Exposing Internal Attentional Brain States using Single-Trial EEG Analysis with Combined Imaging Modalities

Jennifer M. Walz

Submitted in partial fulfillment of the
requirements for the degree
of Doctor of Philosophy
in the Graduate School of Arts and Sciences

COLUMBIA UNIVERSITY

2014

ABSTRACT

Exposing Internal Attentional Brain States using Single-Trial EEG Analysis with Combined Imaging Modalities

Jennifer M. Walz

The goal of this dissertation is to explore the neural correlates of endogenous task-related attentional modulations. Natural fluctuations in task engagement are challenging to study, primarily because they are by nature not event related and thus cannot be controlled experimentally. Here we exploit well-accepted links between attention and various measures of neural activity while subjects perform simple target detection tasks that leave their minds free to wander. We use multimodal neuroimaging, specifically simultaneous electro-encephalograpy and functional magnetic resonance imaging (EEG-fMRI) and EEG-pupillometry, with data-driven machine learning methods and study activity across the whole brain. We investigate BOLD fMRI correlates of EEG variability spanning each trial, enabling us to unravel a cascade of attention-related activations and determine their temporal ordering. We study activity during auditory and visual paradigms independently, and we also combine data to investigate supra modal attention systems. Without aiming to study known attention-related functional brain networks, we found correlates of attentional modulations in areas representative of the default mode network (DMN), ventral attention network (VAN), locus coeruleus norepinephrine (LC-NE) system, and regions implicated in generation of the extensively-studied P300 EEG response to target stimuli. Our results reveal complex interactions between known attentional systems, and do so non-invasively to study normal fluctuations of task engagement in the human brain.

Table of Contents

List of Figures

List of Tables

Acknowledgments

This thesis would not have been possible without the generous support, understanding, and guidance of my advisor Dr. Paul Sajda (a.k.a. "Supreme Overlord of the LIINC Lab"), and it certainly would not have been as much fun! Paul encourages a friendly laboratory environment in which all the members (a.k.a. "stone-cold super freaks") are quirky individuals who genuinely enjoy sharing ideas and helping each other. I'm honored to have been a part of it, and part of me is sad to finally leave. However, I'm excited to move on to the post-doc position of my dreams, and Paul enabled success on that front as well. He funded conference travel that allowed me to present my work all over the world, and in the process to build a network of researchers in the specific field I wish to pursue. He also allowed me to experience the industry environment via a summer internship despite that it meant time away from my projects, and this confirmed the direction of my academic career path. I was trusted to train and mentor other students who joined the lab, and watching them learn to be productive researchers further solidified my desire to remain in academia.

It is no secret that I'm forced to deal with chronic health issues, and Paul's tremendous understanding and patience during times of struggle constantly amaze me. He never expressed frustration during these periods, knowing that I had an overwhelming supply of my own. He did everything in his power to lessen the difficulties associated with my condition.

Secondly and importantly, I would like to thank the rest of my thesis committee: Drs. Truman R. Brown, Andreas H. Hielscher, Elizabeth M.C. Hillman, and Andrew F. Laine. They provided valuable feedback and insight during my proposal defense, and I appreciate their time and consideration in reviewing this dissertation. Truman additionally provided guidance and critique throughout the seemingly never-ending simultaneous EEG-fMRI projects. His detailed questioning of every step drove me close to insanity at times, but in the end dramatically increased the quality of this thesis.

Other key contributors to the EEG-fMRI projects were Dr. Robin I. Goldman and Jordan

Muraskin, who are respectively the "MacGyvers" of simultaneous EEG-fMRI and FSL. I feel honored to have been introduced to the fascinating and challenging world of EEG-fMRI by Robin, since she is a well-respected pioneer of this growing technology. I also give my thanks (and apologies) to the rest of the lab for tolerating the disruptive chaos of our weekly EEG-fMRI meetings. Linbi Hong deserves a special thanks for her integral role in every step of the simultaneous EEG-pupillometry project, including performing all the grunt work. I can genuinely and whole-heartedly say it has been a pleasure to work with her.

fMRI data acquisition would have taken even longer if not for the impressive knowledge and assistance of Stephen Dashnaw and Glenn Castillo at the MRI center formally known as Hatch. During the summer of 2010, Glenn spent almost every Friday night and weekend with me in the cold basement of the Neurological Institute at Columbia University Medical Center. No other technologist could match his relationship with the finicky 3T MRI scanner affectionately called Gertrude.

Of course this work would not have been possible without funding sources, which included the National Institutes of Health (grant R01-MH085092), Army Research Office (W911NF-11-1-0219), and the National Science Foundation's Graduate Research Fellowship Program (GRFP). The latter offered supplementary funding for assistive technology and assistants to ease the burden of my health condition, and the Columbia University Office of Disabilities Services funded structural changes to my work environment to minimize seizure triggers.

The experience of brain mapping from a patient's perspective is what sparked my initial interest in brain research, and for that I'm grateful to my neurologist Dr. Orrin Devinsky and my neurosurgeon Dr. Werner Doyle. However, I had no plans to pursue a Ph.D. until I was motivated to do so by Drs. Beth Pruitt and Marni Goldman. At a time when formal academic advisement blatantly questioned my ability to ever hold a job, Beth and Marni treated my condition as a non-issue, focusing instead on the quality of my work. I am grateful to the AAAS Entry Point! Summer Undergraduate Research Fellowship Program for introducing me to these women. Marni is remembered as an inspiration.

When the inevitable frustrations of scientific research and/or my health condition got out of control, my friends were there to refocus my attention to the big picture and remind me of my accomplishments. In addition to support, many of them provided beautiful EEG and fMRI BOLD

signals. My workout buddies enforced physically strenuous breaks from data analysis, which provided an outlet for my stress and kept my health in check.

Finally, my parents contributed enormously to the success of this thesis, albeit indirectly. They stressed the importance of education from my infancy and encouraged me to pursue any goal of interest. They never put limitations on my choices, and were patient as I clumsily found my educational path. They provided financial support and healthcare for many more years than expected. And I sincerely thank them for instilling in me the frugality that allowed me to live on a graduate student stipend for the past 6 years.

For Marni Goldman.

Chapter 1

Introduction

1.1 Specific Aims

The main goal of this research is to demonstrate that combined imaging modalities can reveal more information about endogenous attentional brain states than can any independent modality. Specifically, we investigated methods of combining electroencephalography (EEG) with functional magnetic resonance imaging (fMRI) and EEG with pupillometry.

The high temporal resolution of scalp EEG allows observation of dynamic neural processes and high frequency oscillations, but source localization is an ill-posed problem and skull impedance results in poor spatial resolution. On the other hand, blood oxygen level dependent (BOLD) fMRI can provide mm-scale spatial resolution, but its temporal resolution is on the order of seconds due to the innately sluggish and somewhat ambiguous BOLD response (Logothetis, 2008). By simultaneously recording EEG and fMRI, the strengths of each modality can be exploited to compensate for intrinsic inadequacies. However, a number of challenges exist with removal of cardiac and radio frequency (RF) gradient artifacts, and optimal approaches to combining the data are yet to be determined.

Perceptual decisions, even in a simple target detection task, involve a complex cascade of neural processes including attention, stimulus detection, target recognition/rejection, motor planning, and response (Philiastides & Sajda, 2007). This begins with modulation of sensory and cognitive attention by locus coeruleus (LC) activations, which enable humans to optimize the allocation of our limited attentional resources (Aston-Jones & Cohen, 2005). This allocation plays an important

role in decision-making, from confidence in one's perceptual decisions to the ability to solve complex problems. The LC is a tiny nucleus of cells at the top of the brainstem associated with primitive physiological processes resulting from arousal, stress, and attention. Its widespread excitatory and inhibitory projections result in correlated effects on multiple sensory areas, deep brain structures, and the oculomotor system. We will capitalize on this link by combining EEG with pupillometry.

Hypothesis 1: When attention to a task wanes, there is an increase of attentional allocation in brain regions not associated with the task.

Aim 1a: Transition previously-used custom-built MR-compatible EEG system for use in a higher-field 3T scanner.

Traditional fMRI analysis enables observation of the event-related average response evoked by stimuli. An oddball paradigm, during which subjects respond only to rare stimuli, can be used to detect activations associated with exogenous bottom-up shifts of attention (Stevens et al., 2000). However, task engagement inevitably varies on a single-trial basis throughout the run of the experiment, particularly during easy tasks that leave the mind free to wander. By recording EEG simultaneously with fMRI, and exploiting the single-trial variability (STV) of the electrophysiological response in the general linear model (GLM) of the fMRI data, we can reveal discriminating components in deep brain structures and more precisely locate cortical components. This was demonstrated by Goldman et al. (2009), who used simultaneous EEG and 1.5T fMRI with an auditory oddball paradigm. Our first aim was to replicate the results of Goldman et al. (2009), using a higher field 3T scanner and the same custom-built MR-compatible 34-electrode EEG system (Chapter 3). A higher static field boosts the SNR of the fMRI data, but the simultaneously-acquired EEG suffers from increased magnitude of magnetically induced artifacts.

Aim 1b: Using simultaneous EEG-fMRI and single-trial analysis, observe the time course of activity linked to the redistribution of attentional resources during a visual task.

After demonstrating feasibility of these methods in the higher field scanner, our next aim was to expand upon this auditory experiment using an analogous visual oddball paradigm (Chapter 4). It is probable that a subset of regions involved in maintaining task-related attention depend on the sensory input modality of the task.

Aim 1c: Identify brain regions that show common modulatory activity across auditory and visual tasks.

We next combined auditory and visual task EEG-fMRI data to investigate coupling between supra-modal attentional systems (Chapter 5). We used the same data-driven single-trial EEG variability methods to find areas that modulate BOLD activity with task-related attention, in a common way across the auditory and visual sensory input domains. We expanded upon our findings by performing a Dynamic Causal Modeling (DCM) analysis (Friston et al., 2003; Stephan et al., 2010) to investigate directionality of functional connectivity between these regions.

Hypothesis 2: Endogenous attentional state influences evoked EEG and fMRI BOLD responses to the subsequent stimulus.

Aim 2a: Investigate correlates of prestimulus alpha power variability and fMRI BOLD response.

Despite the common association of EEG alpha power with attention, not much is known about the function of these oscillations or the mechanisms and brain structures driving them (Klimesch et al., 1998; van Dijk et al., 2008). Alpha activity is easily detected using EEG but cannot be studied using traditional or single-trial fMRI analysis due to the slow nature of the BOLD response. In order to derive EEG-based regressors for the fMRI GLM, the high-dimensional electrode space must be reduced. However, the broad posterior distribution characteristic of alpha activity makes electrode selection arbitrary. To circumvent this we will perform independent component analysis (ICA) to

determine the projection containing maximum EEG alpha power. We will then generate regressors for the GLM analysis by finding the alpha power of that projection immediately preceding each trial. Trials will be grouped by high and low alpha power to investigate effects of prestimulus alpha activity on strength and spatial distribution of the event-related BOLD response (Chapter 6).

Aim 2b: Investigate correlation of pre-stimulus pupil size with EEG attention index.

The locus coeruleus (LC) is a widely-projecting nucleus of cells in the brainstem, which plays an important role in target detection, focused attention, and behavioral responses to sensory stimuli (Aston-Jones & Cohen, 2005). Two modes of LC activity have been proposed: tonic (i.e. baseline) and phasic (i.e. event-related) (Aston-Jones & Cohen, 2005). However, due to its tiny size and deep subcortical location, studies are normally limited to highly invasive experiments in primates. Pupil diameter has been shown in monkeys to closely track LC activity (Aston-Jones & Cohen, 2005), and we plan to exploit this link in humans by simultaneously recording EEG and pupillometry during LC activation. Since tonic LC activity underlies the endogenous state of attention and arousal, pupil size should be correlated with task engagement (and thus with our EEG attention index). We will investigate this by correlating the pupil size prior to the onset of the stimuli with the EEG discriminator output, to temporally and spatially localize components associated with attention (Chapter 7). Significant correlations would provide further evidence for the role of the LC in endogenous modulations of arousal and attention.

1.2 Motivation

1.2.1 Scientific Motivation

Humans continuously rely on our ability to optimally allocate our attentional resources. Top-down attention affects nearly all cognitive processes, from perceptual decision-making to complex problem-solving. Even healthy individuals are commonly affected by temporary deficiencies in attention allocation, and attention deficit hyperactivity disorder (ADHD) can have disabling effects. This may result in decreased task performance (e.g. digesting a journal article) or dangerous oversights (e.g. inattentive driving).

A deeper understanding of the neural mechanisms underlying top-down attention will ultimately lead to more accurate diagnoses and more effective treatments for ADHD and other impairments. Our work will enable future research to link deviations from characteristic temporal and spatial activations to specific pathologies. In the long-term, it may also lead to applications that increase productivity and learning rate of both diseased and healthy individuals. A brain-computer interface could be developed to detect unwanted changes in attentional allocation, and then alter stimuli in response. Such a closed-loop system could potentially switch stimulus delivery to another sensory modality to optimize information transfer, or even retain attention to the initial modality to maximize performance of the task at hand.

1.2.2 Technical Motivation

Internal attentional brain states are challenging to study because their fluctuations are not always event-related. Traditional event-related neuroimaging analysis methods enable observation of the average response evoked by stimuli. However, task engagement inevitably varies on a single-trial basis throughout the run of an experiment. Single-trial EEG analysis enables observation of natural fluctuations of evoked (phase-locked) responses.

The high temporal resolution of scalp EEG allows observation of dynamic neural processes, but source localization is an ill-posed problem and skull impedance results in poor spatial resolution. On the other hand, BOLD fMRI can provide mm-scale spatial resolution, but its temporal resolution is on the order of seconds due to the complex and indirect nature of the BOLD response (Arthurs & Boniface, 2002). By simultaneously recording EEG and fMRI, the strengths of each modality can be exploited to compensate for intrinsic inadequacies. However, optimal approaches to combining the data are yet to be determined.

Aim 1a is to replicate and expand upon previous simultaneous EEG-fMRI results (Goldman et al., 2009), acquired at 1.5T, by using a 3T MR System. The higher static field provides a higher SNR of the fMRI BOLD signal compared to that recorded from the previously used 1.5T scanner. It also enables us to obtain higher resolution functional images with the same repetition time. However, it comes at the cost of reduced SNR in the EEG due to increased magnitude of gradient and BCG artifacts. To remove non-stationary artifacts, many technical difficulties need to be overcome, including loss of task-relevant EEG frequencies.

The locus coeruleus (LC) is a nucleus of cells in the brainstem that is closely tied to both exogenous and endogenous attention, but too small and deep for its activity to be studied noninvasively using currently-existing methods. However, its widespread projections provide a link between measurable responses of the oculomotor system and cortical tissue. Aim 2b exploits these links using simultaneous scalp EEG and pupil diameter recordings, to study the temporal dynamics underlying unprovoked attentional modulations.

1.3 Background

1.3.1 Trial-to-trial EEG variability linked to attention

Specific ERP components have been associated with various stages of attentional and perceptual decision making processes. Exogenously-driven shifts of attention (e.g. resulting from presentation of target stimuli) can be studied with event-related analyses, and have been known to modulate on a single-trial basis with the endogenous attentional state of the subject (Key et al., 2005; Polich & Kok, 1995; Warbrick et al., 2009).

Even a simple target detection task involves a complex cascade of neural processes including attention, stimulus detection, target recognition/rejection, motor planning, and behavioral response. Linear discrimination using logistic regression (LR) applied to EEG signal amplitude has been successfully used to classify and localize the cortical activity correlated with various cognitive tasks (Parra et al., 2002, 2005; Philiastides & Sajda, 2006, 2007).

Evoked response potentials (ERPs) to sensory stimuli have been extensively studied using scalp EEG. These neural responses are phase-locked to the onset of the stimulus or the behavioral response.

1.3.2 BOLD correlates of attentional modulations using simultaneous EEG and fMRI

Simultaneous EEG-fMRI is a relatively new tool with proven utility in brain function studies, but its use comes with many challenges in data collection/quality (Figure 1.1), and there remain open questions with regard to meaningful analysis methods.

Firstly, EEG data acquired in the scanner are inevitably contaminated with RF gradient arti-

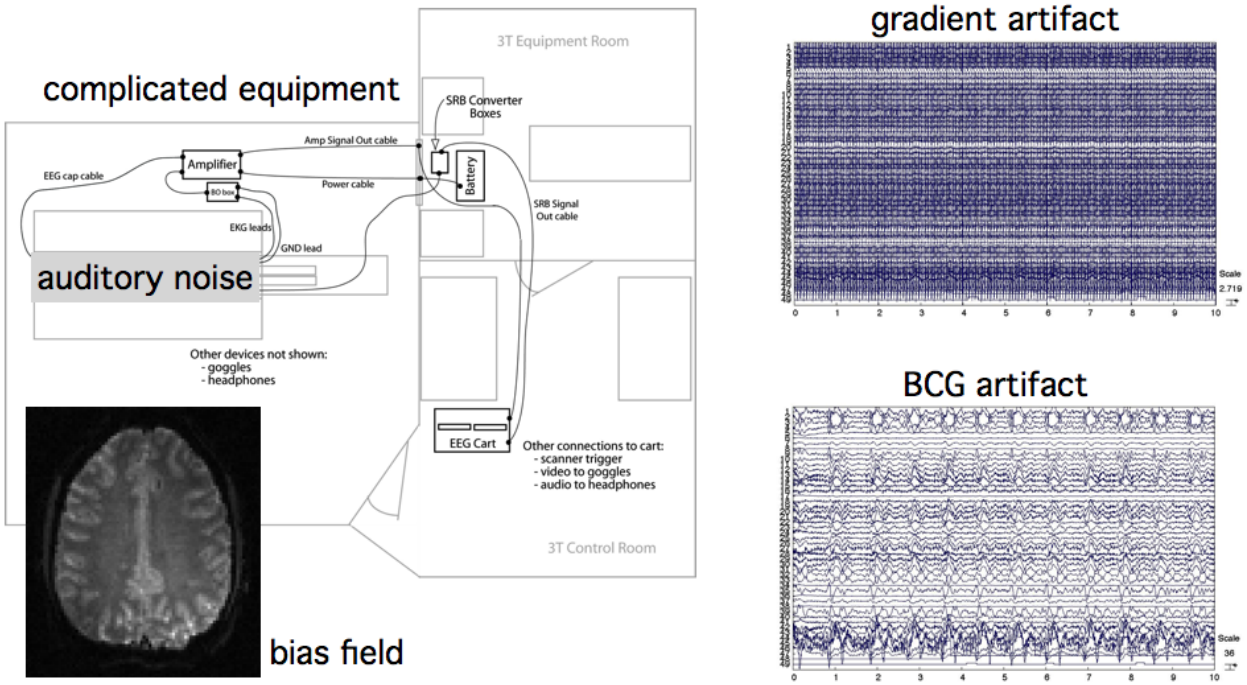

Figure 1.1: Challenges When Acquiring Simultaneous EEG-fMRI. Additional challenges when acquiring EEG in the fMRI scanner include complicated hardware setup, auditory noise from the changing magnetic fields, bias field artifact in the fMRI images due to presence of the EEG wires, and magnetically-induced artifacts in the EEG data, both from the rapidly changing fields (gradient artifact) and movement of the EEG wires within the static field (BCG pulsation artifact).

facts as the changing magnetic field induces current in the wires. Special MR-compatible amplifier designs and modified electrode cap configurations can help to make these artifacts more manageable (Hill et al., 1995; Ives et al., 1993). Second, motion artifacts are greatly magnified, since even small movement of the wires in the strong static field induces unwanted current. It is imperative that subjects are positioned and padded comfortably in the scanner to minimize movement, with care taken not to allow subjects to wiggle around during placement in the head coil, since this can result in impedance increases or even loss of signal. An additional motion-related artifact that is not present in stand-alone EEG is ballistocardiogram (BCG), which are caused by the tiny movement of the electrodes with each pulse of the subject (Ives et al., 1993; Muri et al., 1998). RF artifacts are regular enough to easily remove with simple mean subtraction methods, and only become a problem when head position changes cause non-stationarities. BCG, on the other hand, is highly non-stationary and irregular, making template-matching ineffective. ICA methods can reduce this artifact, but sometimes remove neurologically-relevant frequency content. Furthermore, EEG wires can cause field inhomogeneities that result in signal dropoff in the fMRI images. Despite these challenges and due to the development of effective preprocessing techniques and increased availability of commercial data acquisition systems, EEG-fMRI is growing fast in popularity.

One useful approach is to exploit the single-trial variability of the electrophysiological response in the fMRI general linear model (GLM) (Fuglo et al., 2012; Warbrick et al., 2009). The event-related potential (ERP) component measurements vary across electrodes though, leading to a challenge selecting an electrode subset for the model. On the other hand, independent component analysis (ICA) can blindly find projections of the EEG data, but the functional meaning of these components is unclear. Goldman et al. (2009) demonstrated the utility of single-trial EEG analysis using machine learning techniques to find a functionally relevant projection of the EEG data, which was then used to construct the fMRI GLM. This method can reveal meaningful discriminating components in deep brain structures and more precisely locate cortical components. Furthermore, analysis of discriminating components at various latencies allows the study of the temporal progression of task-relevant neural activity.

In Aim 1b, we expand upon the auditory oddball paradigm results of Goldman et al. (2009), using an analogous visual oddball paradigm, to further investigate whether decreased task engagement is due to an increased rationing of attention in task-irrelevant areas or a uniform downregulation

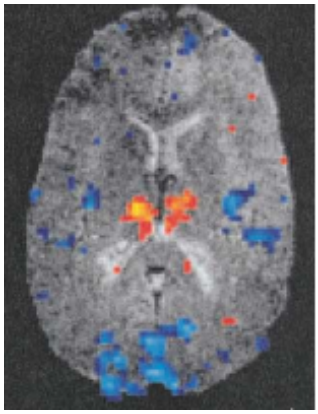

Figure 1.2: BOLD Correlates of Posterior EEG Alpha. BOLD signals in subcortical and cortical structures have been shown to (respectively) positively and negatively correlate with natural fluctuations in ongoing posterior EEG alpha activity. Reproduced from Goldman et al. (2002).

throughout the brain. We used a higher-field 3T scanner, providing a greater signal-to-noise ratio (SNR) of the fMRI signal and higher resolution functional images. However, this came at the potential cost of EEG discrimination performance, due to reduced SNR in the EEG caused by increased magnitude of magnetically-induced artifacts.

1.3.3 Prestimulus EEG alpha power related to endogenous attentional state

One particular EEG frequency band that is commonly associated with attention modulations is alpha (8–12 Hz); there is a commonly known inverse relationship between posterior alpha power and attention, both in baseline activity and responses to stimuli (Klimesch et al., 1998; Makeig et al., 2002; Min & Park, 2010; van Dijk et al., 2008). Many of these studies, however, have analyzed data with respect to behavioral responses (e.g. segregating correct and error trials and looking at differences in the power spectrum for these two cases). However, during easy tasks that leave our minds free to wander (and thus allow greater natural alpha fluctuations to occur), errors are too rare for these methods to be used. In these tasks, variability in the EEG response, instead of task performance, can be related to baseline alpha fluctuations (Barry et al., 2000).

Neurophysiological oscillatory activity is too fast to be studied with BOLD fMRI alone, since its signal comes from the blood flow response to changes in neural activity. The advent of simultaneous EEG-fMRI has allowed investigators to unveil BOLD correlates of endogenous alpha fluctuations in brain regions previously associated with vision and attention (Goldman et al., 2002; Laufs et al.,

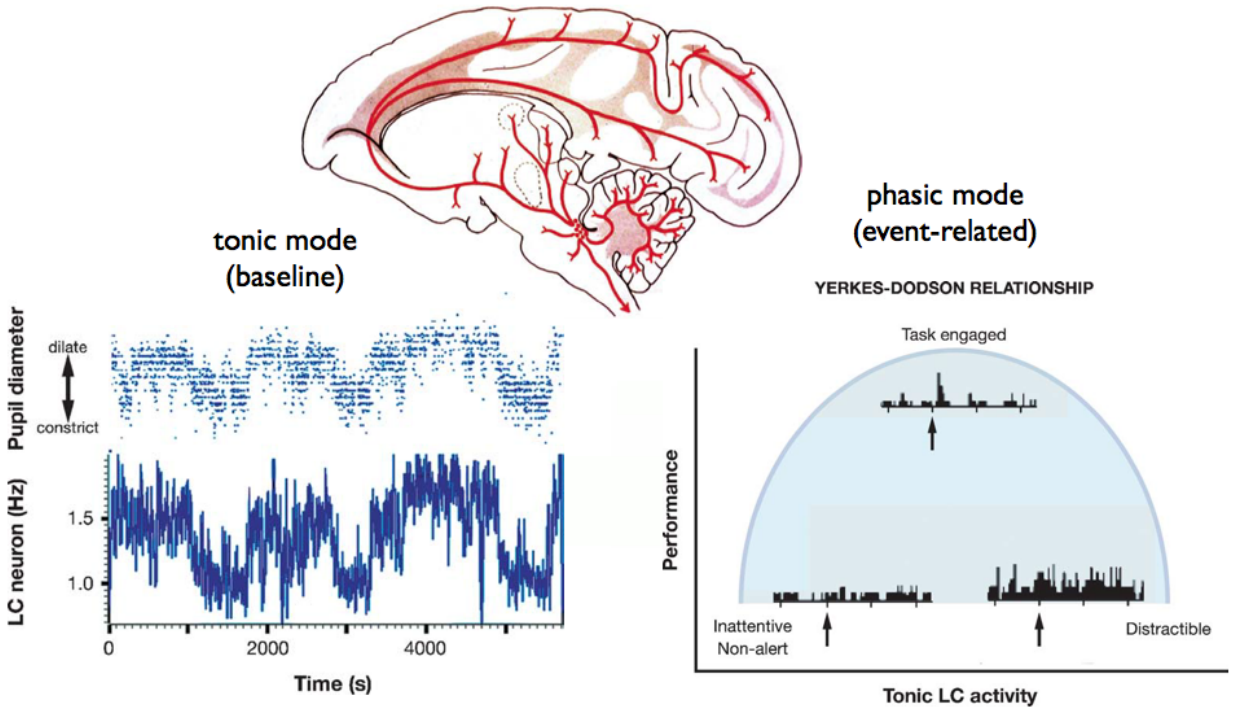

Figure 1.3: The Locus Coeruleus Norepinephrine System. The LC is a small nucleus of cells in the dorsal pons that projects widely to cortical and subcortical structures. Top: diagram of LC projections in the monkey brain. Tonic LC activity has been shown to closely track pupil diameter changes (left). Phasic activity has been related to task performance (right). Figures reproduced from Aston-Jones & Cohen (2005).

2006) (see Figure 1.2). However, little has been done to investigate effects of baseline alpha activity modulations on the event-related BOLD response. In Aim 2a, we use simultaneous EEG-fMRI with the oddball paradigm to study the effects of EEG alpha power fluctuations on the elicited BOLD response; we hypothesize that modulations in baseline alpha result in a change in the extent of cortex necessarily recruited to process the target stimuli.

1.3.4 Pupil diameter strongly linked to attention

Activity of the locus coeruleus (LC) has been shown to modulate electrophysiological and pupillary responses (phasic mode), and closely track pupil diameter (PD) and attentional fluctuations (tonic mode) (Aston-Jones & Cohen, 2005; Gilzenrat et al., 2010) (see Figure 1.3). As previously mentioned, EEG response variability has been associated with a variety of endogenous states, including attention (i.e. task engagement) and anticipation (Key et al., 2005; Polich & Kok, 1995; Smit et al.,

2009; Warbrick et al., 2009). Pupil diameter has also been shown to modulate with these internal states (Einhauser et al., 2008; Steinhauer & Hakerem, 1992; Waszak & Herwig, 2007).

Since these EEG, pupil diameter, and internal brain state modulations are associated with underlying LC activity, the LC provides a link between the cortical activity of the central nervous system (CNS) and the unconscious pupil diameter changes of the peripheral nervous system (PNS), both of which can be observed non-invasively. In Aim 2b, we exploit the LC's link between the CNS and PNS to investigate correlations of EEG discriminating components at various latencies with measures of attention and anticipation, using PD to index attention on each trial, and number of pre-target standard trials to index the subjects' anticipation.

Chapter 2

Materials and Methods

This chapter describes the core materials and methods that are used repeatedly throughout this dissertation. Materials and methods specific to individual projects are described within the corresponding chapters.

2.1 Oddball Paradigm

For each of the projects within this thesis, healthy human subjects performed a classic oddball task. This is a simple and well-studied paradigm that leaves subjects' minds free to wander while still maintaining near-perfect behavioral performance, so it was ideal for studying naturally occurring endogenous shifts of attention. In Chapters 3, 6, and 7 an auditory oddball experiment was used, in Chapter 4 a visual oddball experiment was used, and in Chapter 5 commonalities across both sensory input domains were studied. Figure 2.1 diagrams the visual oddball paradigm. The auditory paradigm was analogous. Both are described below.

All stimuli were presented for 200 ms each with a 2 to 3 s uniformly-distributed variable inter-trial interval (ITI) and probability of target was $\frac{1}{5}$. The first two stimuli of each run were constrained to be standards. The visual target and standard stimuli were, respectively, a large red circle and a small green circle on isoluminant gray backgrounds (3.45° and 1.15° visual angles). The larger target stimuli boosted EEG discriminator performance, and did not confound our final results, since we interpreted only the variability within the target class. Auditory standard stimuli were a pure 390 Hz tone, and target stimuli were a broadband "laser gun" sound. These choices are

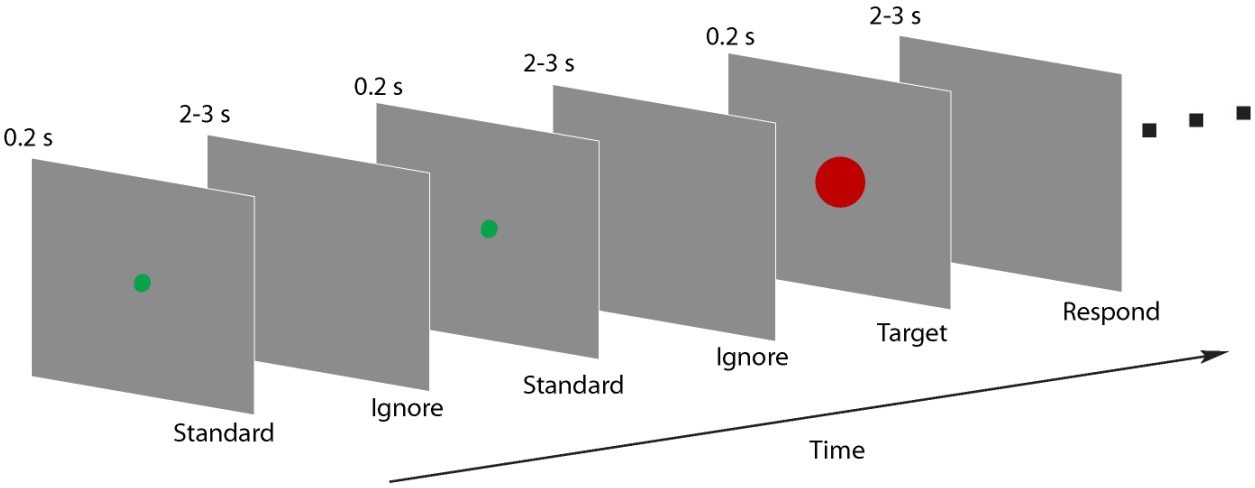

Figure 2.1: Visual Oddball Paradigm.

explained in Chapter 3, which is focused on transitioning previously used EEG-fMRI single-trial analysis methods from the 1.5T to higher field 3T scanner. Stimuli were presented to subjects using E-Prime software (PST, Pittsburgh, PA) for all experiments. Because our study focused on task-related attentional states, subjects were asked to respond to target stimuli, using a button press with the right index finger.

In the auditory oddball experiment performed outside of the fMRI scanner (Chapter 7), sounds were presented through speakers and subjects responded using a gamepad. In the EEG-fMRI studies, stimuli were presented via a VisuaStim Digital System (Resonance Technology, Northridge, CA), comprised of headphones and a 600×800 goggle display. Behavioral responses were acquired using an MR-compatible button response pad. All subjects gave written informed consent following the protocol of the Columbia University Institutional Review Board.

2.2 Data Acquisition

All of the studies within this thesis use EEG in combination with other types of neurological data and explore data fusion methods to study endogenous fluctuations of task-related attention. The study described in Chapter 7 used simultaneous EEG-pupillometry, and all other studies used simultaneous EEG-fMRI. The pupillometry data acquisition and preprocessing is described within Chapter 7, and the simultaneous EEG-fMRI data are described below.

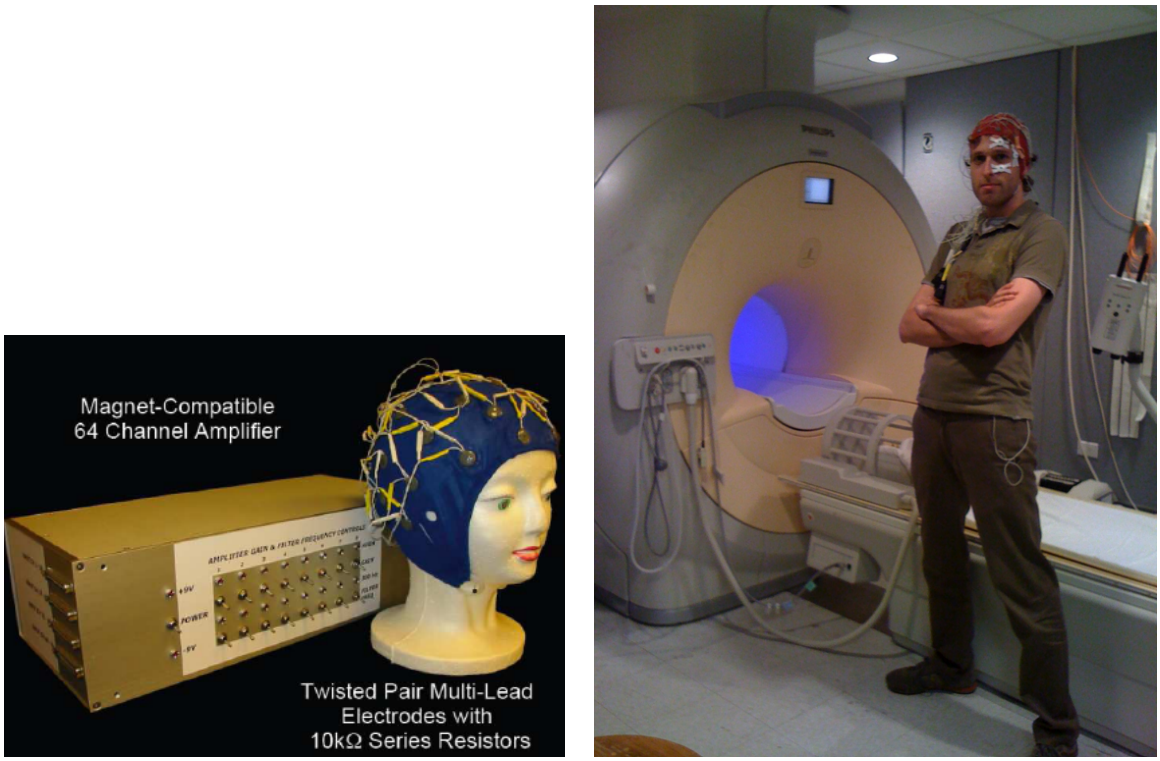

Figure 2.2: Custom-built MR-Compatible EEG System. Left: 64-channel EEG amplifier and bipolar electrode cap. Right: Subject setup for EEG-fMRI experiment. The (model) subject is standing in front of the 3T MRI scanner, wearing an electrode cap embedded with 36 EEG electrodes arranged as 43 bipolar pairs (see Figure2.3) as well as external electro-oculogram (EOG) and echo-cardiogram (ECG) channels.

2.2.1 EEG recorded in the fMRI scanner

We simultaneously and continuously recorded EEG using a custom-built MR-compatible EEG system (Goldman et al., 2009; Sajda et al., 2010), with differential amplifier and bipolar EEG cap (Figure 2.2). The caps are configured with 36 Ag/AgCl electrodes including left and right mastoids, arranged as 43 bipolar pairs (Figure 2.3). Bipolar pair leads are twisted to minimize inductive pickup from the magnetic gradient pulses and subject head motion in the main magnetic field. This oversampling of electrodes ensures data from a complete set of electrodes even in instances when discarding noisy channels is necessary. To enable removal of gradient artifacts in our offline preprocessing, we synchronized the 1-kHz-sampled EEG with the scanner clock by sending a transistor-transistor logic (TTL) pulse to a field-programmable gate array (FPGA) card (National Instruments, Austin, TX) at the start of each of 170 functional image acquisitions. All

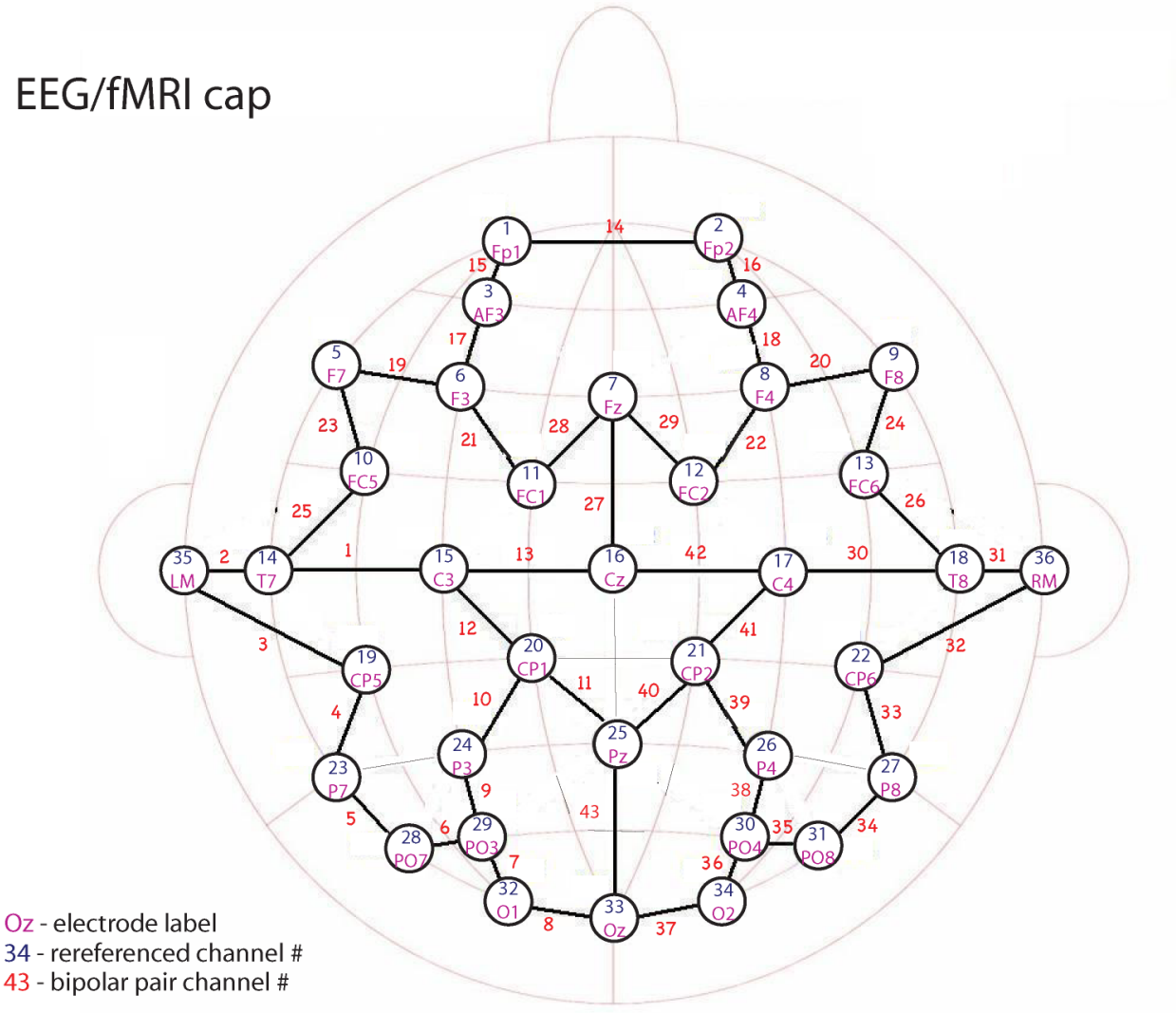

Figure 2.3: MR-compatible EEG cap diagram. The custom-built EEG cap is configured with 36 electrodes arranged as 43 bipolar pairs. Leads are twisted to minimize induction of current due to magnetic field changes.

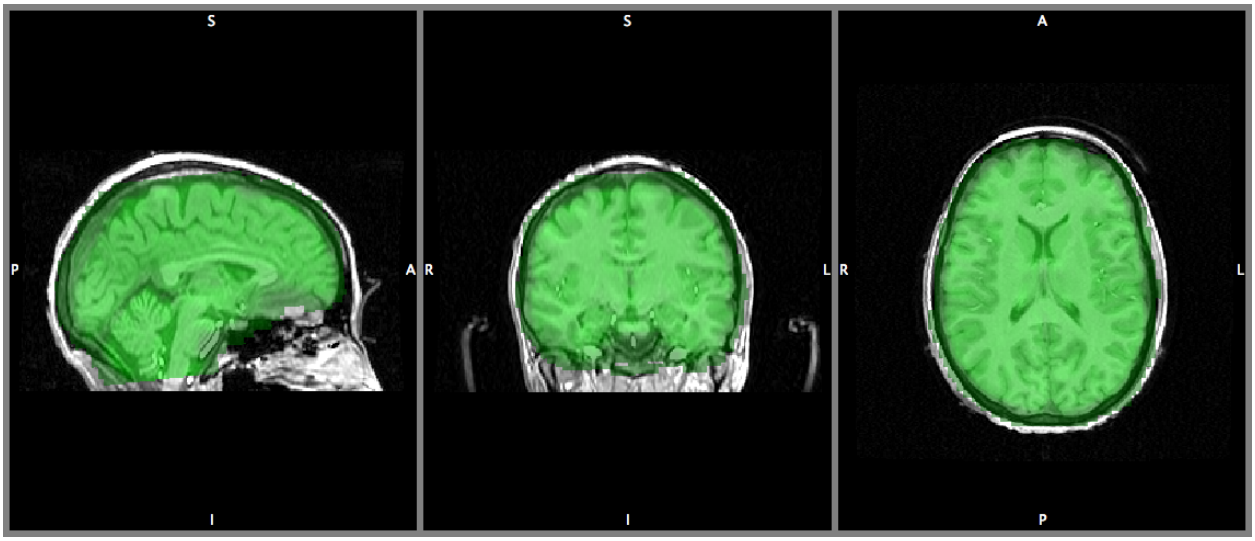

Figure 2.4: fMRI Whole-brain Data Coverage. Example of whole brain EPI data coverage (green) including cortical and subcortical regions, shown for one subject (overlaid on subject's structural scan). Headphones and goggles can be seen in the images.

electrode impedances were kept below 20 kΩ, including 10 kΩ resistors built into each electrode for subject safety. A comprehensive description of the hardware, along with many of the preprocessing and analysis methods described throughout the remainder of this section, can be found in Sajda et al. (2010).

2.2.2 fMRI

A 3T Philips Achieva MRI scanner (Philips Medical Systems, Bothell, WA) was used to collect functional echo-planar image (EPI) data continuously with 3 mm in-plane resolution and 4 mm slice thickness. We covered the entire brain (Figure 2.4) by obtaining 32 slices of 64×64 voxels using a 2000 ms repetition time (TR) and 25 ms echo time (TE). We also acquired a single-volume high resolution ($2 \times 2 \times 2$ mm) EPI image and a $1 \times 1 \times 1$ mm spoiled gradient recalled (SPGR) image for each subject for purposes of registration.

Great care was taken when placing the subjects in the scanner to ensure subject safety and maximize data quality. Subjects were instructed to avoid shifting their head in the coil after lying down on the scanner bed. This would have interfered with the impedances and even disrupted connections between the posterior electrodes and the scalp. We padded the subjects' heads as

much as their comfort allowed, in order to minimize head motion during the scans. Head motion exceeding half a voxel (1.5 mm) could decrease SNR substantially enough to warrant discarding the data. Furthermore, even minuscule head movement within the static 3T field was enough to cause huge deflections in EEG amplitude caused by magnetic induction in the wires. EEG wires were arranged such that they were as far from the subjects' heads as possible without penetrating the cage of the coil (see right side of Figure 2.2) and separated from them with padding.

2.3 Data Preprocessing

2.3.1 Standard EEG data preprocessing

We performed EEG preprocessing offline using Matlab (Mathworks, Natick, MA), using the following digital Butterworth filters: 0.5 Hz high pass to remove DC drift, 60 Hz and 120 Hz notches to remove electrical line noise and its first harmonic, and 100 Hz low pass to remove high frequency artifacts not associated with neurophysiological processes. These filters were applied together in the form of a linear phase finite impulse response (FIR) filter to avoid distortions caused by phase delays.

2.3.2 Additional preprocessing for EEG data acquired simultaneously with fMRI

In addition to standard EEG artifacts, electrophysiological signals recorded inside the MRI scanner are contaminated with gradient artifacts and ballistocardiogram (BCG) artifacts due to magnetic induction in the EEG wires. First we removed the gradient artifacts by subtracting the mean artifact across all functional volume acquisitions. We then applied a 10 ms median filter to remove any residual spike artifacts. Because we sync the scanner with the EEG we are able to remove the gradient artifact at the commonly-used 1 kHz sampling rate of stand-alone EEG. Next we removed standard EEG artifacts, using the filters described above (Section 2.3.1).

BCG artifacts are more challenging to remove, since they share frequency content with EEG activity. Currently-existing BCG removal algorithms cause loss of signal power in the underlying EEG, so we performed single-trial classification (described in Section 2.4) on the data prior to BCG artifact removal. This is a justified practice because our classifier identifies discriminating components that are likely to be orthogonal to BCG. In order to compute scalp topographies

of these discriminating components, BCG artifacts were removed from the continuous gradient-free data using a principal components analysis (PCA) method (Goldman et al., 2009; Sajda et al., 2010). First the data were low-passed at 4 Hz to extract the signal within the frequency range where BCG artifacts are observed, and then the first two principal components were determined. The channel weightings corresponding to those components were projected onto the broadband data and subtracted out. These BCG-free data were then re-referenced from the 43 bipolar channels to the 34-electrode space to calculate scalp topographies of EEG discriminating components. They were also necessarily used to calculate the average event-related potentials (ERPs) on each electrode.

We investigated both stimulus-locked and response-locked activity because some cognitive processes are more tightly time-locked to stimulus onset and others to behavioral responses (Gerson et al., 2005; Makeig et al., 2004). We extracted 1000 ms stimulus-locked and response-locked epochs (with baseline removal on the 200 ms prior to stimulus) from both the 43-channel gradient-free dataset and the 34-electrode re-referenced dataset. By visual inspection we discarded trials containing motion or blink artifacts, evidenced by sudden high-amplitude deflections, and also those with incorrect responses, identically for both datasets. This left approximately 95% of the target trials remaining. Because the paradigm does not require a behavioral response to standard stimuli, we randomly assigned reaction times (RTs) to standard trials chosen from the probability distribution of target trial RTs (Goldman et al., 2009). This provided a baseline activity for response-locked single-trial EEG analysis, and it did not affect interpretation of results since we only viewed results derived from the variability within the target class.

2.3.3 fMRI data preprocessing

Using FSL (Smith et al., 2004), we performed bias-field correction on all images to adjust for artifacts caused by the EEG wires. We then performed slice-timing correction, motion correction, 0.01-Hz high-pass filtering, and 5-mm full width half max (FWHM) spatial smoothing on the functional data. Motion correction provided motion parameters that were later included as confounds in the general linear model (GLM). Functional and structural images were registered to a standard Montreal Neurological Institute (MNI) brain template following brain extraction, and each subject's registration was checked manually to ensure proper alignment.

2.4 Single-Trial Analysis of EEG

Every study within this thesis, with the exception of the EEG alpha study described in Chapter 6, uses the following EEG single-trial analysis methods.

We applied a linear classifier to the multi-dimensional EEG signal amplitude using the sliding window method of Parra et al. (2005). Specifically, we find a projection of the multidimensional EEG signal, $\mathbf{x}_i$(t), $i = \{1...T\}$ (where i indexes trials and T is the total number of trials) within a short time window that achieves maximal discrimination between target and standard trials. All time windows had a width of $N = 50$ ms and the window center, τ, was shifted from 0 ms to 1000 ms relative to stimulus onset, in 25 ms increments. We used logistic regression to learn the multi-channel spatial weighting, $\mathbf{w}(\tau)$, that maximally discriminated conditions, arriving at the projection, $y_i(\tau)$, for each trial i and a given window τ.

$$y_i(\tau) = \frac{1}{N} \sum_{t=\tau-\frac{N}{2}}^{\tau+\frac{N}{2}} \mathbf{w}(\tau)^T \mathbf{x}_i(t) \tag{2.1}$$

Note that we use the average projection in each temporal window, τ, which tends to be less sensitive to noise. The result is a hyperplane, for each τ, that maximally discriminates the target vs. standard trials given the EEG amplitudes for each trial (see Figure 2.5).

The classifier output, $y_i(\tau)$, represents the classifier's confidence in its prediction based on the training data and the model. We assessed classifier performance with the area under the receiver operating characteristic (ROC) curve (Green & Swets, 1966), denoted AUC, using leave-one-out (LOO) cross validation (Duda et al., 2001). AUC was calculated for multiple temporal windows, enabling observation of the temporal progression of task-relevant components and localization of the event-locked time with maximal discrimination between conditions. To obtain a significance threshold for the AUC values, we used a permutation test in which we randomly permuted the trial labels and ran the classifier using the LOO approach. We repeated this procedure 1000 times for each subject to generate a distribution of AUC values from which we computed the null hypothesis distribution for AUC values and the corresponding AUC threshold for p = 0.01.

For each window τ we also generated the forward model $\mathbf{a}(\tau)$,

$$\mathbf{a}(\tau) = \frac{\mathbf{X}(\tau)\mathbf{y}(\tau)}{\mathbf{y}(\tau)^T\mathbf{y}(\tau)} \tag{2.2}$$

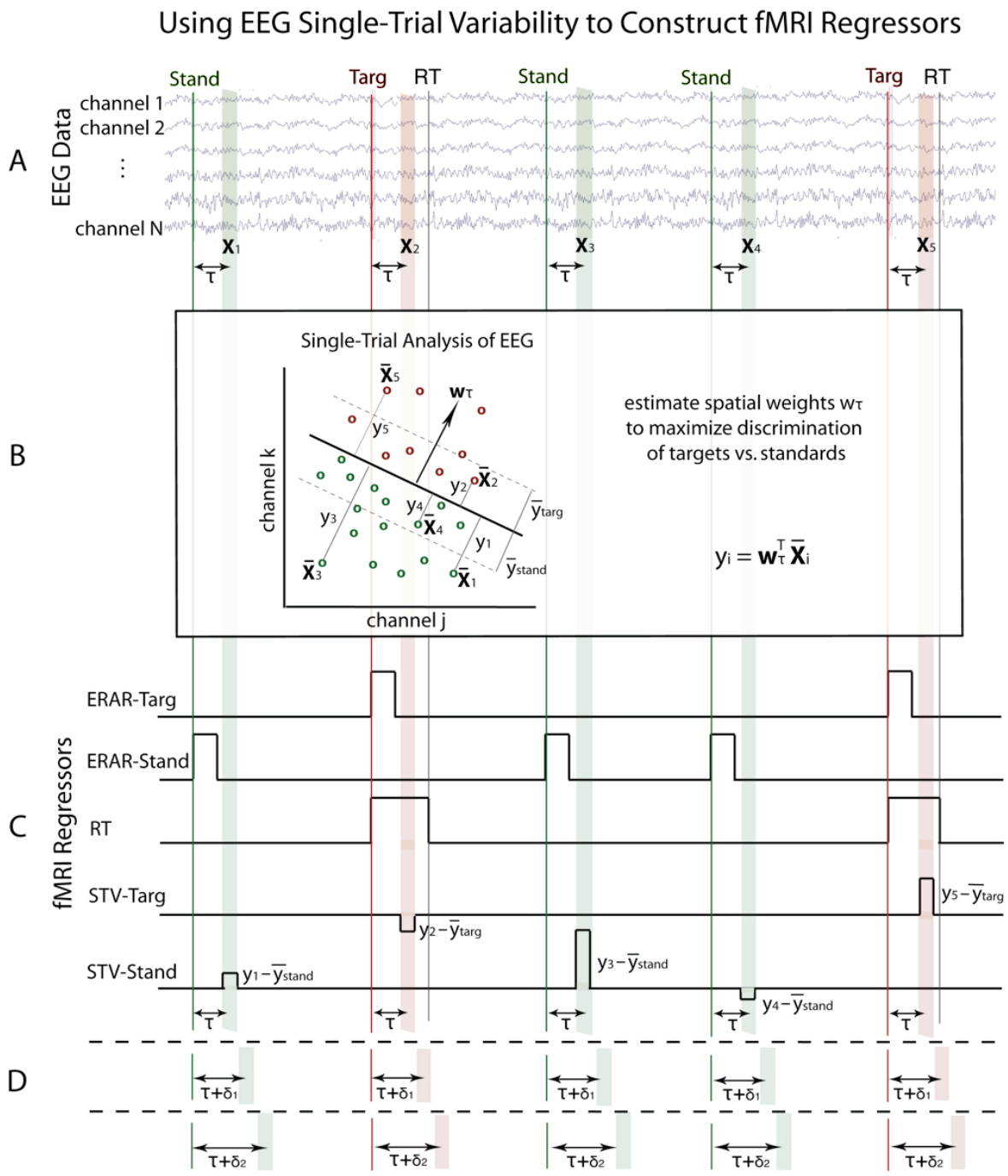

Figure 2.5: Method for constructing fMRI regressors from simultaneously-acquired EEG data. A. For each trial (i), select a training window of EEG data ($\mathbf{X}_i$) with offset τ from the stimulus (or behavioral response). **B.** Train linear classifier on EEG data within the time window to estimate a set of spatial weights ($\mathbf{w}$) that maximize discrimination of the two conditions (shown using only 2 EEG channels for visualization purposes). **C.** In addition to traditional event-related average response (ERAR) and reaction time (RT) regressors, construct single-trial EEG variability (STV) regressors by modulating boxcar height with classifier output (y) for each trial. **D.** This technique is repeated for multiple window offsets spanning the epoch to view temporal progression of discriminating components spanning the trial.

where we now organize $y_i(\tau)$ as a vector $\mathbf{y}(\tau)$, where each row is from trial i, and we organize $\mathbf{x}_i(t)$ as a matrix, $\mathbf{X}(\tau)$, where rows are channels and columns are trials, all for time window τ. These forward models can be viewed as scalp plots and interpreted as the coupling between the discriminating components and the observed EEG (Goldman et al., 2009; Parra et al., 2002, 2005; Sajda et al., 2010). Given that we estimate a linear weighting for temporal windows spanning the trial, we are able to track the progression of the spatial components across time.

2.5 Traditional fMRI Analysis

We first ran a traditional fMRI analysis, using event-related and RT variability regressors in our GLM. The event-related regressors were comprised of boxcar functions with unit amplitude and onset and offset matching that of the stimuli. RT variability was modeled using unit amplitude boxcars with onset at stimulus time and offset at response time, and these were orthogonalized to the event-related regressors. Orthogonalization was implemented using FSL, which utilizes the Gram-Schmidt procedure (Strang, 2003) to de-correlate the RT regressor from all other event-related regressors. All regressors were convolved with the canonical hemodynamic response function (HRF), and temporal derivatives were included as confounds of no interest. An event-related target vs. standards contrast was also constructed. A fixed effects model was used to model activations across runs, and a mixed effects approach used to compute the contrasts across subjects. Statistical image results for these traditional analyses were thresholded at $z > 2.3$, and clusters were multiple-comparison-corrected at $p = 0.05$ (Worsley, 2001).

2.6 EEG-Based fMRI Analysis

For the single-trial variability (STV) fMRI analysis, we modeled the variability of the neural response using an additional two regressors: one each for targets and standards. These EEG-based regressors were designed with duration 100 ms, centered on the classifier training window. The STV regressor height was modulated using the demeaned output $\tilde{y}_i = y_i - y_{\text{mean}}$ of the EEG discriminator for each trial (i). These regressors were convolved with the HRF and orthogonalized with respect to all traditional regressors, with temporal derivatives included as confounds. It was especially important to regress out the RT variability, since RT is known to be negatively correlated

with attention (Eason et al., 1969; Weissman et al., 2006), and our aim was to study variability in task engagement that cannot be detected using an external measure. This entire analysis was run independently for all stimulus-locked and response-locked EEG training windows exceeding a mean AUC value of 0.75, which is a common psychophysical threshold used in signal detection theory and here represents substantial performance of the classifier. To avoid stimulus-type confounds, we focused on within-class variability, using only the target stimuli STV statistical maps in our results interpretation.

We used a randomization method motivated by deBettencourt et al. (2011) and threshold-free cluster enhancement (Smith & Nichols, 2009) to correct for multiple comparisons, by running a complete STV fMRI analysis after permuting the $y_{\tau=450\text{ms}}$ values randomly within each class. 100 permutations were run for each subject. We carried these randomization results through to the group level and thresholded the statistical maps at per-voxel $p = 0.005$. For each cluster in the resulting null distribution, we summed the negative logarithm of the p-value over each voxel in the cluster. This provided a score for each cluster that, while highly dependent on cluster size, also accounted for some variation in the magnitude of the z-scores within the cluster. We determined a threshold based on the 99^{th} percentile of these null-distribution cluster scores, or a p-value of 0.01.

We took extra care to investigate the possibility of pulsation artifacts confounding our results, by constructing fMRI regressors from BCG-artifact pulse timing. This timing was determined using a peak detection algorithm on temporal lobe EEG channels, which are the channels most strongly contaminated with BCG artifact. We fit this regressor to the functional data, and thresholded the resulting maps at an uncorrected $p < 0.005$. We do not report any results that overlap with these pulse correlates.

Chapter 3

Transition of EEG-fMRI Methods from 1.5T to 3T Scanner

3.1 Introduction

Our group previously demonstrated that single-trial variability (STV) of EEG components recorded simultaneously with 1.5T fMRI can yield task-relevant BOLD activations that are unobservable using traditional fMRI analysis methods (Goldman et al., 2009). A higher field MR system provides greater signal-to-noise ratio (SNR) of the fMRI BOLD signal, and it enables acquisition of functional images with increased resolution in both time and space. However, this comes at the cost of reduced SNR in the EEG due to increased magnitude of gradient, BCG, and motion artifacts. Since our STV method depends upon high fidelity EEG, a major concern was loss of statistical power in the BOLD correlates due to reduced discrimination of EEG acquired during 3T scanning.

3.2 Methods

Upon completion of preliminary stand-alone EEG tests (purpose and results described below), seventeen subjects (6 female, mean 27.7 years, range 20–40) participated in three runs of the traditional auditory oddball paradigm described in Section 2.1. Each run consisted of 100 standard stimuli and 25 oddball stimuli. Subjects were instructed to keep their eyes closed to minimize eye movement artifacts in the EEG. All of the EEG-fMRI data acquisition, preprocessing, and analysis

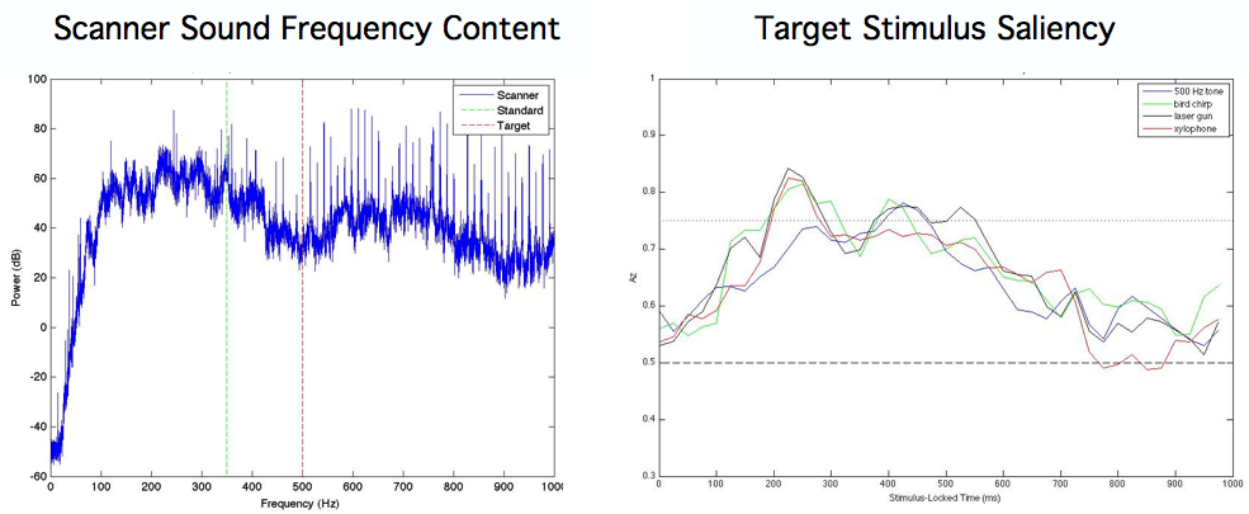

Figure 3.1: Overcoming the challenges of increased acoustic noise in the higher 3T field scanner. Left: The 3T scanner sound frequency spectrum, and the positions of the pure tone stimuli used in the previous experiment at 1.5T. Standard tone was shifted to a trough, and a broadband target stimulus was selected. Right: EEG discrimination results, comparing broadband target sounds in the auditory oddball task. The laser gun sound was selected due to its high saliency relative to the background scanner noise, which we played as background noise during the stand-alone EEG tests.

methods that were employed in this study were described in Chapter 2.

3.3 Results

3.3.1 Transition of methods to higher field strength

As a first test of transition to the higher field 3T scanner, we repeated the auditory oddball EEG-fMRI experiment of Goldman et al. (2009) and extended the paradigm to include an analogous visual task (Chapter 4). Because the high dB acoustic noise produced by the 3T scanner can easily mask the auditory stimuli, we shifted our previously used standard tone to 390 Hz, to fall within a trough of the scanner sound frequency spectrum (Figure 3.1, left). The auditory oddball target stimulus was changed from a pure tone to a broadband sound, which increased the saliency of the target relative to the background scanner sounds (difference in salience between 1.5T and 3T). The broadband target tone was selected so that EEG single-trial classification classifier performance was maximized (Figure 3.1, right) and matched that of the visual paradigm in stand-alone EEG

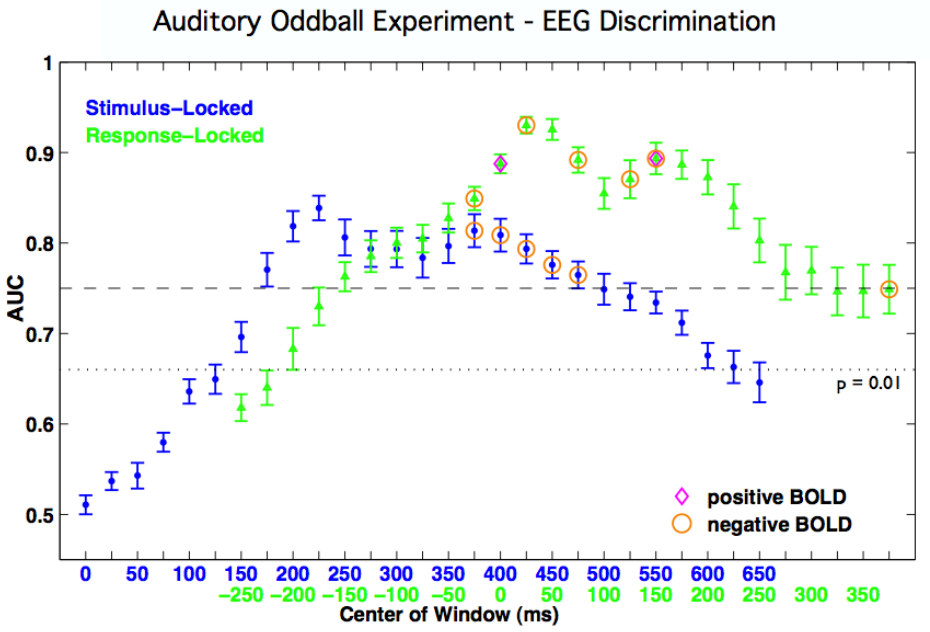

Figure 3.2: Auditory Oddball Experiment EEG Discrimination. Averages and standard errors of single-trial EEG discrimination performance across 17 subjects for the auditory oddball paradigm. Results of both the stimulus-locked (blue) and response-locked (green) analyses are shown, aligned by mean RT. Since we are interested in the BOLD correlates of single-trial EEG variability, we only consider EEG components with discrimination that is both significant (AUC > 0.66, $p < 0.01$) and substantial (AUC > 0.75). Windows resulting in significant positive and negative BOLD correlations are indicated with magenta diamonds and orange circles, respectively.

tests (i.e. EEG outside the scanner).

3.3.2 EEG discrimination

Despite the increased amplitude of magnetically-induced EEG artifacts, we were able to successfully remove gradient artifacts. Following artifact removal and standard EEG preprocessing offline, we utilized our binary logistic regression classifier with the sliding window technique (Parra et al., 2002, 2005) (refer to Section 2.4). For both stimulus-locked and response-locked epochs, we selected a training window of width 50 ms and varied the window onset in 25 ms increments. Area under the ROC curve (AUC) with leave-one-out (LOO) cross validation was used to assess classifier performance.

We were able to discriminate oddball vs. standard EEG trials at a higher AUC level than our prior results (Goldman et al., 2009) despite the decrease in EEG SNR. We also found a similar

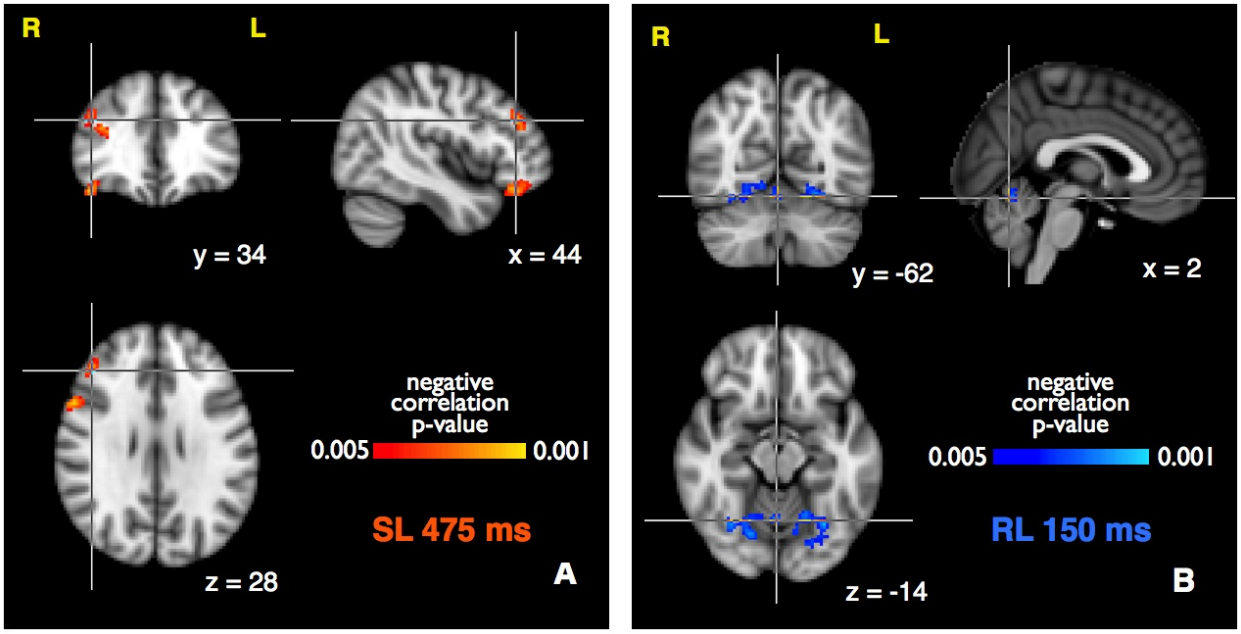

Figure 3.3: fMRI Correlates of EEG Variability in the Auditory Oddball Experiment. Significant (z-score $p < 0.005$, cluster $p < 0.01$) group mean negative BOLD correlations with EEG single-trial variability for the (A) stimulus-locked 475 ms window, and (B) response-locked 150 ms window, displayed in radiological coordinates on an MNI template brain (MNI coordinates are specified).

double-peaked temporal pattern of discrimination (Figure 3.2), which was consistent with the previous auditory paradigm results. Maximum 17-subject group mean performance of AUC = 0.84 was achieved at 225 ms. Response-locked classification, also similar to previous results (Goldman et al., 2009), yielded peaks at response time and shortly thereafter, with max AUC = 0.93 at 25 ms.

Traditional fMRI results were consistent with previous findings (Stevens et al., 2000), showing widespread activations throughout cortical and subcortical structures. In the EEG-based analysis, we found significant positive and negative BOLD correlations in multiple windows for both tasks (denoted with magenta diamonds and orange circles on Figure 3.2). We compared our results at 3T to the previous results at 1.5T.

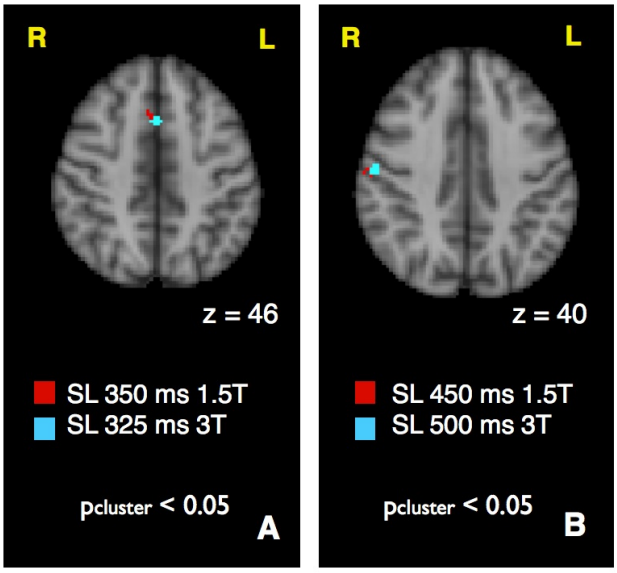

Figure 3.4: fMRI Results at 1.5T vs. 3T. Superposition of previous 1.5T results (red) and current 3T results (blue) for similar EEG windows. Negative activations thresholded at $p < 0.005$ are shown, for clusters in (A) paracingulate and (B) postcentral gyrus, displayed in radiological coordinates on an MNI template brain. Note that clusters are displayed as binary masks (i.e. containing no statistical information within each cluster).

3.3.3 BOLD fMRI correlates of EEG STV consistent with previous auditory task results

Our analysis at 3T revealed activations undetectable at 1.5T, including frontal regions for the 475 ms stimulus-locked window (Figure 3.3), and increased the strength and size of previously found clusters (Figure 3.4). Most notably, we found bilateral occipital negative correlations for the response-locked 150 ms window (Figure 3.3). This is consistent with our previous result (not shown) that found right occipital negative correlations in the same window. Our right occipital cluster exceeded our previous result in both voxel size (260) and max z-score (3.18) but did not spatially overlap with it. However, this repeated finding that visual areas are negatively correlated with endogenous auditory attention further supports our hypothesis of inter-modal latent attentional modulation (Goldman et al., 2009).

3.4 Conclusion

In this chapter we demonstrated the feasibility of our previous EEG-fMRI STV analysis methods in the more challenging environment of the higher-field 3T scanner. We were able to discriminate the EEG with greater accuracy than our previous results, despite the decreased SNR of the EEG signal. The increased fMRI SNR improved BOLD correlations, resulting in larger clusters with higher peak z-scores.

Chapter 4

A Temporal Cascade of Task Related and Default Mode Activations During a Simple Target Detection Task

4.1 Introduction

Internal attentional brain states are challenging to study because their fluctuations are not always event related and can dynamically ebb and flow at multiple timescales. Traditional blood oxygen level dependent (BOLD) functional magnetic resonance imaging (fMRI) enables observation of the average response evoked by stimuli and/or behavioral response. However, task engagement inevitably fluctuates on a single-trial basis throughout the run of an experiment. Even simple target-detection perceptual decisions involve a complex cascade of neural processes including stimulus detection, target recognition/rejection, motor planning, and behavioral response, all of which are associated with evoked responses that vary on a single-trial basis (Philiastides et al., 2006). Many of these processes are time locked to stimulus onset, but others are more closely locked to the behavioral response (Gerson et al., 2005).

The high temporal resolution of scalp EEG allows observation of dynamic neural processes, but activity in deep subcortical structures is difficult to detect. Furthermore, source localization is essentially an ill-posed problem, with skull and cerebral spinal fluid (CSF) impedance resulting

in poor spatial resolution. On the other hand, BOLD fMRI can localize both superficial and deep sources of activity with mm-scale resolution, but its temporal resolution is limited due to the slow nature of the BOLD response and the low sampling rate required for acquisition of whole-brain fMRI data.

Perhaps the most well-studied evoked response to a task-related sensory stimuli is the P3 (also called P300), which peaks at approximately 450 ms post-stimulus (Key et al., 2005; Linden, 2005; Polich, 2007). The P3, which is typically measured via electroencephalography (EEG), is known to have amplitude that is modulated by the endogenous state of the subject (Key et al., 2005; Polich, 2007). Extensive evidence from intracranial, lesion, and EEG-fMRI studies shows this response to be generated by a widespread network that includes frontal and temporal-parietal areas (Linden, 2005; Polich, 2007). Frontal activity has been associated with the earlier novelty-related P3a subcomponent, and temporal-parietal activity with the later task-related P3b subcomponent, consistent with their EEG scalp topographies (Polich, 2007).

Endogenous brain states that have been linked to inattention to sensory stimuli are often referred to as "resting states." Both functional connectivity analysis and independent component analysis (ICA) of fMRI data have identified many consistent resting-state networks (De Luca et al., 2006; Fox & Raichle, 2007). These networks are characterized by "infra-slow" fluctuations on the order of 0.01–0.1 Hz (Palva & Palva, 2012) and can be observed by recording fMRI on undirected subjects while they lie in the scanner doing no specific task. The most extensively studied of these is the default-mode network (DMN), a co-activation of the posterior cingulate cortex, medial prefrontal cortex, and angular gyri that was originally defined to represent a baseline brain state (Raichle et al., 2001). It is commonly associated with self-monitoring, auto-biographical, and social functions, reflecting attention to the internal world (Bressler & Menon, 2010). However, recent work has uncovered evidence for a more active role of the DMN related to task performance (Eichele et al., 2008), including its deactivation by cognitive load during task engagement (Esposito et al., 2006).

In this project we use simultaneously-recorded EEG and fMRI during a simple visual oddball task. We investigate the relationship between neural correlates of processing task-relevant sensory stimuli and brain states reflective of inattention to the task and sensory input. We use the single-trial analysis methodology of Goldman et al. (2009), whereby machine learning methods are used to find a maximally discriminative projection of the EEG data, and the single-trial variability of

that projection is used to construct the BOLD fMRI univariate model. Previous studies of the BOLD correlates of single-trial event-related EEG variability have focused mainly on the P3 and only a few other well-known components at selected stimulus-locked latencies, and have often used an arbitrary selection of electrodes (Benar et al., 2007; Warbrick et al., 2009), and many have studied this coupling without regressing out the effect of the externally-observable reaction time variability. Eichele et al. (2005) were one of the first to investigate the spatio-temporal evolution for BOLD correlates of event-related potential (ERP) components spanning the entire trial. Their approach, applied to an auditory oddball paradigm, used ICA to de-noise the EEG from which they then selected a specific subset of electrodes to construct single-trial variability regressors for well defined ERPs (e.g. P2, N2 and P3).

Instead of a priori defining ERP components of interest, we use a purely data-driven approach to identify temporally specific, maximally discriminative task-relevant projections of the EEG data. Specifically, our multivariate discrimination improves identification of task-relevant components in low signal-to-noise ratio environments, such as EEG recorded during MRI acquisition. It also enables us to study the BOLD correlates of continuously-evolving components linked to the task (i.e. defined by trial labels). Since we analyze the BOLD signal by first regressing out the variance linked to observed stimulus and behavioral events (Feige et al., 2005; Goldman et al., 2009), these methods also allow us to investigate the BOLD correlates of modulations in task engagement that are undetectable with traditional methods, and dissociate them from observable behavioral variability. Furthermore, we investigate the correlates of these modulations only for target trials (i.e. identical stimuli), thus ensuring that the trial-to-trial variation in neural processes is reflecting a latent state. Despite making no prior assumptions about functional connectivity between brain regions and without aiming to study functional networks, we find that for this simple target detection task, regions associated with task-dependent and default-mode networks transiently correlate with the trial-to-trial variability of the EEG discriminating components, and they do so on a millisecond timescale with a distinct temporal ordering.

4.2 Methods

Seventeen subjects (6 female, mean 27.7 years, range 20–40) participated in three runs of the traditional visual oddball paradigm described in Section 2.1. Each run consisted of 100 standard stimuli and 25 oddball stimuli. All of the EEG-fMRI data acquisition, preprocessing, and analysis methods that were employed in this study were described in Chapter 2.

4.2.1 fMRI Analysis for Localizing the DMN

Because our single-trial findings included correlates consistent with DMN, we performed ICA on the functional image data to locate the DMN, which is an established method used to study resting-state functional networks not associated with any task (De Luca et al., 2006; Fox & Raichle, 2007). To prevent investigator bias, we used a template-matching algorithm to automatically determine the DMN component for each subject (template obtained from the Neurosynth database of Yarkoni et al. (2011)), and we found the group mean DMN component in MNI space. Manual DMN component selection was consistent with our algorithm output.

4.3 Results

All subjects responded with high accuracy and speed. $98.4\% \pm 3.1\%$ of targets were correctly detected, with 397.2 ± 38.9 ms RT.

4.3.1 EEG Analyses

Traditional stimulus-locked event-related potentials (ERPs) displayed a strong visual P2 peak over frontal and posterior sites and a prominent P3 over central sites (Figure 4.1, left), consistent with previous literature (Hopfinger & West, 2006; Makeig et al., 1999). N1 and N2 responses were also visible. The response-locked ERPs showed a double peak that was most pronounced at central and posterior sites (Figure 4.1, right), and which was highly replicable across subjects. This matches the post-motor theta-band synchronization described by Makeig et al. (2004).

We were able to discriminate target vs. standard EEG trials with highly significant accuracy (Figure 4.1). We surpassed the corrected $p = 0.01$ value (AUC = 0.66) for all consecutive stimulus-locked training windows from l50 to 750 ms and for all analyzed response-locked windows centered

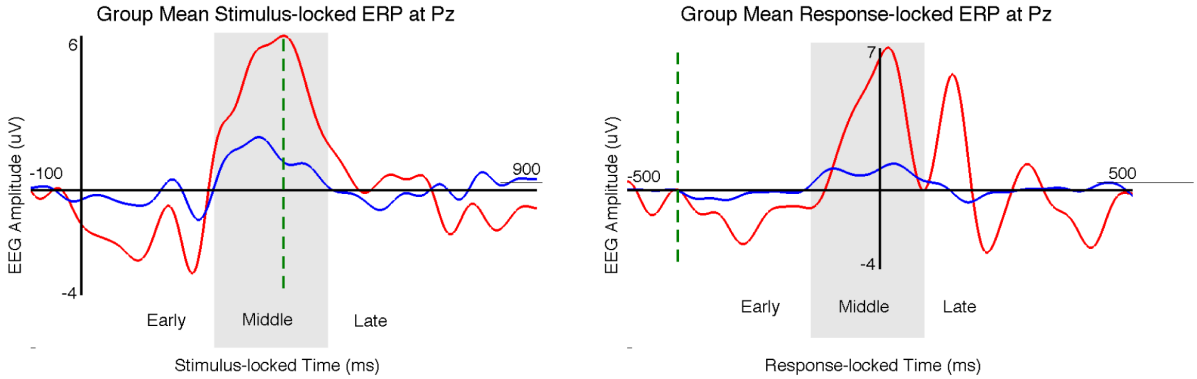

Figure 4.1: Stimulus-locked (left) and response-locked (right) ERPs recorded at the Pz electrode for targets (red) and standards (blue). Mean RT and mean stimulus time are denoted with green dashed lines. Our definition of early, middle, and late window ranges (see main text for discussion) are indicated with shading.

at –250 ms or later. Maximum discrimination of AUC = 0.86 ± 0.04 was reached at 325 ms for the stimulus-locked classification, with a broad temporal peak. Response-locked classification yielded even higher AUC values, with a double peak shortly after reaction time. A maximum AUC of 0.93 ± 0.04 was reached at 25 ms following RT, and 0.91 ± 0.07 AUC was reached at 150 ms. The window ranges exceeding 0.75 mean AUC (and thus subsequently included in the EEG-based fMRI analysis) were 175 to 600 ms for stimulus-locked and –175 to 375 ms for response-locked discrimination.

Discriminator output was significantly ($p < 0.01$) negatively correlated with RT for multiple stimulus- and response-locked windows. This result demonstrated the need to orthogonalize our STV fMRI regressors to RT-variability regressors, being that our aim was to study residual variance not observable with behavioral response.

The grand mean forward models displayed an early frontal positivity that was strongest at the 250 ms stimulus-locked window. They also revealed a central negativity around 325 ms, which occurred prior to behavioral responses and corresponded to the middle of the broad stimulus-locked discrimination peak. A posterior positivity first appeared near the RT and slowly became more centrally distributed, reaching its highest strength late in the trial. The progression of these discriminating components was consistent with the visual target detection results of Gerson et al. (2005). We show EEG topographies alongside their corresponding BOLD activations in Figures 4.5, 4.6, and 4.7.

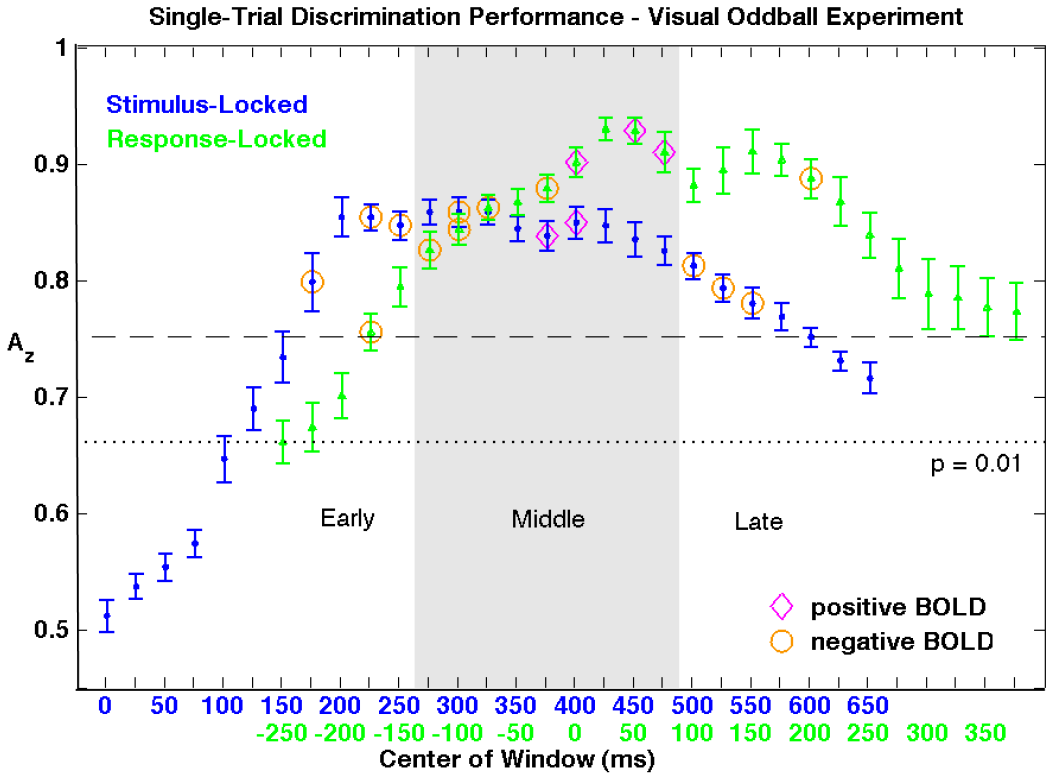

Figure 4.2: Group mean averages and standard errors of single-trial EEG discrimination performance. Results of both the stimulus-locked (blue) and response-locked (green) analyses are shown, aligned by mean RT. Since we are interested in the BOLD correlates of single-trial EEG variability, we only consider EEG components with discrimination that is both significant (AUC > 0.66, $p > 0.01$) and substantial (AUC > 0.75). Windows resulting in significant positive and negative BOLD correlations are indicated with magenta diamonds and orange circles, respectively. Early, middle, and late windows (as grouped for discussion) are indicated with shading.

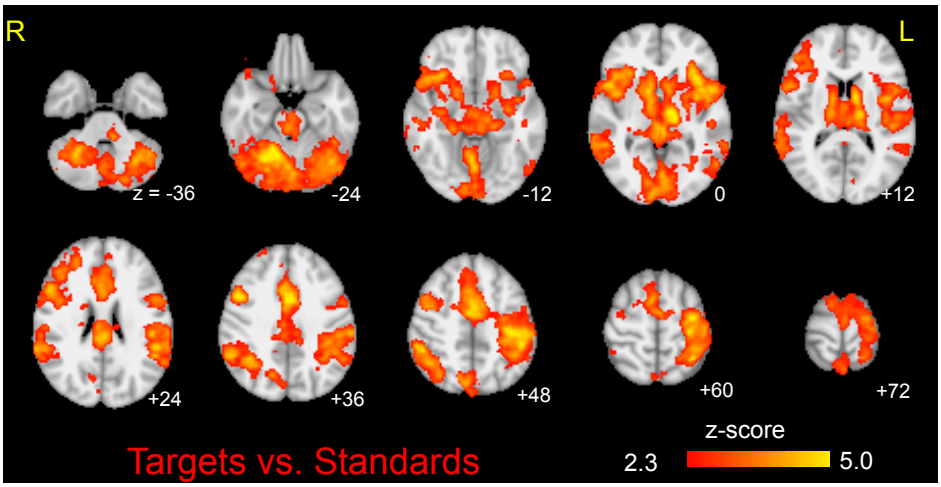

Figure 4.3: Traditional event-related average BOLD response target vs. standard contrast. Group-level positive activations thresholded at $z > 2.3$, cluster corrected at $p < 0.05$. Images are displayed in radiological coordinates.

4.3.2 Traditional fMRI Analysis

Event-related BOLD responses to target stimuli were present in multiple brain areas, including bilateral supramarginal gyri, insular cortices, cingulate cortices, angular gyri, precentral gyri, thalamus, cerebellum, and brainstem. Postcentral activations were strong and left-lateralized, consistent with right-handed button press. These activations matched previous visual oddball paradigm results (Laurens et al., 2005; Stevens et al., 2000; Warbrick et al., 2009), and were even stronger and more widespread in the traditional event-related target vs. standard contrast (Figure 4.3). This contrast additionally resulted in right-lateralized clusters in precuneus and middle frontal gyrus. RT-variability statistical maps (Figure 4.4) showed activations in anterior cingulate cortex (ACC), supplementary motor area, and right precentral gyrus.

4.3.3 Single-trial EEG Variability fMRI Analysis

Our randomization method, which we used to correct for multiple comparisons, determined a $p = 0.01$ threshold which corresponded to a 60-voxel cluster size (24 voxels for $p = 0.05$). At the $p = 0.01$ threshold, the EEG-derived regressors resulted in significant group-level positive and negative correlations for multiple stimulus-locked and response-locked EEG training windows, indicated with diamonds and circles on Figure 4.2. Interestingly, all significant clusters correlating

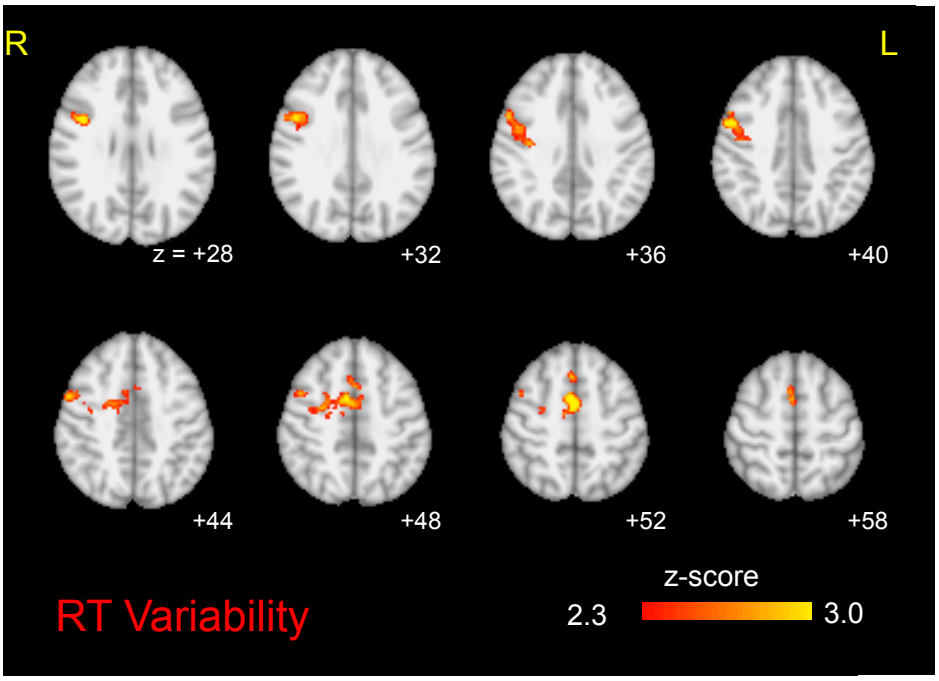

Figure 4.4: fMRI BOLD correlates of reaction time variability. Group-level positive activations thresholded at $z > 2.3$, cluster corrected at $p < 0.05$. Images are displayed in radiological coordinates.

with single-trial variability in windows prior to the RT were negatively correlated with classifier output. Near the mean RT, we saw a reversal to positive correlations, and this effect lasted approximately 100 ms, after which all significant clusters were negative.

Since our analysis separately identifies EEG discriminating components at different time windows relative to the stimuli and responses, we are able to study the temporal cascade of neural involvement related to modulations of internal attentional states. For simplification and clarity in the following discussion, we divided our results into three stages (indicated in Table 4.1 and Figures 4.1 and 4.2): early (prior to behavioral response), middle (at or near RT), and late (after the response while the subject is waiting for the subsequent stimulus). We based these temporal ranges on timing of ERP components at the Pz electrode (Figure 4.1) such that the early stage corresponds to the P2 and N2, the middle stage corresponds to the P3, and our late windows are those that occur after the P3.

Table 4.1 contains a complete list of activations exceeding multiple-comparison-corrected $p = 0.01$ with their corresponding EEG windows.

The early stimulus-locked EEG discriminating components revealed negatively-correlated acti-

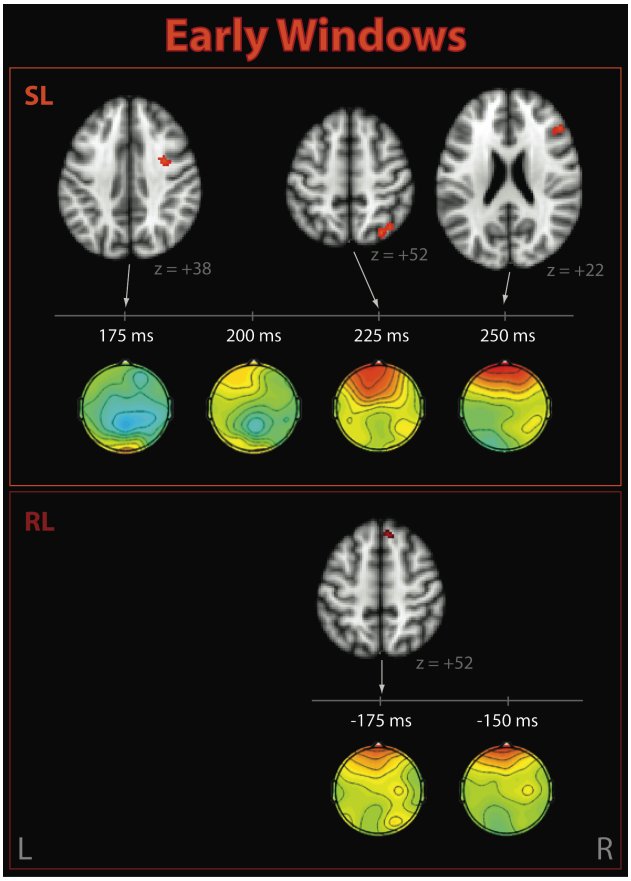

Figure 4.5: Significant clusters correlating with EEG single-trial variability early in the trial. Shown for stimulus-locked (SL, top) and response-locked (RL, bottom) windows. Corresponding EEG discriminant component scalp projections (forward models) are also shown, where color represents correlation between the discriminating component and the data (red = positive, blue = negative, green = 0). Note that images are displayed in neurological coordinates.

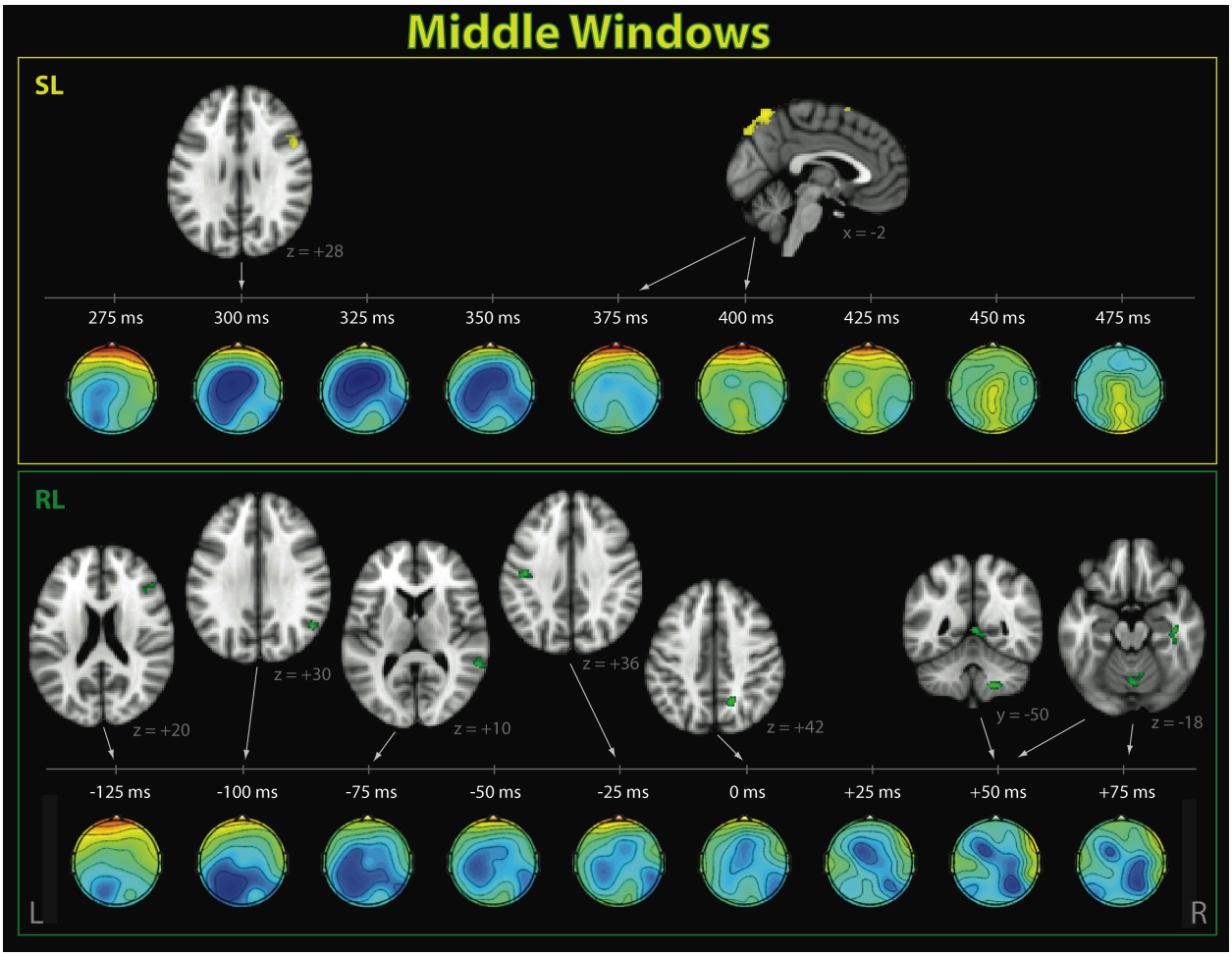

Figure 4.6: Significant clusters correlating with EEG single-trial variability in middle windows. These activations occurred near the behavioral response time and in the range of the P3, shown for stimulus-locked (SL, top) and response-locked (RL, bottom) windows. Corresponding EEG discriminant component scalp projections (forward models) are also shown, where color represents correlation between the discriminating component and the data (red = positive, blue = negative, green = 0). Note that images are displayed in neurological coordinates.

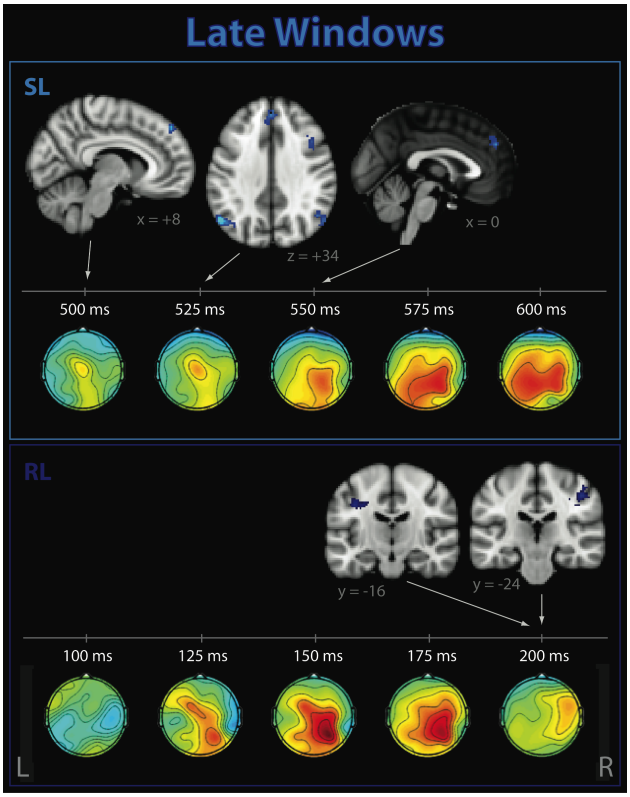

Figure 4.7: Significant clusters correlating with EEG single-trial variability late in the trial. These activations occurred after the subject has made his/her response, for stimulus-locked (SL, top) and response-locked (RL, bottom) windows. Corresponding EEG discriminant component scalp projections (forward models) are also shown, where color represents correlation between the discriminating component and the data (red = positive, blue = negative, green = 0). Note that images are displayed in neurological coordinates.

STIMULUS-LOCKED										
window	AUC	+/-	Nvox	max z	$p_{cluster}$	MNIx	MNIy	MNIz	hem	region
175ms	0.80	neg	66	3.29	0.0094	32	0	38	R	precentral gyrus, white matter
225ms	0.85	neg	69	3.44	0.0083	30	-70	52	R	superior lateral occipital cortex
250ms	0.85	neg	82	3.25	0.0062	48	32	22	R	middle frontal gyrus, dorsolateral prefrontal cortex
300ms	0.86	neg	89	3.28	0.0052	52	10	28	R	middle frontal gyrus, inferior frontal gyrus, precentral gyrus
375ms	0.84	pos	192	3.65	0.0008	0	-78	56	L/R	superior sagittal sinus, L precuneus
		pos	93	3.06	0.0047	-2	-48	2	L	posterior cingulate gyrus
		pos	74	3.02	0.0083	6	-24	14	L/R	white matter, ventricle
400ms	0.85	pos	340	3.70	0.0005	-2	-66	62	L/R	superior sagittal sinus
		pos	70	3.20	0.0086	-6	10	68	L	superior frontal gyrus
500ms	0.81	neg	63	3.33	0.0094	8	48	46	R	frontal pole, superior frontal gyrus
525ms	0.79	neg	293	3.59	0.0005	40	6	44	R	middle frontal gyrus
		neg	212	3.29	0.0005	2	46	40	L/R	superior frontal gyrus, paracingulate gyrus, R frontal pole
		neg	109	3.74	0.0029	-52	-66	34	L	superior lateral occipital cortex, angular gyrus
		neg	90	3.28	0.0047	56	-66	32	R	superior lateral occipital cortex, angular gyrus
550ms	0.78	neg	87	3.23	0.0057	0	48	32	L/R	superior frontal gyrus, paracingulate gyrus
RESPONSE-LOCKED										
window	AUC	+/-	Nvox	max z	$p_{cluster}$	MNIx	MNIy	MNIz	hem	region
-175ms	0.75	neg	83	3.34	0.0062	8	32	52	R	superior frontal gyrus
-125ms	0.82	neg	63	2.95	0.0104	40	26	26	R	middle frontal gyrus
-100ms	0.84	neg	65	3.33	0.0094	52	-60	30	R	superior lateral occipital cortex, angular gyrus
-75ms	0.86	neg	88	3.25	0.0052	60	-44	10	R	middle temporal gyrus, auditory cortex
-25ms	0.88	neg	86	3.32	0.0049	-42	-18	36	L	postcentral gyrus, precentral gyrus
0ms	0.90	pos	59	3.46	0.0099	16	-58	42	R	white matter, precuneus
50ms	0.93	pos	80	3.33	0.0070	2	-48	4	L/R	posterior cingulate gyrus
		pos	79	3.54	0.0060	20	-48	-48	R	cerebellum VIIIb
		pos	72	3.25	0.0078	40	-20	-18	R	temporal fusiform cortex
		pos	69	3.12	0.0091	4	-70	-18	L/R	cerebellar vermis
75ms	0.91	pos	82	3.39	0.0065	4	-70	-18	L/R	cerebellar vermis
200ms	0.89	neg	184	3.36	0.0010	46	-24	44	R	postcentral gyrus, white matter, hand sensorimotor
		neg	71	3.17	0.0083	-38	-16	36	L	precentral gyrus, white matter

Table 4.1: Significant clusters resulting from the stimulus-locked and response-locked EEG-based fMRI analyses. Dotted lines denote cutoffs between early, middle, and late windows, as per our discussion.

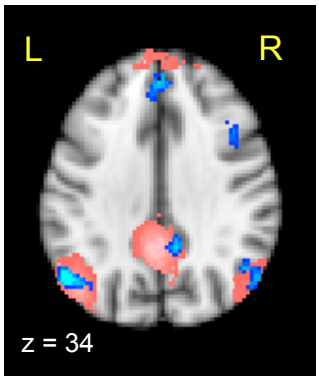

Figure 4.8: DMN determined independently with EEG single-trial variability and ICA. 525 ms stimulus-locked window EEG single-trial variability (STV) negative correlates in medial frontal gyrus, bilateral angular gyri, and posterior cingulate (in blue, with hue representing p-value in the range 0.005–0.001), overlaid with the mean default-mode network (DMN) as determined using ICA (pink). STV results shown are multiple-comparison corrected at $p < 0.05$. An additional cluster in right middle frontal gyrus can also be seen. Note that images are displayed in neurological coordinates.

vations in the precentral gyrus, superior lateral occipital cortex (LOC), and frontal regions including dorsolateral prefrontal cortex (DLPFC). Components close to the response time (but not locked to response) were correlated positively with superior frontal gyrus (SFG) and areas consistent with draining veins. The later stimulus-locked discriminating components showed additional negative correlations with regions in the left and right angular gyrus/LOC, the SFG/paracingulate gyrus, and the right middle frontal gyrus.

The response-locked EEG components revealed an early negative correlate in superior frontal gyrus, but most of the significant BOLD activations appeared in windows close to the RT. These included negative activations in LOC, middle temporal and frontal gyri, and precentral and postcentral gyri. We saw positive activations in cerebellum, posterior cingulate, and precuneus immediately following response time. Later response-locked components revealed additional negative activations in postcentral and precentral gyri. Supra-threshold negative and positive activations also appeared in white matter for our response-locked analysis.

The late stimulus-locked windows showed regions consistent with the default-mode network. Since the DMN is commonly detected using ICA, we confirmed the location of the subject mean DMN using ICA and template matching on the functional data. Our supra-threshold clusters in the medial frontal gyrus and angular gyri overlapped with this ICA-determined DMN, as did a

negative 58-voxel activation in the posterior cingulate that achieved a cluster p-value of 0.0125, with max z = 3.185 at MNI coordinates (10, –48, 34) (Figure 4.8).

4.4 Discussion

Based on the difference ERPs and the scalp distributions and timing of our EEG discriminating components, we believe we are tracking variation related primarily to the P2, N2, and P3 responses (Key et al., 2005), so we discuss our results partly in light of these. More specifically, our topographies are consistent with discrimination of the target-related P3b, frontal P3f, and post-motor potential (Pmp) subcomponents of the P3 (Makeig et al., 1999), as expected for our visual oddball task. Since amplitudes of these components are known to modulate with arousal and attention (Key et al., 2005; Luck et al., 2000; Nieuwenhuis et al., 2005), we use the classifier output (i.e. its decision certainty) to index the subjects' attentional state (i.e. task engagement) during each trial. Our EEG-based fMRI regressors are thus revealing the BOLD correlates of modulations in task engagement.

Electrophysiological activity and BOLD responses are coupled in a complex way that is not yet completely understood. There is evidence to suggest that the sign of the EEG-BOLD correlate is both a function of space and of frequency, and the sign of the BOLD response itself is affected by the excitation-inhibition balance within local neuronal circuits (Logothetis, 2008). It has been shown that low-frequency electrophysiological variations, such as those measured by scalp EEG in the 0–20 Hz range, are negatively correlated with the BOLD response (Goldman et al., 2002; Mukamel et al., 2005; Scheeringa et al., 2011a). Additionally, commonly-studied fMRI resting state networks have been shown to correlate with specific frequency bands in magneto-encephalography (MEG) studies (Brookes et al., 2011; de Pasquale et al., 2010) and show some (though lesser) frequency-dependency using EEG-fMRI (Mantini et al., 2007). Since there is still some question about the physiological meaning of directionality of electrophysiological BOLD correlates, the following sections do not attempt to interpret the sign of the correlation between the BOLD signal and the STV regressor.

4.4.1 Early EEG discriminating components reveal BOLD correlations in task-relevant brain areas

Early EEG windows resulted in right-lateralized activations in brain regions associated with task-relevant neural processes (Figure 4.5). These included frontal activations in DLPFC and posterior SFG, which are most commonly associated with working memory and higher-level cognitive processing during demanding tasks (Fuster, 2001; MacDonald et al., 2000), and the superior LOC. These areas have been linked to P3 modulations and are discussed further in Section 4.4.2, which focuses on components in that time range. To the best of our knowledge, BOLD correlates of variability in the early P2 and N2 ERP components have not been studied in the visual domain; however, Eichele et al. (2005) found correlates of auditory oddball N2 variability in both of these areas at similar latencies. Using a visual target detection task, Novitskiy et al. (2011) found these regions correlated with variability in the even earlier N1 component, but their activations were left-lateralized.

4.4.2 EEG discriminating components during the P3 and around reaction time reveal a period of transition from externally driven task-related to internally-driven processing

Our middle windows, which occurred close to the behavioral response and in the range of the P3, revealed a superposition of task-related and endogenous attention areas (Figure 4.6). Similar to the early windows, task-related BOLD correlations were found in right middle frontal gyrus and superior LOC. We also found an activation in right inferior frontal gyrus, an area associated with reorienting to salient behaviorally-relevant stimuli and is a main node in the right-hemisphere ventral attention network (VAN) (Corbetta et al., 2008; Corbetta & Shulman, 2002). Right-hemisphere frontal areas have been shown by a number of recent EEG-fMRI studies to modulate with P3 amplitude during visual (Bledowski et al., 2004a) and auditory (Eichele et al., 2005) tasks, and were reported for the latter case at a similar latency.

Our superior LOC correlate is an expected finding, given its common association with visual attention (Murray & Wojciulik, 2004). However, similar regions have also been shown to couple with EEG components in the P3 time range for auditory tasks. Benar et al. (2007) linked the parieto-occipital junction to P3 modulations during an auditory oddball task. In our previous study

that used an analogous auditory oddball paradigm and the same EEG discriminating component methods (Goldman et al., 2009), we also detected a correlate in the right LOC in the P3 range, but that cluster was located slightly inferior to our current finding. These collective findings suggest a supra-modal role for the LOC in attention.

An activation also appeared in right temporal fusiform cortex, an area commonly known to be involved in high-level visual processing. Bledowski et al. (2004b) also found that higher visual areas in inferior temporal gyrus contribute to the visual P3b, and their correlate appeared at similar latency. We also detected right-lateralized activations in auditory cortex. This co-activation of auditory and visual processing areas supports the presence of cross-modal attentional modulations, suggesting that modulations in auditory-directed attention (e.g. listening to scanner noise) affect attention to the visual modality.

As expected for EEG windows close to reaction time, we found BOLD correlates in several regions related to the button press. This included the motor areas of the left precentral and post-central gyri, which is consistent with a right-handed button press and has previously been associated with P3 coupling in visual (Bledowski et al., 2004a,b; Warbrick et al., 2009) and auditory (Benar et al., 2007) tasks. We also saw activations in the cerebellar vermis, which coordinates and monitors movement (Ghez & Fahn, 1985), and right cerebellum area VIIIb, which plays additional roles in motor control, coordination, and accurate timing of movements, and which has been particularly associated with right-handed finger tapping (Stoodley & Schmahmann, 2009; Stoodley et al., 2012).

The precuneus has been associated with a variety of task-relevant cognitive processes, including attentional orienting, visuo-spatial imagery, coordination of motor behavior, success monitoring, and self-referential thoughts (Cavanna & Trimble, 2006; Taylor et al., 2009). Eichele et al. (2005) found precuneus activations correlated with earlier P2 amplitude modulations, though their study used an auditory task. Our reaction-time precuneus activation supports the idea of a transition from the exogenous attentional state required for the visual perceptual decision to motor coordination required for the button press, followed by a reflection on task performance. Activations associated with other forms of internal thought, including posterior cingulate and SFG, were detected both in middle and late windows, and these are discussed in Section 4.4.3.

BOLD fMRI literature historically has reported activations mainly in gray matter, partially due to the common practice of masking white matter during statistical analyses, but growing evidence

supports the presence of white matter BOLD signals. This is particularly true when single-trial variability is modeled (Yarkoni et al., 2009). Here, our latent variability feature, the EEG single-trial discriminating component, revealed BOLD correlates in white matter regions. Since these activations were adjacent to sensorimotor regions, including right postcentral and precentral gyri and the left precentral gyrus, they are most closely related to the button press.

Reports of BOLD activations in draining veins are also rare in the literature, due to the high spatial resolution required to differentiate veins from cortical tissue. However, Biancardi et al. (2011), using a high-resolution study of visual areas at 7 T, found task-related negative BOLD correlates in large cerebral veins. We found a remarkable 340-voxel cluster that is adjacent to the precuneus but appears to track the superior sagittal sinus, a large cerebral vein that drains widespread areas of cortical tissue. The BOLD signal we detected in cerebral veins is likely due to a transient misbalance between metabolic demands and increased oxygenated blood, and may reflect strongly activated cortices that are functionally but not anatomically overlapping across subjects, but which drain into the same veins. Since the superior sagittal sinus is nearly exclusively responsible for draining the cerebrum (Mattle et al., 1990), this interpretation does not allow speculation regarding particular cortices. An alternative idea for the physiological meaning of this activation is that it reflects a global change in cerebral blood flow. Given the care we took with image registration, pulsation artifact investigation, and multiple comparison correction, and the congruency of our cortical results with the literature, we believe these to be true results that should not be ignored. However, these remain preliminary findings that we are currently validating in new datasets using diffusion tensor imaging and magnetic resonance venography.

4.4.3 Late EEG discriminating components reveal default mode activity between subject response and the next stimulus

BOLD correlates of EEG discriminating components late in the trial (Figure 4.7) appeared in a pattern matching the DMN (Figure 4.8), supporting MEG evidence for a transient nature of functional networks (de Pasquale et al., 2010). Given that we found an earlier activation in a region associated with the VAN, this supports the hypothesis for complementary roles of the DMN and VAN in directed awareness (Boly et al., 2007; Vanhaudenhuyse et al., 2011), and supports the intracranial EEG finding that transient stimulus-related activations in VAN areas occur earlier

than those in DMN (Ossandn et al., 2011).

Our finding is in agreement with a number of recent fMRI and combined EEG-fMRI studies that suggest that the DMN plays an active role in task-related processing. Spontaneous DMN fluctuations have been shown to affect visual task performance (Eichele et al., 2008) and during rest have inversely correlated with the frontal theta rhythm (Scheeringa et al., 2008), which is typically associated with cognitive processing. There is also evidence of transient event-related suppression of DMN regions related to increased cognitive load during a visual N-back task (Esposito et al., 2006, 2009) and during motion discrimination (Singh & Fawcett, 2008) and auditory oddball tasks (Eichele et al., 2005), though in the latter case corresponding to an earlier component. This converging evidence supports the idea that DMN regions modulate selective attention for optimal allocation of attentional resources.

Because our correlate appears after the response, our finding suggests an active role for the DMN in introspective task-relevant processing, such as an active observation of the behavioral response. Such retrospection is not necessarily overtly conscious so it is challenging to investigate experimentally (Schooler, 2011). We do not believe this post-response DMN correlate is reflecting an anticipatory state while subjects await the next stimulus since ERPs (derived from EEG data that were not high-pass filtered) revealed no effect of contingent negative variation (CNV), a slow ERP component with magnitude dependent upon level of expectation of the following stimulus (Palva & Palva, 2012; Scheibe et al., 2010) (data not shown). Previously reported BOLD correlates of CNV did not include the canonical DMN (Scheibe et al., 2010); combined with our result, this loosely suggests that suppression of DMN is not related to increased anticipation. Further evidence for an introspective state late in the trial is an activation in the paracingulate, which has associations with self awareness and theory of mind, and particularly introspection-related activity during visual tasks (Goldberg et al., 2006).

Our bilateral angular gyri clusters, which are subregions of the intra-parietal lobules (IPLs), are consistent with many reports of IPL in P3 coupling (Linden, 2005). Similar to our late (525–550 ms relative to stimulus) activations, Bledowski et al. (2004a,b) found bilateral IPL correlated with EEG amplitude variability, reported around 540 ms (in 2004b). Our stimulus-locked correlates appear later than the peak amplitude of the P3, which suggests that the IPL is more closely linked to P3 latency variability than amplitude variability. This is consistent with findings that activity

in parietal areas correlates with P3 latency but not with amplitude (Warbrick et al., 2009).

4.4.4 BOLD coupling with the EEG response is captured by reaction-time variability for a subset of brain regions

Our results differ from converging evidence of the literature in that we did not find any EEG variability correlates in the ACC. This region is thought to be involved in both top-down and bottom-up attentional control related to sensory processing (Crottaz-Herbette & Menon, 2006) and has been linked to early EEG component modulations. The N1 has been shown to correlate with ACC activity during auditory discrimination tasks using EEG-fMRI (Mulert et al., 2008) and fMRI-constrained EEG source localization (Esposito et al., 2009). The latter technique was applied to both visual and auditory oddball data to find correlates in the early N2b and P3a components (Crottaz-Herbette & Menon, 2006). However, we did find ACC correlates of RT variability, which was not regressed out of the single-trial-variability models in these previous investigations. This finding is in accordance with Warbrick et al. (2009), who used a visual target-detection task to discover similar ACC correlates for both RT variability and P3 latency variability, but did not tease these effects apart. We demonstrate that attention-related ACC coupling with EEG components is reflected in the variability of externally-observable behavioral response events.

Our EEG variability results also differ from the many EEG-fMRI reports of P3-variability correlates in the insula (Bledowski et al., 2004a,b; Eichele et al., 2005; Warbrick et al., 2009). However, we did find bilateral insula correlates of the average event-related response, and additional RT-variability correlates (max z-score 3.78 in right insula and 3.38 in left insula) that were slightly too small to pass cluster threshold. Using a visual target-detection task, Warbrick et al. (2009) also found bilateral insula correlates with a traditional analysis, and conversely with P3 amplitude variability but not RT variability. Together with their findings, our results suggest that variance of the BOLD signal within the insula can be explained primarily via the average event-related response, with only minor contributions observable in EEG-component and RT variability.

4.4.5 Our methods begin to unravel a cascade of neural events associated with endogenous attentional modulations

Precise temporal localizations are difficult in traditional fMRI studies due to the slow, diffuse, and indirect nature of the BOLD measurement and to spatial variations in the HRF. Our method of combining single-trial EEG variability with fMRI was able to circumvent this limitation by finding BOLD correlates of the electrophysiological response at multiple temporal offsets. Because we used EEG STV in our fMRI model design and orthogonalized to event-related regressors, our activations reveal the BOLD correlates of endogenous modulations in attention across trials. This method begins to unravel a complex cascade of neural events, including sensory processing, executive processing, motor planning, and default-mode activity, in high spatial and temporal resolution.

Due to the simplicity of the task, the subjects' minds were free to wander, and this enabled observation of natural fluctuations in task engagement and the underlying spatial redistribution of attentional resources throughout the duration of each trial. Specifically, our results revealed task-relevant and primarily right-lateralized frontal areas engaged immediately following the stimuli, and default-mode-region activations following the behavioral response. These findings are consistent with the role Polich (2007) proposed for the P3 in rapid inhibition of ongoing neural processes to facilitate the transfer of stimulus information from frontal to temporal-parietal areas. They also provide evidence for a role of the default mode network in task-related processing. Furthermore, our findings demonstrate the utility of our methods for non-invasively investigating the temporal ordering of many widely distributed BOLD activations. We believe these techniques will be important in future investigations of brain function, as the information they provide is complementary to that which can be obtained from intracranial-EEG, MEG, and resting state studies.

4.5 Summary

Focused attention continuously and inevitably fluctuates, and to completely understand the mechanisms responsible for these modulations it is necessary to localize the brain regions involved. During a simple visual oddball task, neural responses measured by EEG modulate primarily with attention, but source localization of the correlates is a challenge. In this study we used single-trial analysis of simultaneously-acquired scalp EEG and fMRI data to investigate the BOLD correlates of modula-

tions in task-related attention, and we unraveled the temporal cascade of these transient activations. We hypothesized that activity in brain regions associated with various task-related cognitive processes modulates with attention, and that their involvements occur transiently in a specific order. We analyzed the fMRI BOLD signal by first regressing out the variance linked to observed stimulus and behavioral events. We then correlated the residual variance with the trial-to-trial variation of EEG discriminating components for identical stimuli, estimated at a sequence of times during a trial. Post-stimulus and early in the trial, we found activations in right-lateralized frontal regions and lateral occipital cortex, areas that are often linked to task-dependent processes, such as attentional orienting, and decision certainty. After the behavioral response we saw correlates in areas often associated with the default-mode network and introspective processing, including precuneus, angular gyri, and posterior cingulate cortex. Our results demonstrate that during simple tasks both task-dependent and default-mode networks are transiently engaged, with a distinct temporal ordering and millisecond timescale.

Chapter 5

Temporal Evolution of Coupling Between Supramodal Cortical Attention Networks and the Brainstem

Cortical and subcortical networks have been identified that are commonly associated with attention and task engagement, along with theories regarding their functional interaction. However, a link between these systems has not yet been demonstrated in healthy humans, primarily due to data acquisition and analysis limitations. We record simultaneous EEG-fMRI while subjects perform auditory and visual oddball tasks, and we investigate the BOLD correlates of single-trial EEG variability at latencies spanning the trial. We focus on variability along task-relevant dimensions in the EEG for identical stimuli, and then we combine auditory and visual data at the subject level to spatially and temporally localize brain regions involved in endogenous attentional modulations. Specifically, we find that anterior cingulate cortex (ACC) correlates strongly with both early and late EEG components, whereas brainstem, right middle frontal gyrus (MFG), and right orbito-frontal cortex (OFC) correlate significantly only with late components. By orthogonalizing with respect to event-related activity, we find that variability in insula and temporo-parietal junction is reflected in reaction time variability, OFC and brainstem correlate with residual EEG variability,

and ACC and MFG are significantly correlated with both. To investigate interactions between these correlates of temporally-specific EEG variability, we performed dynamic causal modeling (DCM) on the fMRI data. We found strong evidence for reciprocal effective connections between the brainstem and cortical regions. Our results support current theories of dynamic interaction between attention systems, using noninvasive methods to study the healthy human brain. In particular, our results support the adaptive gain theory of locus-coeruleus-norepinephrine (LC-NE) function and the proposed functional relationship between the LC-NE system, right-hemisphere ventral attention network, and P300 EEG response.

5.1 Introduction

Neural and behavioral responses to external sensory input vary, even for identical stimuli and environmental conditions. Much of this variability is attributable to natural fluctuations in internal attentional state. Simple tasks requiring minimal working memory and executive processing allow for greater fluctuations to occur but endogenous modulations of attention occur regardless of the task difficulty. Some of this internal variation is reflected in behavioral response time (RT), but residual variability remains that cannot be explained by externally observable events. Thus, purely event-related analyses that focus on mean responses to a set of identical stimuli are unable to fully explain the natural waxing and waning of attention.

Evoked responses to sensory stimuli have been studied extensively using electroencephalography (EEG). This event-related potential (ERP) amplitude modulates with a number of exogenous and endogenous factors, and different components are associated with particular tasks and stimulus types (Key et al., 2005). One well-known ERP component, the P300, presents as a positive deflection over central electrodes, begins around 300 ms and peaks at approximately 450 ms after stimulus onset (Donchin & Coles, 1988; Hopfinger & West, 2006; Makeig et al., 1999; Picton, 1992). It appears for both auditory and visual target stimuli, and its amplitude is known to modulate with attention to the task (Luck et al., 2000; Nieuwenhuis et al., 2005; Polich, 2007)). Despite extensive study, the mechanism of P300 generation is still not completely understood, though invasive animal studies suggest it is deep-rooted in the brainstem, involving the locus coeruleus (LC), a tiny nucleus of cells that projects widely and has been found to play a role in target detection, focused

attention, and behavioral responses to sensory stimuli (Aston-Jones & Cohen, 2005; Nieuwenhuis et al., 2005; Sara & Bouret, 2012). Based on results of EEG-fMRI studies using separate auditory and visual tasks (Benar et al., 2007; Eichele et al., 2008, 2005), the P300 has also been shown to couple with activity in cortical regions, including anterior cingulate cortex (ACC), insula, and the right-lateralized frontal and temporo-parietal regions of the ventral attention network (VAN). The common brain regions found using independent auditory and visual studies suggest their modulatory roles are supra-modal. However, to the best of our knowledge such commonalities across sensory input modalities have not been investigated directly. A strong functional link has been proposed between the locus coeruleus-norepinephrine (LC-NE) system, the P300 response, and the VAN (Corbetta et al., 2008), but this hypothesis requires validation in healthy humans.

Dynamic Causal Modeling (DCM) of fMRI data is a useful approach to investigate directed connectivity between brain regions of interest (ROIs) (Friston et al., 2003; Stephan et al., 2010), since it aims to provide neuro-biologically interpretable estimates of effective connectivity between neural populations. ROIs and presence of connections between them are specified based on prior knowledge of brain structure and function. The generative models specify propagation of neural state changes induced by experimental perturbations (both in space and time). Mapping from neural activity to observable fMRI BOLD activity is estimated independently for each ROI, accounting for spatial variability of the hemodynamic response (Stephan et al., 2010). DCM is classically performed on stand-alone fMRI data, but Nguyen et al. (2013) recently demonstrated the value of incorporating EEG-derived information into DCMs of simultaneously-acquired fMRI data. EEG-fMRI data fusion using DCMs remains a promising new research area (Smith, 2012).

In this study, we utilize simultaneous EEG-fMRI to investigate non-invasively in healthy humans the BOLD correlates of natural fluctuations of attention that generalize across auditory and visual sensory domains. We use mundane auditory and visual target detection tasks, which leave the subjects' minds free to wander, and apply well-established EEG machine learning methods to estimate linear classifiers that maximally discriminate target from standard stimuli. We then use the classifier output to index attention to the task on a single-trial basis, and correlate these values with the fMRI BOLD data via the general linear model (GLM). We use the results as priors in a DCM analysis that investigates interactions between these attention-related brain regions. Our findings provide evidence for the role of the LC-NE system in supra-modal attention-related

modulation of evoked EEG responses, and support the hypothesized functional link between the LC-NE system, P300, and VAN.

5.2 Methods

Our seventeen subjects (6 female, mean 27.7 years, range 20–40) participated in three runs each of the analogous visual and auditory oddball paradigms (see Section 2.1). The auditory and visual runs were interleaved, beginning with the visual experiment for approximately half of the subjects and the auditory experiment for the other half. There were 375 (125 per run) total stimuli per task.

We used the same EEG-fMRI single-trial variability methods as in Chapters 3 and 4, and these methods are described throughout Chapter 2. However, the purpose of the study here was to investigate commonalities across the auditory and visual sensory input modalities. This required combining the auditory and visual data.

5.2.1 Traditional fMRI Analyses

We combined individual runs of the experiment at the subject level in three ways: including only auditory runs (Chapter 3), including only visual runs (Chapter 4), and including all six auditory and visual runs together. Each of these three analyses was carried through to the group level. Statistical image results for the traditional analyses were thresholded at $z>2.3$, and clusters were multiple-comparison-corrected at $p<0.05$ (Worsley, 2001). Because it is possible for significant correlations to be driven much more strongly by a subset of the data (in this case by one task), we used the subject-level auditory-only and visual-only results to compute paired t-tests and thus identify any brain regions with BOLD correlates that differed significantly across auditory and visual runs. We discarded any voxels that achieved an uncorrected voxel-wise $p<0.01$ from the statistical maps of the combined analysis, to ensure that our reported findings are common to both auditory and visual tasks. Note that for its role as exclusion criteria, this is a conservative threshold.

Since pulsation artifacts in the ventricles have been attributed to false activations near the brainstem (Astafiev et al., 2010), we similarly excluded any voxels that were correlated with the BCG

pulsation artifact present in the EEG. These voxels were determined with a $p<0.01$ uncorrected threshold, after incorporating the pulse timing into a GLM and carrying through to group level. The pulse timing was obtained using a peak detection algorithm on the EEG signals at temporal electrodes (T7, T8, CP5, CP6), which are the sites most strongly affected by such artifacts.

5.2.2 EEG single-trial variability fMRI Analysis

As in the traditional analysis, we ran the EEG STV fMRI analysis separately three ways: only auditory runs, only visual runs, and with auditory and visual combined at the subject level. The latter method was of primary interest, as it was used to investigate BOLD correlates that generalize across both sensory modalities. As described for the traditional fMRI analysis (Section 2.5), we used the auditory-only and visual-only results to determine voxels with activation that significantly differed between the two tasks. These were then excluded from the statistical maps of the combined analysis, as were any voxels that correlated with BCG pulse timing. This ensured that our reported findings generalize across the auditory and visual domains.

Note that it was especially important to regress out the RT variability, since RT is known to be negatively correlated with attention and our aim was to study variability in task-related attention that cannot be detected using an external measure. This entire analysis was run independently for all EEG training windows exceeding a mean AUC value of 0.75 for both tasks. We continued to focus on within-class variability, using only the task-relevant (target) stimuli STV statistical maps in our results interpretation.

We used the following randomization method to generate a null distribution and correct for multiple comparisons. We ran the full STV fMRI analysis described above after permuting the $y_{\tau=450\text{ms}}$ values randomly within each class. 100 such permutations were done for each subject, from which we generated 10,000 group-level statistical maps via random samplings from the subject-level results. Stelzer et al. (2013) demonstrated the validity of this oversampling method. This null distribution was used to generate family-wise-error (FWE) corrected positive and negative activation p-value maps within the brainstem (one map for each of the EEG windows).

Cluster-size-thresholding is commonly used to correct for multiple comparisons in cortical regions, because true activations are assumed to be widespread and FWE-correction is often too strict for such a large number of voxels. To avoid an arbitrarily-selected cluster size threshold in

our cortical analysis, we applied threshold-free cluster enhancement (TFCE) to account for variable z-score magnitude within each cluster (Smith & Nichols, 2009). After also applying TFCE to all maps comprising the null distribution, we used FWE-correction within a grey matter mask. All corrected maps were thresholded at $p = 0.05$.

5.2.3 Dynamic Causal Modeling of fMRI Data

The EEG-based fMRI analysis described above provided timing information about the BOLD correlates of endogenous attentional modulations, but it did not allow inference of directed relationships between these regional activations. We investigated interactions between our temporally-specific EEG variability correlates by performing an effective connectivity fMRI analysis. In particular, we implemented single-state linear dynamic causal modeling (Friston et al., 2003; Stephan et al., 2010) using DCM10 in SPM8.

We used the results of our EEG-based fMRI analysis (Figure 5.5) to select five regions of interest (ROIs); these were chosen based on supra-threshold significance and particular interest in relation to previous studies of attentional networks.

- brainstem (BS)
- anterior cingulate cortex (ACC)
- right anterior cingulate cortex (rACC)
- right middle frontal gyrus (rMFG)
- right orbito-frontal cortex (rOFC)

The activations were spread across four different EEG time windows (i.e. correlated with variability in temporally-specific EEG discriminating components) and some differed in sign of correlation, so their time series were not necessarily intrinsically correlated. Each ROI was a sphere with 4 mm radius, centered on the peak voxel of the group-level EEG-based GLM results. Time series were extracted from individual subjects' preprocessed functional data in MNI space (down-sampled to $3 \times 3 \times 3$ mm for computational efficiency) by estimation of the first principle component within each ROI. Auditory and visual runs of the experiment were combined since the focus of our study was task-related attentional modulations common across sensory input modalities.

We designed twelve related models (Figure 5.7) to investigate intrinsic directed connectivity between the five ROIs, focusing on cortical projections to and from the brainstem. In models 1-9, we varied the direction of the ACC-brainstem connection (including one-way and bidirectional connections) and the stimulus input region (brainstem, ACC, or both). Directionality of the other connections was based on known structural projections in primates (Aston-Jones & Cohen, 2005), including a directed connection from the brainstem to rMFG and bidirectional connections between brainstem and rACC as well as brainstem and rOFC. Models 10-12 used timing information from the EEG-based analysis in specification of all the connections, only allowing connections to be directed forward in time. Input region was varied similarly to the other models.

We used fixed effects Bayesian model selection (BMS) to compare these 12 models both on a single-subject level and at the group level. BMS balances model fit and complexity, thereby selecting the most generalizable model. It estimates the relative model evidence and provides a distribution of posterior probabilities for all of the models considered. We used fixed effects because focused attention to a simple task involves basic physiological processes that are expected to be common to a healthy subject population (Stephan et al., 2009, 2010). We also compared families of similar models (Penny et al., 2010); the model space was divided into three families based on the direction of connectivity between the brainstem and ACC. Finally, we used Bayesian parameter averaging (BPA) to provide group-mean intrinsic connection strengths and their probabilities for the winning model.

5.3 Results

All subjects responded with high accuracy and speed. For the auditory task, $98.3\% \pm 2.0\%$ of targets were correctly detected, with 404.1 ± 58.3 ms RT. The visual targets were detected with $98.4\% \pm 3.1\%$ accuracy and 397.2 ± 38.9 ms RT.

5.3.1 EEG Analyses

Traditional ERPs following target stimuli displayed strong widespread P300 responses for both the auditory and visual tasks. These were most prominent and discriminative relative to the ERP response to standard stimuli at the Pz electrode site (Figure 5.1). N200 responses were also strongest

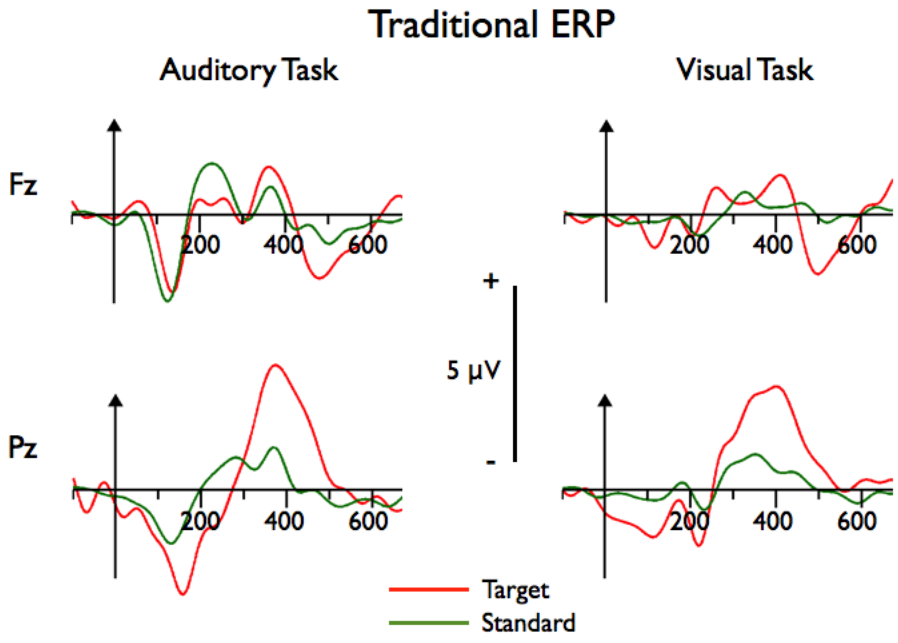

Figure 5.1: Traditional stimulus-locked ERPs. Target and standard EEG responses at the Fz (top) and Pz (bottom) electrode sites for both the auditory (left) and visual (right) oddball tasks. Time is in ms relative to stimulus onset.

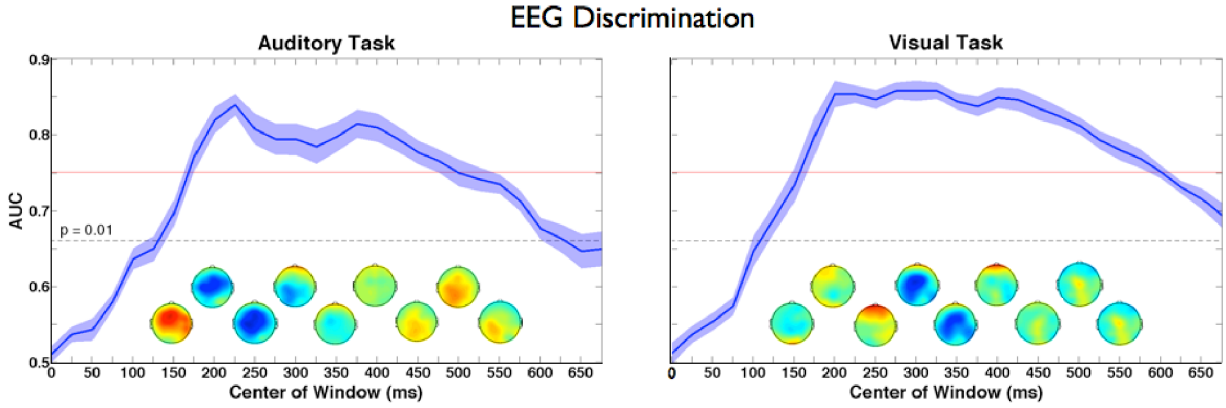

Figure 5.2: Single-trial EEG discrimination results. Group mean discriminator performance for the auditory (left) and visual (right) oddball tasks. Standard error is indicated with shading. Since we are interested in the BOLD correlates of single-trial EEG variability, we only consider EEG components with discrimination that is both significant (AUC > 0.66, $p < 0.01$) and substantial (AUC > 0.75, $p \ll 0.01$). Corresponding EEG discriminant component scalp projections (forward models) are shown for a subset of the windows with significant classifier performance, where color represents correlation between the discriminating component and the data (red = positive, blue = negative, green = 0).

and most discriminative at parietal sites for both tasks. The N100 and P200 components were largest at medial frontal electrodes for the auditory task. Both of these earlier ERP components could also be seen for the visual task, but were stronger at parietal sites. The latencies and scalp topographies were consistent with previous ERP literature (Hopfinger & West, 2006; Key et al., 2005; Makeig et al., 1999), notably that the auditory N100-P200 complex presents over frontal regions, whereas the visual N100-P200 presents more strongly over parietal regions.

For both the auditory and visual tasks and for all subjects, we were able to discriminate target vs. standard EEG trials with highly significant accuracy for multiple EEG windows (Figure 5.2). Our permutation method determined the $p = 0.01$ significance corresponded to AUC $= 0.66$. The auditory stimulus discrimination resulted in a peak group-mean AUC of 0.84 at 225 ms, with a later discrimination peak of 0.81 AUC at 375 ms. The visual stimulus discrimination curve displayed a broad peak with maximum AUC of 0.86 at 325 ms. Discriminator performance exceeded the more conservative AUC > 0.75 threshold for the 175–475 ms windows for the auditory task, and 175–600 ms windows for the visual task. Thus, all windows from 175 to 475 ms were included in the fMRI analysis. Importantly, the high discrimination accuracy with similar temporal profiles

showed the auditory and visual tasks to be well-matched.

The grand mean forward models, which show the scalp distribution of discriminating components as they progress across time, are displayed below the discriminator performance curves in Figure 5.2 for a subset of windows with significant performance. Both auditory and visual EEG data were most discriminative at medial frontal sites very early in the trial, then at medial central sites slightly later, and finally the P300 range data were most discriminative at medial posterior sites. These topographies were consistent with previous reports for auditory (Goldman et al., 2009) and visual (Gerson et al., 2005) target discrimination. Discriminator output was significantly ($p < 0.01$) negatively correlated with RT for multiple EEG windows. This result demonstrated the need to orthogonalize our STV fMRI regressors to RT-variability regressors given our aim to study residual variance unobservable with behavioral response.

5.3.2 Traditional fMRI Analysis

The traditional event-related target vs. standard contrast resulted in extensive activations throughout multiple cortical and subcortical structures. Bilateral activations were observed in cerebellum, thalamus, insula, ACC, and supra-marginal gyri. Left (i.e. contralateral) motor areas and right middle frontal gyrus (MFG) were also strongly activated. These were consistent with previous oddball paradigm results (Laurens et al., 2005; Stevens et al., 2000). RT-variability statistical maps showed strong correlates in anterior and posterior cingulate cortex (PCC), left motor areas, right MFG, right lateral occipital cortex (LOC), right angular gyrus, and bilateral insula (Figure 5.3).

5.3.3 Single-trial EEG Variability fMRI Analysis

The EEG-derived regressors resulted in significant group-level activations for multiple stimulus-locked EEG training windows, including positive correlates for the 200 ms window and negative correlates for the 425-475 ms windows. The early (200 ms) positive activations were observed in ACC and left caudate. EEG variability within all windows from 425 to 475 ms correlated negatively with BOLD activity across right middle and inferior frontal gyrus (MFG/IFG). Negative correlates were also found in right precentral and postcentral gyri for the 425 and 475 ms windows. Right-lateralized negative activations were also detected in paracingulate/ACC at 425 ms, and temporal and frontal poles, including lateral orbito-frontal cortex (OFC), at 475 ms. A neg-

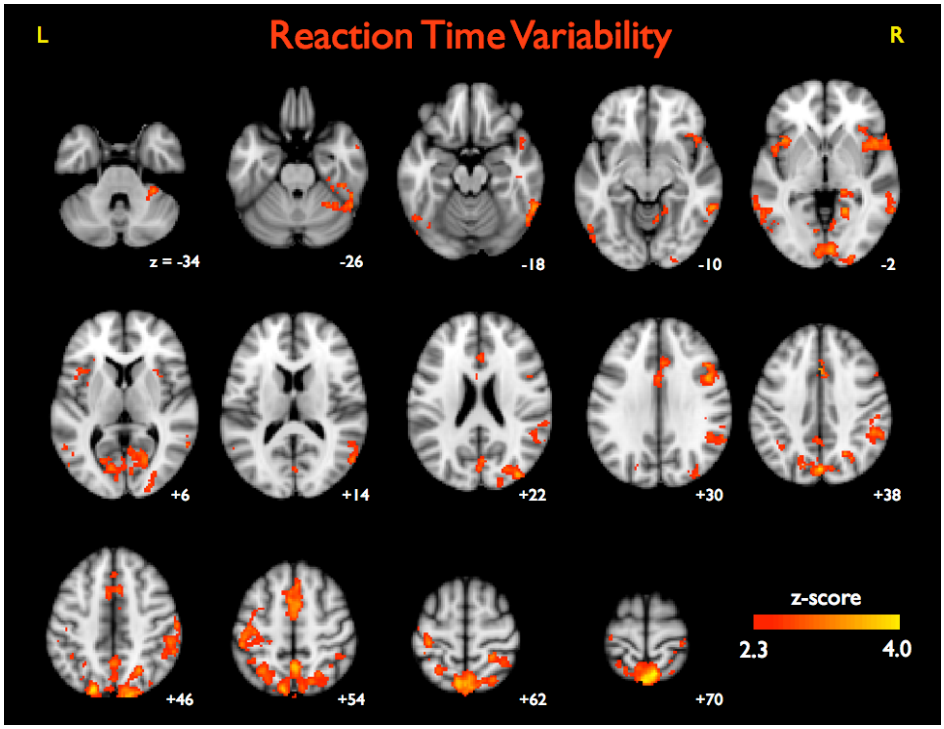

Figure 5.3: fMRI BOLD correlates of reaction time variability. Group-level positive activations thresholded at $z > 2.3$, and cluster corrected at $p < 0.05$. All voxels correlating significantly ($p < 0.01$ uncorrected) with the BCG pulse timing are excluded. Also excluded are all voxels with significantly different activation strength for the auditory vs. visual tasks (paired t-test, $p < 0.01$ uncorrected). Note that images are displayed in neurological coordinates.

window	Nvox	+/-	min p	MNIx	MNIy	MNIz	hem	region
200ms	273	pos	0.0217	2	8	34	L/R	anterior cingulate gyrus
	23	pos	0.0217	-14	2	24	L	caudate
	4	pos	0.0482	-60	4	14	L	precentral gyrus
	2	pos	0.0491	-64	-14	-12	L	middle temporal gyrus (posterior, anterior, superior)
425ms	578	neg	0.0242	52	26	26	R	middle frontal gyrus, inferior frontal gyrus
	211	neg	0.0377	42	-2	58	R	precentral gyrus, middle frontal gyrus
	49	neg	0.0340	12	22	34	R	paracingulate gyrus, anterior cingulate gyrus
	11	neg	0.0449	48	-18	44	R	postcentral gyrus
	8	neg	0.0487	32	26	46	R	middle frontal gyrus, superior frontal gyrus
450ms	59	neg	0.0402	52	26	26	R	middle frontal gyrus, inferior frontal gyrus
	21	neg	0.0018	0	-28	-20	L/R	brainstem
475ms	758	neg	0.0161	44	36	26	R	middle frontal gyrus, precentral gyrus, frontal pole
	213	neg	0.0381	44	40	0	R	frontal pole, inferior frontal gyrus, frontal operculum cortex
	207	neg	0.0260	50	-20	34	R	postcentral gyrus, precentral gyrus, anterior supramarginal gyrus
	72	neg	0.0367	40	42	-16	R	frontal pole, orbito-frontal cortex
	43	neg	0.0418	56	10	-26	R	temporal pole

Table 5.1: BOLD Correlates of EEG Variability Common to Auditory and Visual Tasks. Shown for each cluster are center of stimulus-locked EEG training window, number of voxels in cluster, sign of correlation, minimum FWE-corrected p-value within cluster and its coordinates in MNI template space, hemisphere, and anatomical brain region. FWE correction was performed independently within a grey matter mask following TFCE and within the brainstem.

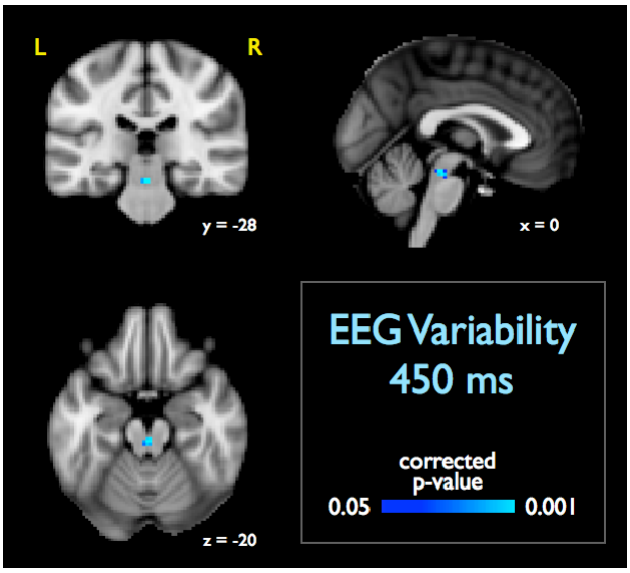

Figure 5.4: BOLD fMRI correlate of EEG single-trial variability detected in brainstem. EEG discriminating component variability in the 450 ms window correlated negatively with a 21-voxel cluster in the midbrain. Minimum FWE-corrected p-value of 0.0018 was located at MNI coordinates (0, –28, –20). Note that images are displayed in neurological coordinates.

ative 21-voxel activation in the brainstem was observed for the 450 ms window (Figure 5.4); this cluster had a minimum corrected p-value of 0.0018 at MNI coordinates (0, –28, –20). Table 5.1 contains a complete list of activations exceeding multiple-comparison-corrected $p = 0.01$ with their corresponding EEG windows. Figure 5.5 shows axial slices through the peak voxel of each of these clusters. Despite the high EEG discrimination accuracy in the middle window range, we did not detect significant activations at those latencies (225–400 ms) in this supra-modal analysis, which used a paired t-test to exclude areas that were more strongly correlated with EEG during one task (either auditory or visual).

In addition to the stimulus-locked analysis, we investigated response-locked activity, as some cognitive processes and subcomponents of the P300 are more tightly time-locked to behavioral responses than stimulus presentation (Gerson et al., 2005; Makeig et al., 2004; O'Connell et al., 2012). Although discrimination performance for response-locked EEG windows exceeded that of the stimulus-locked analysis, we were unable to detect significant BOLD correlates of response-locked discriminating activity common to both auditory and visual tasks.

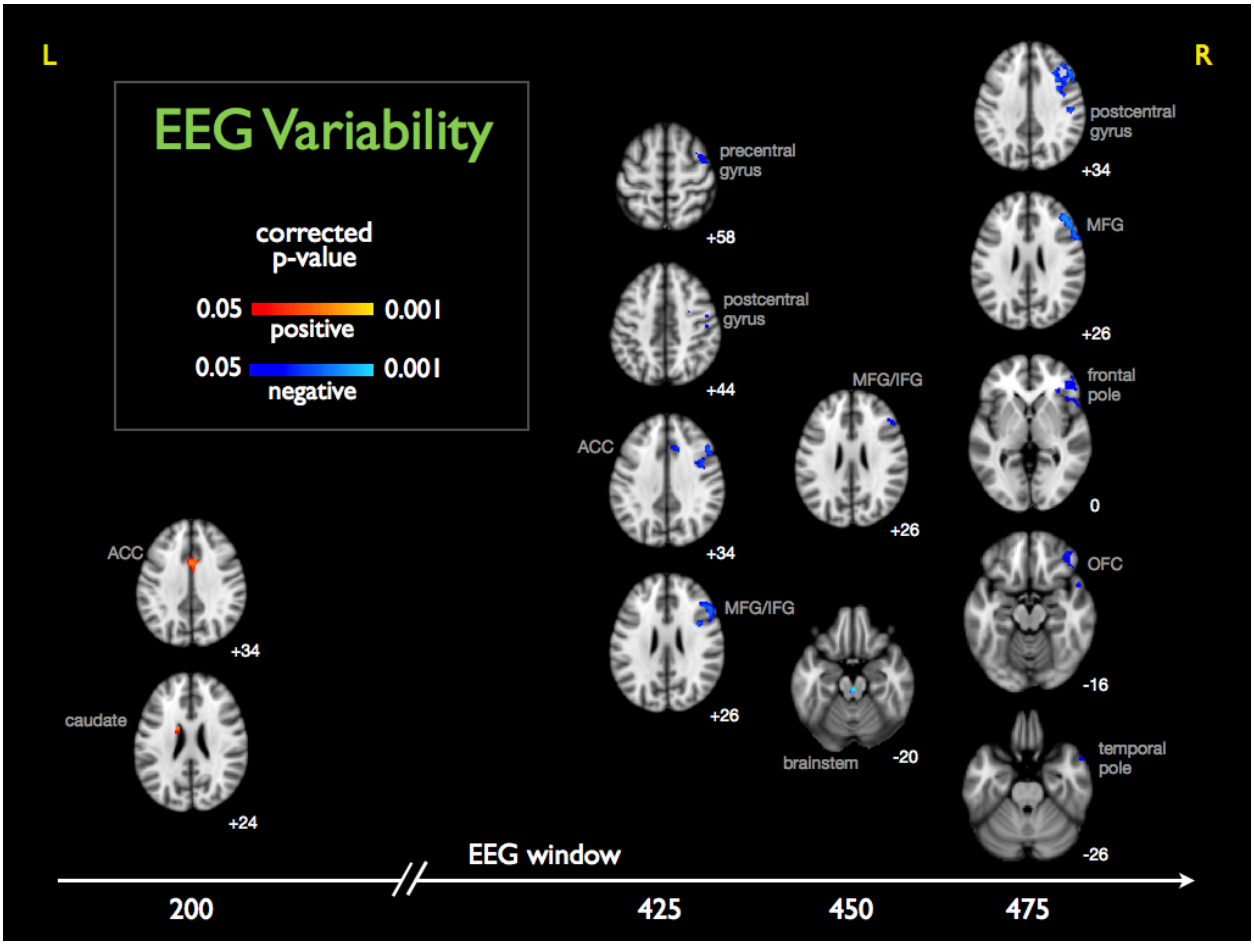

Figure 5.5: BOLD fMRI correlates of EEG single-trial variability spanning the trial. Timing diagram showing axial slice through peak voxel of each significant cluster. Time is in ms relative to stimulus onset. Red-yellow denotes positive correlation with the single-trial EEG classifier output (attentional index), and blue-cyan denotes negative correlation. MNI z-coordinate is specified to lower right of each slice. Note that images are displayed in neurological coordinates.

5.3.4 Separating BOLD correlates of RT variability and latent EEG variability

Using our methods we were able to separate variance in the BOLD data explainable purely by RT variability from that explainable by single-trial EEG variability. Figure 5.6 summarizes these results. Specifically we find strong bilateral insula correlates of RT variability, but no significant correlates of the EEG variability in these regions. We also found right angular gyrus/TPJ correlated with RT variability, but not with single-trial EEG variability. Conversely, other regions that have been associated with P300 correlated significantly with EEG variability but not RT. This included right precentral and postcentral gyri and left caudate. Lastly, we find that the ACC and MFG/IFG regions correlate significantly with both RT variability and the residual EEG discriminating component variability, suggesting that some but not all of ACC and MFG/IFG BOLD response variation is observable in the RT variation.

5.3.5 DCM Selection and Parameter Estimation

Across the 17 individual subjects, Model 4 (Figure 5.8) was the DCM chosen most frequently by the Bayesian model selection method (5 wins), with Model 5 in 2nd place (3 wins). Both of these models were members of the bidirectional model family, which was defined based on the presence of a bidirectional connection between the ACC and brainstem. All other connectivity was specified identically for these two models (with drives from BS to all other ROIs, and connections directed toward the BS from ACC, rACC, and rOFC). The only difference was the input region for the stimulus events, which was the brainstem for Model 4 and the ACC for Model 5.

On the group level, Bayesian model selection chose Model 4 as an overwhelming winner, with posterior probability 0.9997. Model 5 placed a distant 2nd with probability 0.0003. When BMS was applied to the partitioned model space, the bidirectional family won with a posterior probability of 1.0000 on the group level. (The other two partitions, which were defined by unidirectional ACC-BS connections, were each estimated to have probabilities less than 10^{-9}.)

All group-mean coupling and input parameters estimated by Bayesian parameter averaging of Model 4 (Figure 5.8) achieved a posterior probability greater than 0.9975. Input parameters for the target and standard stimuli were 0.10 and -0.04, respectively. Connectivity internal to each of the 4 cortical ROIs was negative (representative of self-inhibition), whereas brainstem self-connectivity had a low-magnitude positive coupling parameter estimate. Connectivity parameters from the

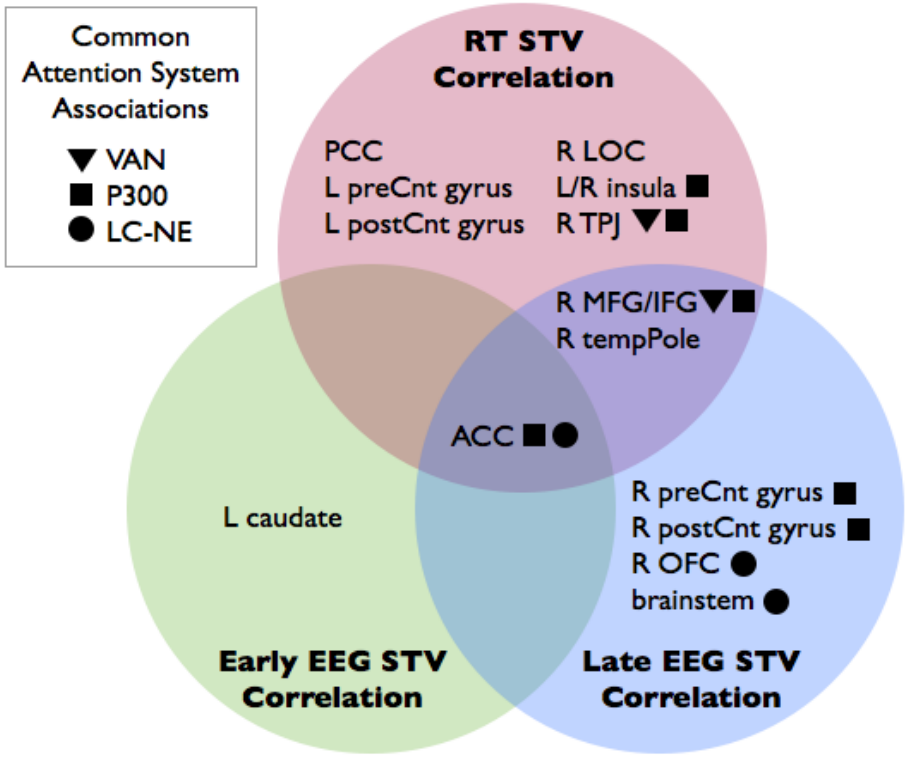

Figure 5.6: Reflection of neural activity in reaction time is region-specific. By regressing out RT variability from EEG variability in our fMRI model, we find that single-trial BOLD activity in a subset of attention- or P300-linked regions is reflected in the behavioral response. Listed are regions where BOLD signal significantly ($p < 0.05$ corrected) correlates with RT single-trial variability, latent early-window EEG single-trial variability, the late-window EEG variability, or their intersections. Common associations within the literature are indicated. TPJ = temporoparietal junction, LOC = lateral occipital cortex, PCC = posterior cingulate cortex, preCnt = precentral, postCnt = postcentral, ACC = anterior cingulate cortex, MFG = middle frontal gyrus, IFG = inferior frontal gyrus, OFC = orbitofrontal cortex.

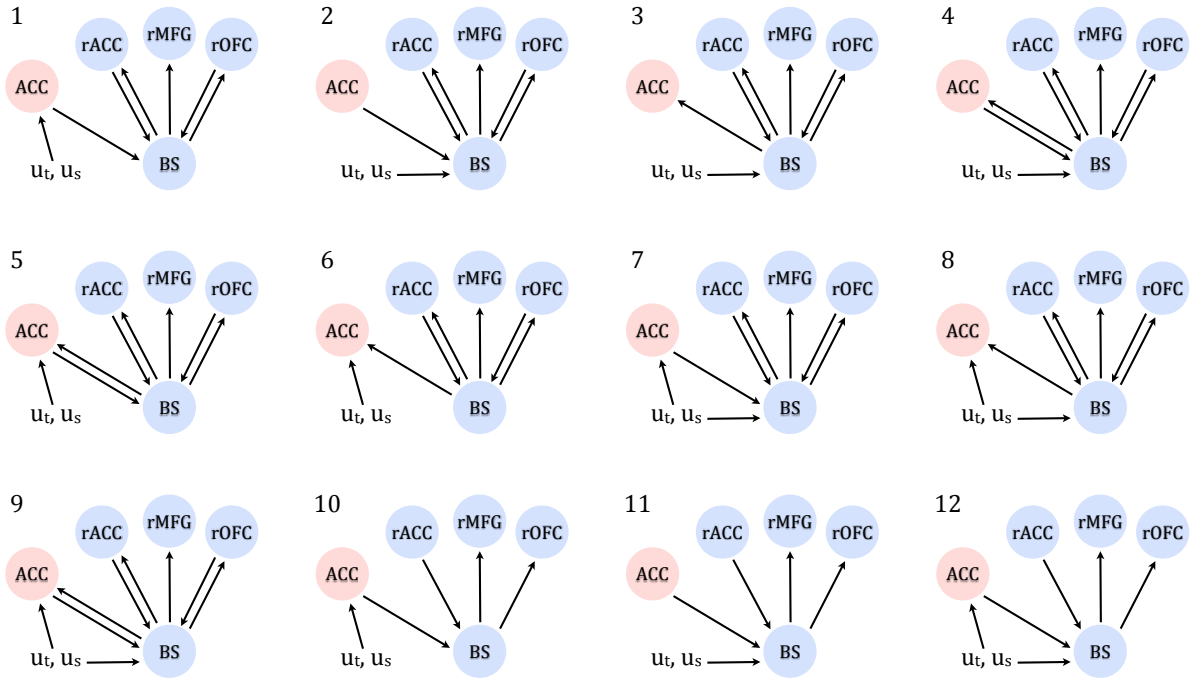

Figure 5.7: Dynamic Causal Models. We designed, estimated, and compared 12 related models. 5 ROIs were selected from results of the EEG-based fMRI analysis, and therefore were correlated with temporally-specific EEG discriminating component variability. Red circles represent ROIs positively correlated with the EEG variability, and blue negative. Diagram is arranged such that these EEG correlates are in temporal order from left to right. See Table 5.1 and Figure 5.5 for cluster details. Event timing for target (u_t) and standard (u_s) stimuli were used as input to the DCMs, applied either to ACC, BS, or both. ROIs: BS = brainstem, ACC = anterior cingulate cortex, rACC = right anterior cingulate cortex, rMFG = right middle frontal gyrus, rOFC = right orbito-frontal cortex. Model space was partitioned for family analysis based on ACC-BS connectivity. ACC to BS: models 1, 2, 7, 10, 11, 12; BS to ACC: models 3, 6, 8; bidirectional connectivity: models 4, 5, 9.

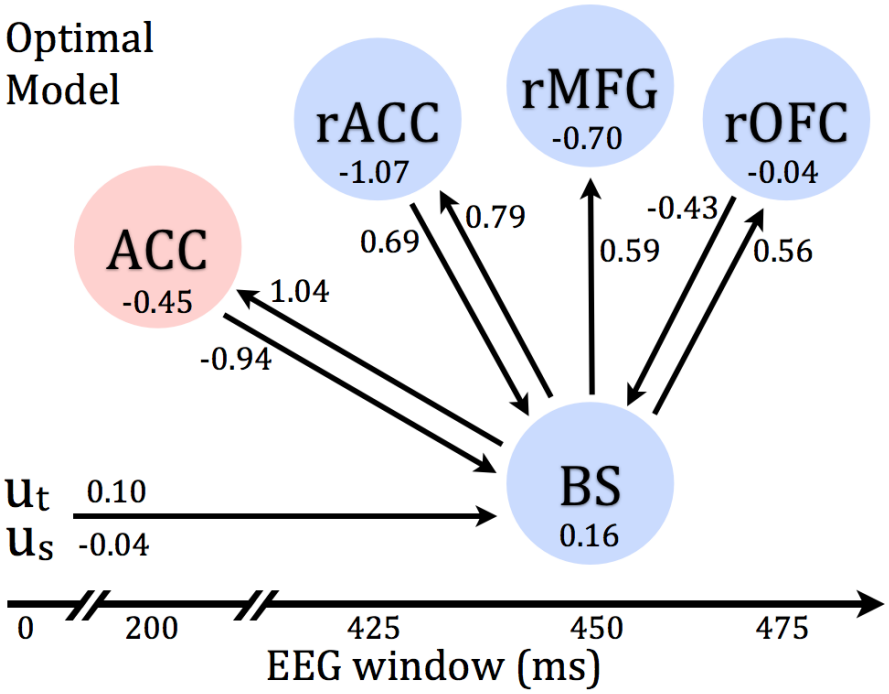

Figure 5.8: Group Average DCM for the Optimal Model. Results of Bayesian parameter averaging for Model 4 (see Figure 5.7), which won the Bayesian model selection on the group level (posterior probability 0.9997) and had more wins than any other model on the individual subject level. Intrinsic connection strengths are displayed next to their corresponding connectivity arrows; all values had posterior probability exceeding 0.9975. Time axis and circle color relate the model to the EEG-based fMRI results (see Figure 5.5), from which these ROIs were derived.

brainstem directed to all ROIs were positive (excitatory), ranging from 0.56–1.04 Hz. Strongest coupling strength was estimated for the "earliest" ROI (i.e. derived from correlates of early EEG variability) and monotonically decreased to the lowest strength for the "latest" ROI. The ACC and rOFC connections directed toward the brainstem had negative (inhibitory) coupling parameters (–0.94 Hz and –0.43 Hz, respectively), and the rACC showed a positive value (0.69 Hz).

5.4 Discussion

5.4.1 Our methods reveal BOLD correlates of attentional modulations

Our aim in this study was to tease apart the cascade of neural involvement related to natural fluctuations in focused attention using the high temporal resolution of EEG to find fMRI correlates of task-related EEG-components derived from a weighted average of all electrodes. Previous studies investigating BOLD correlates of single-trial event-related EEG variability have focused on only a few well-known ERP components at selected latencies and electrodes (Benar et al., 2007; Esposito et al., 2006; Fox & Raichle, 2007), though some work has investigated ERP components spanning the trial (Eichele et al., 2005; Goldman et al., 2009). These single electrode measurements can be particularly noisy when recorded simultaneously with fMRI due to scanner-related artifacts.

Our method uses EEG discrimination to separately identify the most task-relevant data projections of the entire EEG dataset at different event-locked time windows. We are thus able to study activity related to stimulus detection, target recognition/rejection, motor planning, and behavioral response as these processes evolve following the stimulus (Philiastides & Sajda, 2006). Further we regress out the variance correlated with RT (Feige et al., 2005; Goldman et al., 2009), so that we are investigating only BOLD correlates of modulations in focused attention that are not reflected in externally-observable behavioral events. Finally, because we combine data from analogous auditory and visual tasks, our methods reveal activity that generalizes across sensory input modalities. We take care to ensure that our results are not driven by activity related to only one task or to physiological artifacts in the images.

We do not attempt here to interpret the sign of fMRI correlates of EEG single-trial variability, since the BOLD response is related to electrophysiological activity in a complex way that is not yet completely understood (Arthurs & Boniface, 2002; Brookes et al., 2011; de Pasquale et al., 2010;

Goense et al., 2012; Goldman et al., 2002; Logothetis et al., 2010; Mantini et al., 2007; Mukamel et al., 2005; Scheeringa et al., 2011a).

5.4.2 fMRI correlate of EEG variability in brainstem supports LC adaptive gain theory

The LC-NE system is commonly associated with optimization of task performance by engaging and refocusing attention (Aston-Jones & Cohen, 2005; Bouret & Sara, 2005; Dayan & Yu, 2006; Sara & Bouret, 2012). Current theories of its specific functional role rely heavily on animal studies, with confirmation in humans needed. Brainstem imaging using fMRI poses a number of challenges, notably close proximity to pulsatile vessels, proper image alignment, and the small size of brainstem nuclei relative to BOLD spatial resolution. Nevertheless, fMRI activations in midbrain nuclei have been previously reported (D'Ardenne et al., 2008; Payzan-Lenestour et al., 2013; **?**), including EEG-fMRI evidence for an effective relationship between ACC and brainstem during a simple auditory target detection task (Crottaz-Herbette & Menon, 2006). Our brainstem correlate of the 450-ms EEG variability lies between and in close proximity to LC (Astafiev et al., 2010; Keren et al., 2009) and ventral tegmental area (VTA) (Carter et al., 2009). Since the LC strongly innervates other nearby neuromodulatory midbrain nuclei and receives their projections to a lesser extent (Sara & Bouret, 2012), our cluster of activation likely arises from LC activity. The LC also projects to multiple subcortical structures and broadly across the cortex (Loughlin et al., 1986), but its only cortical inputs come from the ACC and OFC, which receive information from sensory cortices. These prefrontal regions are thought to regulate LC activity both by directly driving its phasic responses and via changes to baseline excitatory drive (Aston-Jones & Cohen, 2005).

Our methods revealed BOLD correlates of EEG variability in ACC for the 200-ms and 425-ms windows, consistent with multiple reports of ACC coupling with various components of the evoked EEG response. In previous EEG-fMRI studies, the ACC was shown to couple with the N100 component during auditory tasks (Esposito et al., 2009; Mulert et al., 2008), and fMRI-constrained ERP-source-modeling suggested that it is the major generator of the N2b and P3a components during both auditory and visual tasks (Crottaz-Herbette & Menon, 2006). Note that our early ACC cluster is not representative of sensory-evoked activity that differs between targets and standards; we do not study the discriminating projection of the EEG data itself but instead

investigate BOLD correlates of single-trial variability along that projection. We also only interpret results within the target class to avoid stimulus-type confounds. O'Connell et al. (2012) minimized the potential confound of early sensory-evoked processing using a gradual evidence accumulation target detection task. They studied EEG activity related to general supra-modal decision processes and found a relationship with the P300, which given their experimental design was expectedly locked to behavioral response. However, keep in mind that the P300 has many specialized subcomponents linked to multiple processes; some are more stimulus locked and some more response locked (Gerson et al., 2005).

As part of the adaptive gain theory, modulatory drive from the ACC and OFC to the LC is proposed to result from outcome of decision processes (Aston-Jones & Cohen, 2005), an idea which stems from known latency of the LC and P300 responses and evidence to suggest that LC activity is more tightly locked to RT than stimulus presentation (Clayton et al., 2004). We might therefore expect to find significant correlates of response-locked EEG variability (which we did not detect here common to auditory and visual tasks). However, since variability in response-locked EEG components is highly correlated with RT variability (O'Connell et al., 2012), orthogonalization of the EEG-based regressors to RT regressors left too little residual variance for response-locked EEG correlates to achieve significance.

Our late correlates in right ACC, brainstem, and right OFC all occur in the range of the P300 (respectively at 425, 450, and 475 ms), and are all coupled with modulations of discriminating components closely related to the P300 ERP component (see scalp distribution of discriminating components in Figure 5.2). Their latency supports the decision outcome hypothesis of the adaptive gain theory and provide support for the role of ACC and OFC in direct modulation of the LC phasic response. Furthermore, they show that modulatory activity in ACC occurs prior to that in OFC. The late ACC activation is also consistent with previous reports that link it to P300 modulations (Benar et al., 2007; Bledowski et al., 2004b; Crottaz-Herbette & Menon, 2006; Linden, 2005); OFC is not commonly associated with ERP variability. Note, however, that our early ACC correlate suggests that it also has a role in tonic (i.e. baseline) modulation, which occurs prior to the decision. Our inability to detect correlates for middle EEG windows suggests that in the middle time range EEG and BOLD are coupled only in regions specific to the sensory input modality.

According to the adaptive gain theory of LC-NE function, behavioral performance is optimal

during states of intermediate tonic activity, which result in a maximal phasic response to sensory stimuli. Changes in tonic activity drive transitions between high and low attentional states, where very low or high activity results in inattentive or distractible states, respectively. The phasic LC response only occurs for task-relevant stimuli, but is not specific to sensory modality (Aston-Jones et al., 1994). Because pupil diameter is closely tracked by tonic LC activity (Aston-Jones & Cohen, 2005) and pupil size to single-trial EEG variability (Murphy et al., 2011), we hypothesize that our midbrain correlates of EEG variability reflect underlying LC tonic activity and subsequent LC phasic response and the P300. The concurrent EEG-pupillometry study of Murphy et al. (2011) found a relationship between baseline pupil diameter and variability of the P300 EEG response to auditory targets; that finding was also interpreted as support for the adaptive gain theory. Similar studies using simultaneous EEG, pupillometry, and fMRI would be of great benefit to this field.

There are limited reports of caudate coupling with P300 in both auditory (Crottaz-Herbette & Menon, 2006) and visual (Warbrick et al., 2009) tasks. Because the caudate is highly innervated by dopaminergic neurons (mainly from the VTA and substantia nigra within the midbrain), this cluster provides further support for the adaptive gain theory, which proposes that the LC-NE system interacts with many other brain circuits and works in synergy with the dopaminergic system (Aston-Jones & Cohen, 2005).

5.4.3 Right hemisphere cortical activations provide link between LC-NE system, VAN, and P300

The LC phasic response has also been theorized to drive transitions that refocus attention in a more complex way, by facilitating an interruption (Dayan & Yu, 2006) and reset (Bouret & Sara, 2005) of the current endogenously-driven target network and the LC tonic activity, thus reorienting attention to an updated task. This switch is facilitated by the right-lateralized VAN, which is activated by salient behaviorally-relevant stimuli (Bouret & Sara, 2005; Corbetta et al., 2008; Corbetta & Shulman, 2002; Fox et al., 2006). Since the VAN, P300 potentials, and LC phasic responses all similarly show enhanced responses to behaviorally-relevant stimuli in multiple sensory modalities, a functional link between them has been proposed, both in relation to tonic transitions of attention and to phasic responses (Corbetta et al., 2008).

We found correlates of P300-range EEG variability in the right MFG/IFG, a main node in the

VAN. This region has been previously implicated in P300 modulations (Benar et al., 2007; Bledowski et al., 2004a,b; Eichele et al., 2005), as were the activations we detected in right precentral gyrus (Bledowski et al., 2004b; Crottaz-Herbette & Menon, 2006; Eichele et al., 2005) and postcentral gyrus (Crottaz-Herbette & Menon, 2006; Eichele et al., 2005) for the same windows. Nearly all our significant correlates of EEG STV were right-lateralized, consistent with the VAN and other reports showing the majority of regions coupling with EEG responses are in the right hemisphere (Eichele et al., 2005). Bilateral precentral gyrus is commonly associated with a more goal-driven and dorsal attention network, but the right precentral gyrus has also been linked to exogenous processing (Corbetta et al., 2008; Kincade et al., 2005).

Our concurrent brainstem, ACC, OFC, and right MFG/IFG activations, which all occur in the P300 range, provide evidence for a strong link between the LC-NE neuromodulatory system, VAN, and the P300. They support the hypothesis that VAN suppression during focused attention is partly due to decreased tonic activity of the LC-NE system (Corbetta et al., 2008).

5.4.4 Dynamic interactions underlie task-related attentional modulations

ROIs for fMRI DCM analyses are commonly selected based on peaks within traditional event-related GLM statistical maps. One obvious approach to incorporate single-trial EEG variability into a DCM analysis is to build a bilinear model that includes single-trial EEG measurements as modulators to connectivity strength. However, two issues arise with this approach. Firstly, voxels selected by a traditional GLM contrast are not necessarily affected by the trial-to-trial variability of interest and may instead have variability dominated by noise (Smith, 2012). Secondly, the trial-to-trial variability of the EEG response differs across the temporally-specific components of the response. One EEG component may be of particular interest for certain task-specific studies (e.g. the face perception study of Nguyen et al. (2013), but selection of a single component is insufficient to study modulations of attention that generalize across simple tasks in multiple sensory domains. To circumvent these issues, we utilized the results of our EEG-based fMRI analysis to define ROIs for our DCM analysis. We selected a subset of our supra-threshold clusters that were of particular interest based on previous literature. These included the ACC correlate of early (200 ms) EEG variability, a non-spatially-overlapping rACC P300-range correlate, other cortical P300-range correlates in rMFG and rOFC, and the brainstem cluster. Single-trial variability within these ROIs

was thus meaningful for the effective connectivity we aimed to study.

Our DCM analysis of 12 competing models resulted in substantially greater evidence (0.9997 posterior) for a model with multiple reciprocal (bidirectional) intrinsic connections. Furthermore, the only two models that showed consistently large model evidence on the individual subject level both belonged to the model family with bidirectional connection between the brainstem and early ACC clusters. These results provide support for the idea that dynamic interactions between attentional systems play a role in modulations of task-related attention during simple tasks. Other DCM studies have reported interactions of attention systems, but these focused on linking the VAN with the dorsal attention network during tasks related to spatial attention (Vossel et al., 2012) and attentional reorienting (Diquattro et al., 2013), and these studies did not incorporate EEG-derived information.

Connectivity parameter magnitudes and signs (determined by Bayesian parameter group averaging) suggest that the brainstem's role in these modulations is excitatory across the duration of the trial and multiple cortical regions, whereas the rOFC plays an inhibitory role late in the trial. The integral role of the ACC in attentional modulations is likely more complex, with dependencies both in space (bilateral ACC vs. right paracingulate/ACC region) and time (early 200 ms vs. later 425 ms post-stimulus). Specifically, activity within bilateral ACC may act to inhibit evoked brainstem activations early in the trial, but then rACC may drive this activity later in the trial. Studies specifically designed to investigate causality will be required to validate such claims. Our DCM results further support the adaptive gain theory of the LC-NE system, and together with the EEG-based GLM results they expand upon it by providing additional information regarding the timing of involvement of these regions.

5.5 Conclusions

Using machine learning, we tracked variability in temporally-specific task-relevant projections of EEG data, and spatially localize their BOLD correlates. We investigated neural response variability for identical target stimuli, and then combined fMRI data to report regions involved in endogenous attentional modulations that generalize across auditory and visual sensory input. Without restricting our investigation to regions traditionally associated with attention, we found numerous

activations almost entirely within the LC-NE system, VAN, and areas previously implicated in P300 generation. We show that the attentional fluctuations observable via single-trial reaction time are region-specific, but not specific to the attention network. A final DCM analysis expanded upon these results to demonstrate effective connectivity between these regions. Our results shed light on the complex dynamic links between these systems in the human brain, and the relative timing of their involvement, when performing even the simplest auditory and visual tasks.

Chapter 6

Pre-stimulus EEG Alpha Oscillations Modulate fMRI BOLD Responses

6.1 Introduction

The amount of attention allocated to any external task (e.g. listening to a thesis defense) affects the extent to which incoming sensory information is processed and the efficiency of that neural processing. Internal attentional states such as task-related attention are by nature difficult to study. Since they are by definition not event-related, any experimental paradigm attempting to control them would be confounded. Instead it is necessary to obtain a measure of this naturally fluctuating state.

EEG power in the alpha band (8–12 Hz) is commonly associated with endogenous attention, with high power known to correlate with decreased task engagement. This "alpha rhythm" peaks around 10 Hz and is the dominant ongoing oscillation recorded by scalp EEG. While it is widespread, posterior alpha is the most commonly studied, mainly due to its high power in scalp EEG recordings. This component of the alpha rhythm has a scalp distribution over parietal and occipital regions (Min & Park, 2010). Extensive evidence shows that the power of alpha oscillations prior to stimulus correlates negatively with behavioral performance related to visual perceptual ability (Hanslmayr et al., 2007; Mazaheri et al., 2009; van Dijk et al., 2008). Many studies also show a similar correlation with visuo-spatial attention (Kelly et al., 2009; Thut et al., 2006) and multi-sensory attention (Banerjee et al., 2011; Lange et al., 2013). In addition to correlation, a causal effect has been

demonstrated using transcranial magnetic stimulation (TMS) (Romei et al., 2008).

Amplitude of EEG responses is also affected by alpha magnitude (Rajagovindan & Ding, 2011), but evidence suggests the phase of alpha at stimulus onset has a greater effect (Fellinger et al., 2011; Mathewson et al., 2009). Alpha phase has also been associated with behavioral performance related to visual perception (Dugue et al., 2011; Mathewson et al., 2009).

fMRI BOLD activity has also been shown to correlate with EEG alpha. Resting-state EEG-fMRI studies have suggested that the EEG alpha is driven by thalamo-cortical loops (Liu et al., 2012), in particular showing a negative correlation with posterior regions and positive with thalamic regions (Goldman et al., 2002). Three published studies have explored the correlates of the EEG alpha rhythm and the visually-evoked fMRI response, both with respect to power (Becker et al., 2011; Mayhew et al., 2013; Scheeringa et al., 2011b) and phase (Scheeringa et al., 2011b). These studies all focused on task-irrelevant stimulus processing and were limited to the BOLD response within visual regions of interest (ROIs). Until now, the role of prestimulus alpha oscillations on the BOLD response to auditory stimuli has not been explored.

Here we investigate the effects of endogenous attention on the evoked BOLD response to auditory stimuli, and hypothesize that the distribution of recruited brain regions depends on the prestimulus brain state. We use prestimulus EEG alpha to represent the subjects' task engagement on each trial, and contrast the BOLD response for the high and low attention conditions. In contrast to previous studies, we investigate not just stimulus-processing but also task-relevant processing related to perceptual decision making.

6.2 Methods

6.2.1 EEG-fMRI Data

The auditory oddball simultaneous EEG-fMRI data used in Chapter 3 was also used in this study. Data from two of the seventeen subjects were discarded due to a slow EEG alpha power drift across the entire experiment, which left us with an incomplete fMRI model for some runs of the experiment. Demographics of the fifteen remaining subjects were: 6 female, mean 27.5 years, range 20–40. We used only the auditory task data because posterior EEG alpha power is highly confounded by visual stimulus presentation. Furthermore, power in this frequency band is higher with the eyes-closed

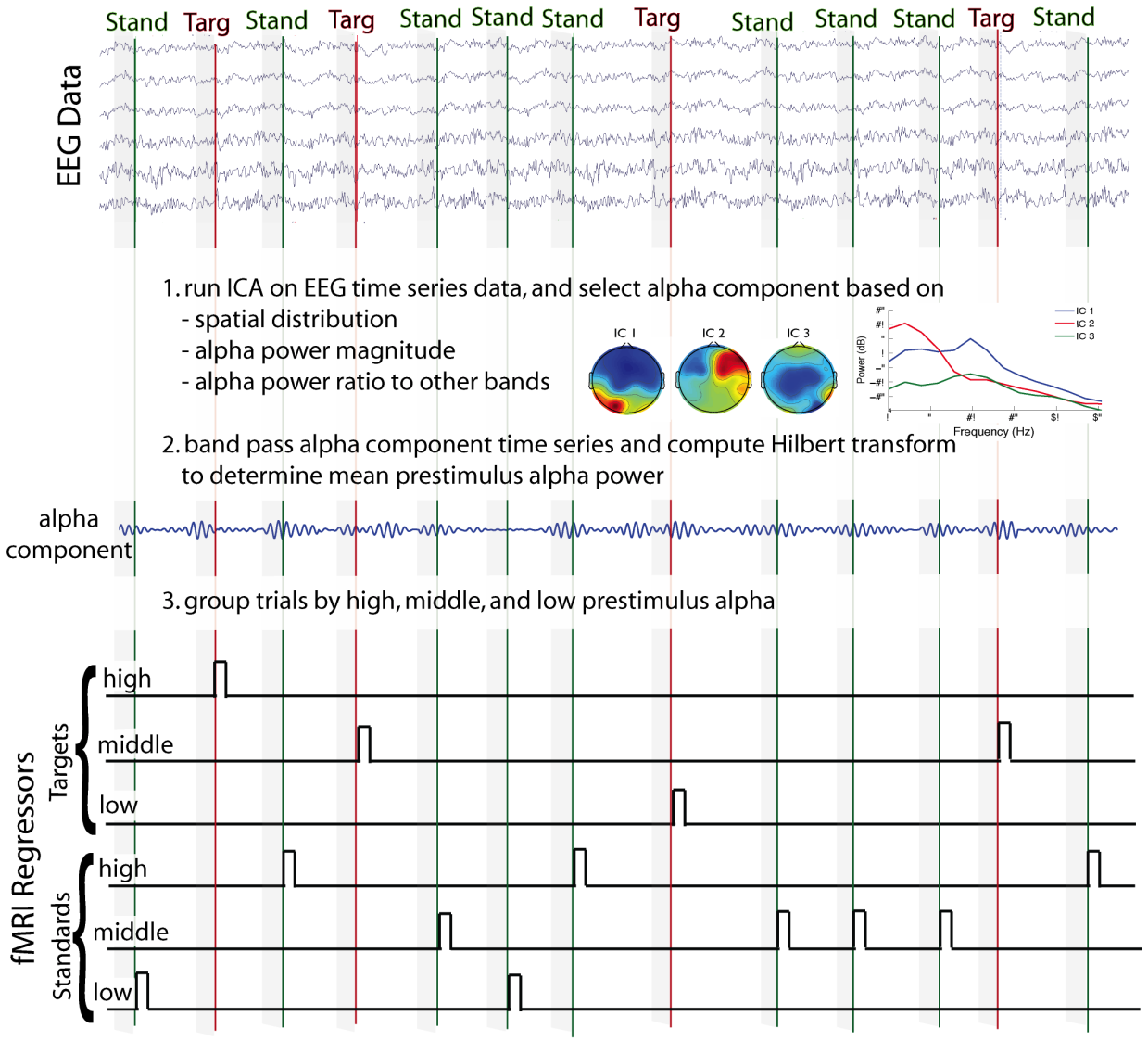

Figure 6.1: Construction of fMRI Model Based on EEG Alpha Activity. EEG was collected in the fMRI scanner while subjects performed an auditory oddball task (top). ICA was run on the continuous EEG data, and an "alpha component" was selected based on its power spectra and scalp topography. A Hilbert transform was used to decompose the alpha-band-passed alpha component into magnitude and phase. Trials were then grouped within class into 3 bins based on high, medium, or low alpha magnitude prior to each stimulus (bottom). These groups were modeled separately so contrasts could be computed. In a separate but similar alpha phase analysis, trials were binned into 4 groups according to instantaneous phase at stimulus onset (refer to Figure 6.2).

condition of the auditory experiment compared to the eyes-open visual experiment (Liu et al., 2012), which gave us a boost to the SNR. This was especially helpful since BCG artifacts contain high alpha power and heavily contaminate EEG recorded in the MRI scanner.

6.2.2 Prestimulus EEG Alpha Estimation

We first preprocessed the EEG data using the methods described in Section 2.3.2. Figure 6.1 shows a diagram of the remainder of our methods, which are described below.

To estimate the alpha in the multi-dimensional EEG data and determine a projection containing the alpha activity of interest, we performed an independent component analysis (ICA) by implementing the FastICA algorithm (Hyvarinen, 1999) in Matlab. This method was chosen over individual electrode selection to boost SNR of the EEG signal. We selected a single "alpha component" based on three main criteria: (1) high alpha power, in particular relative to surrounding frequency bands, (2) no peak in the 1 Hz range, which would represent a contaminant from the BCG pulsation artifact, and (3) typical posterior scalp distribution.

Evaluation of these selection criteria involved the following. To each component's time series we applied a 2^{nd} order Butterworth bandpass filter with cutoffs at 8 and 12 Hz, and then estimated the mean power in the alpha band by squaring and summing the resulting signal. We estimated the mean broadband EEG power similarly, using cutoff frequencies at 5 and 20 Hz. Next we calculated the ratio of mean alpha power to mean broadband power for each component, and ranked the components according to this ratio. Spatial topographies of the top five components were displayed to manually select the alpha component with typical posterior distribution, i.e. heavy weighting on occipito-parietal electrodes.

We took care to ensure that the selected component was not contaminated with BCG artifacts. The top five ranked "BCG components" were chosen using a similar method to that just described for selecting the alpha component, but using a 0.5–2 Hz pass band. These components had heavy lateralized weighting on the electrodes, as expected since temporal electrodes (sites T7, T8, CP5, CP6) are most strongly affected by such pulsation artifacts.

Once the final alpha component was confirmed, we repeated the alpha bandpass filtering with cutoffs at ± 2 Hz around the subject-specific peak alpha frequency. This modal frequency was selected by visual inspection of the power spectral density of that unfiltered component. There was

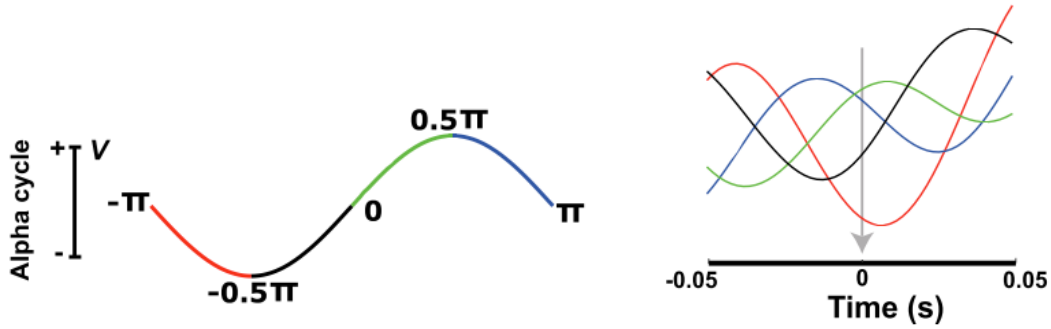

Figure 6.2: Method for Prestimulus Alpha Phase Binning. Trials were grouped into 4 bins according to the instantaneous phase of the alpha oscillation at stimulus onset. Red: $-\pi$ to $\frac{-\pi}{2}$ (negative, waxing, decreasing). Black: $\frac{-\pi}{2}$ to 0 (negative, waning, increasing). Green: 0 to $\frac{\pi}{2}$ (positive, waxing, increasing). Blue: $\frac{\pi}{2}$ to π (positive, waning, decreasing). These groups were then used in construction of the BOLD model (refer to Figure 6.1). Reproduced from Scheeringa et al. (2011b).

a further BCG pulse contaminant check here to ensure no peak was present in the 1 Hz range.

We computed the Hilbert transform of this band-passed alpha component to decompose the alpha oscillation into its magnitude and phase. This provided a single envelope of alpha activity across the run of the experiment. For each trial we computed the mean alpha envelope in the half second prior to stimulus onset, and within each of the two stimulus classes we grouped trials according to high, medium, or low prestimulus alpha magnitude.

For the phase analysis, we divided trials into four groups according to their instantaneous phase at stimulus onset time, as was done previously by Scheeringa et al. (2011b) (see Figure 6.2). This was equivalent to categorizing based on the sign (positive or negative), derivative (increasing or decreasing), and direction of deviation from zero (waxing or waning), giving the following four groups:

- 0 to $\frac{\pi}{2}$ – positive, waxing, increasing
- $\frac{\pi}{2}$ to π – positive, waning, decreasing
- π to $\frac{3\pi}{2}$ – negative, waxing, decreasing
- $\frac{3\pi}{2}$ to 2π – negative, waning, increasing

6.2.3 Effect of EEG Alpha Oscillations on Auditory Stimulus Processing

We first preprocessed the auditory oddball fMRI data and ran the traditional fMRI analysis that was described in Chapter 2, specifically Sections 2.3.3 and 2.5.

The fMRI model for the EEG alpha investigation of this chapter (bottom of Figure 6.1) differed from the traditional analysis in two ways. Firstly, RT variability was not incorporated into the model but instead included as noise regressors. Secondly and key to this study, trials were grouped by alpha (see Section 6.2.2) and each group modeled in separate regressors. The alpha magnitude and alpha phase analyses were performed independently, involving three and four groups of trials, respectively.

We computed a high vs. low alpha contrast within the target class to observe the effect of prestimulus alpha magnitude on the BOLD response to identical target stimuli. We investigated phase effects similarly by contrasting positive vs. negative, waxing vs. waning, and increasing vs. decreasing phase at stimulus onset.

A randomization test was used to generate a null distribution of cluster activations and correct for multiple comparisons. For each subject, we randomly grouped trials 100 times and carried each of the randomizations through to group level. Each of these randomization maps were thresholded at $p < 0.005$ to provide a null distribution of clusters. Within each of these clusters we summed the negative log of each voxel's p-value to create a null distribution of cluster p-values, from which we calculated the $p < 0.05$ cluster threshold. This method of integrating statistics within each cluster is closely related to a cluster size thresholding, but gives a higher weighting to clusters with stronger voxel-wise statistical strength. These randomizations were run independently for the magnitude and alpha phase analyses to generate distributions based on three and four random groups, respectively. The alpha magnitude randomizations resulted in a null distribution of 3955 clusters, and the phase randomizations resulted in a null distribution of 4691 clusters. The $p_{cluster} < 0.05$ threshold was approximately 24 voxels for the magnitude analysis and 26 voxels for the phase analysis.

6.2.4 Effect of EEG Alpha Oscillations on Task-specific Processing

Scheeringa et al. (2011b) suggested that a correlation between the underlying BOLD signal and slow alpha fluctuations could confound the analysis described above (high vs. low contrast), so we also investigated the effect of prestimulus alpha on task-specific stimulus-related processing.

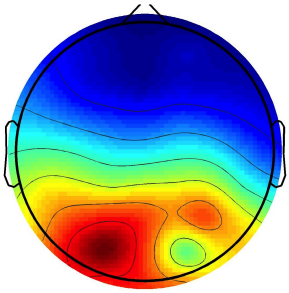

Figure 6.3: Group Mean Alpha Component Topography Across 15 Subjects A typical posterior distribution is seen, without any visible contribution from BCG artifact, which would be evident from a bilateral weighting at temporal sites.

For each of the trial groups (magnitude investigation: high alpha, low alpha; phase investigation: positive waxing increasing, positive waning decreasing, negative waxing decreasing, negative waning increasing) we computed target vs. standard contrasts to give maps of the most task-relevant fMRI activity for each subject. This included areas involved in processes such as target detection, perceptual decision making, and response planning. We then performed paired t-tests to identify effects of prestimulus alpha oscillations on task-relevant BOLD activity. One t-test was performed for the prestimulus alpha magnitude analysis: high vs. low alpha. These results were thresholded at $z > 2.3$, and clusters were FWE multiple-comparison-corrected at $p < 0.05$ (Worsley, 2001). Three t-tests were performed for the phase analysis: positive vs. negative, waxing vs. waning, increasing vs. decreasing.

6.3 Results

All fifteen included subjects responded with high accuracy and speed: $98.8\% \pm 2.1\%$ of targets were correctly detected, with 403.0 ± 60.1 ms RT. As reported in Chapter 3 the mean event-related BOLD response to target stimuli was consistent with previous findings (Stevens et al., 2000), showing the largest activations in thalamus, auditory cortex, insular cortex, and supplementary and primary motor areas.

MAGNITUDE

contrast	Nvox	max z	$p_{cluster}$	MNIx	MNIy	MNIz	hem	region
low > high	190	3.69	0.0003	-6	-82	50	L	superior lateral occipital cortex, precuneus cortex
low > high	71	3.44	0.0053	-2	-62	60	L	precuneus cortex, superior lateral occipital cortex
low > high	63	3.20	0.0073	-32	-88	26	L	superior lateral occipital cortex, occipital pole
low > high	54	2.99	0.0116	-48	-70	-22	L	inferior lateral occipital cortex, inferior temporal gyrus
low > high	51	3.44	0.0116	-2	-86	-20	L/R	lingual gyrus, occipital fusiform gyrus
low > high	48	3.39	0.0129	28	-88	-4	R	lateral occipital cortex, occipital fusiform gyrus, occipital pole
low > high	35	3.12	0.0240	-2	-78	-4	L	lingual gyrus, intracalcarine cortex, occipital fusiform gyrus
low > high	33	2.97	0.0291	-20	-94	0	L	occipital pole, lateral occipital cortex
low > high	29	3.06	0.0362	-4	-44	8	L/R	posterior cingulate gyrus
low > high	26	3.27	0.0369	14	-42	-4	R	posterior cingulate gyrus, lingual gyrus, parahippocampal gyrus
high > low	25	3.02	0.0448	-38	-60	-42	L	cerebellum

Table 6.1: Effect of Prestimulus EEG Alpha Magnitude on BOLD Response to Auditory Targets. Per-voxel thresholded at $p < 0.005$ then cluster-corrected at $p < 0.05$.

6.3.1 EEG Alpha Components

The subjects' modal alpha frequencies ranged from 9.5–12 Hz, with mean 10.6 Hz and median 10.5 Hz. The mean scalp topography of the EEG alpha components across the 15 subjects is shown in Figure 6.3. A typical posterior distribution is clearly seen, without any visible contribution from BCG artifact, which would be evident from a bilateral weighting at temporal sites.

6.3.2 Effect of alpha magnitude on BOLD response to target stimuli

Negative correlation between BOLD signal and prestimulus alpha magnitude was found throughout posterior regions for the high vs. low alpha contrast of the response to target stimuli (Figure 6.4). These regions included left and right lateral occipital cortices (LOC) and lingual gyri, as well as left precuneus and occipital pole. We also found a positive correlate in the left cerebellum. A complete list of activations exceeding the FWE cluster corrected $p < 0.05$ threshold can be found in Table 6.1.

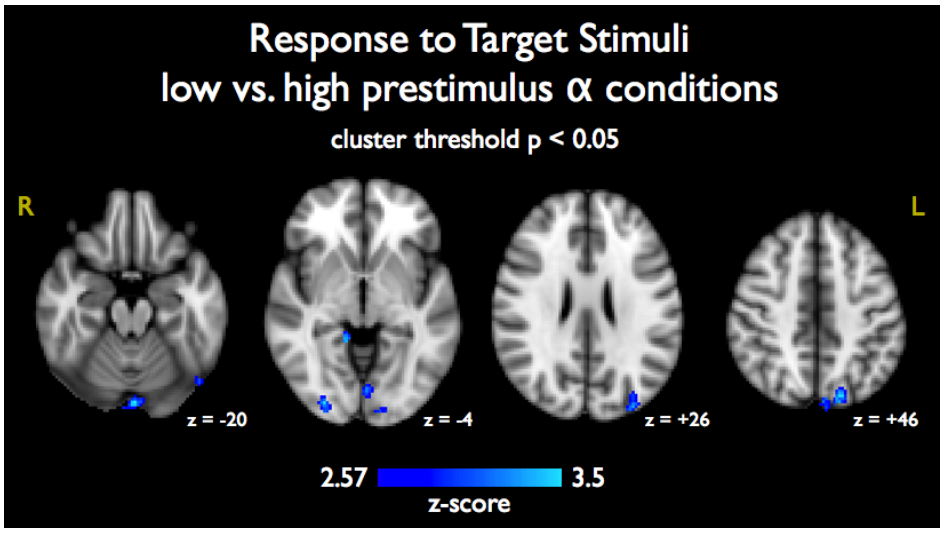

Figure 6.4: Event-Related Average BOLD Response to Targets for Low vs. High Prestimulus Alpha Conditions. An inverse correlation between prestimulus alpha magnitude and the BOLD response was seen throughout many posterior regions. Results shown were per-voxel thresholded at $p < 0.005$ then cluster-thresholded at $p < 0.05$ and are displayed in radiological coordinates on an MNI template brain.

6.3.3 Effect of alpha phase on BOLD response to target stimuli

BOLD correlates of phase at stimulus onset were less extensive, though a few activations exceeded the cluster threshold (Table 6.2). The positive vs. negative phase contrast resulted in positive activations in right precuneus and left cerebellum as well as negative correlates in left and right thalamus. The increasing vs. decreasing phase contrast resulted in a negative BOLD correlate in the left middle frontal gyrus.

PHASE

contrast	Nvox	max z	$p_{cluster}$	MNIx	MNIy	MNIz	hem	region
positive > negative	112	3.19	0.0028	6	-56	56	R	precuneus
negative > positive	109	3.54	0.0028	-18	-18	8	L	thalamus
positive > negative	80	3.09	0.0043	-38	-78	-26	L	cerebellum, occipital fusiform gyrus
negative > positive	43	3.25	0.0192	14	-16	6	R	thalamus
decreasing > increasing	39	3.20	0.0233	-38	-4	60	L	middle frontal gyrus, precentral gyrus

Table 6.2: Effect of Prestimulus EEG Alpha Phase on BOLD Response to Auditory Targets. Per-voxel thresholded at $p < 0.005$ then FWE-cluster-corrected at $p < 0.05$.

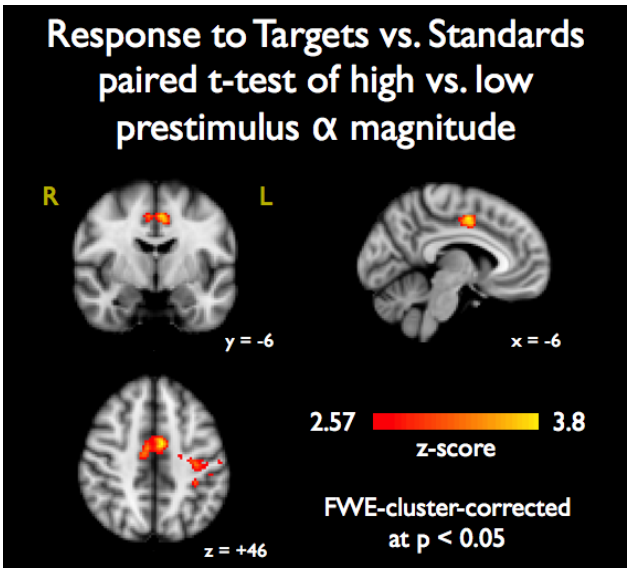

Figure 6.5: BOLD Correlates of Alpha Magnitude and Decision-Related Processing. Results of paired t-test comparing the target vs. standard contrast for low vs. high alpha magnitude prior to stimulus. Images are shown in radiological coordinates on an MNI template.

6.3.4 Effect of prestimulus alpha magnitude on task-related processing

We found a greater difference in the BOLD response to targets as compared to standards (i.e. target vs. standard contrast) in cingulate and contralateral motor areas for the high alpha (low attention) condition (Figure 6.5). Ipsilateral motor areas were also activated, but less extensively. Right inferior, middle, and superior frontal gyri and left LOC were also activated. A complete list of all clusters containing at least 10 voxels can be found in Table 6.3.

6.3.5 Effect of alpha phase on task-related processing

Table 6.4 contains a complete list of all clusters containing 10 or more voxels for the alpha phase paired t-tests of the target vs. standard contrast. For the paired t-test of waxing vs. waning phase (refer to Figure 6.2) we found positive correlates in precuneus, frontal pole, left occipital pole, left superior LOC. Small correlates were detected in left (contralateral) motor areas and right superior temporal gyrus. The positive vs. negative phase t-test (i.e. trough vs. peak) revealed positive correlates in left superior LOC and precuneus. Large negative correlates were found in bilateral thalamus (121 voxels for left and 61 for right, Figure 6.6) along with a smaller correlate in the

MAGNITUDE

paired t-test	Nvox	max z	MNIx	MNIy	MNIz	hem	region
high > low	254	3.77	-6	-4	46	L/R	cingulate gyrus
high > low	105	3.22	-34	-22	46	L	postcentral gyrus, precentral gyrus
high > low	88	3.41	48	40	4	R	frontal pole, inferior frontal gyrus
high > low	86	3.11	-32	-18	70	L	precentral gyrus, postcentral gyrus
high > low	57	3.28	-34	-36	48	L	postcentral gyrus
high > low	51	2.97	50	10	30	R	precentral gyrus
high > low	43	2.87	28	-38	54	R	postcentral gyrus
high > low	32	3.21	-16	-84	26	L	superior lateral occipital cortex
high > low	30	3.09	42	6	38	R	middle frontal gyrus, precentral gyrus, inferior frontal gyrus
high > low	30	2.96	16	-14	62	R	precentral gyrus
high > low	29	3.32	30	-6	64	R	precentral gyrus, superior frontal gyrus, middle frontal gyrus
high > low	28	3.10	24	-16	72	R	precentral gyrus, superior frontal gyrus, postcentral gyrus
high > low	27	3.23	-2	-14	60	L/R	precentral gyrus
high > low	25	2.98	56	-6	-24	R	middle temporal gyrus
high > low	24	3.19	-52	10	34	L	middle frontal gyrus, precentral gyrus, inferior frontal gyrus
high > low	21	2.90	-60	-28	22	L	anterior supramarginal gyrus, postcentral gyrus
high > low	18	3.23	-34	-48	70	L	superior parietal lobule, superior lateral occipital cortex, postcentral gyrus
high > low	17	2.82	-54	18	8	L	inferior frontal gyrus, precentral gyrus
high > low	16	2.83	-36	-62	-42	L	cerebellum
high > low	16	2.94	52	-28	48	R	supramarginal gyrus, postcentral gyrus
high > low	13	2.88	-12	-92	38	L	occipital pole, superior lateral occipital cortex
high > low	12	2.75	42	0	-22	R	planum polare, anterior superior temporal gyrus, insular cortex
high > low	12	2.93	-38	-38	30	L	supramarginal gyrus
high > low	12	2.99	32	10	38	R	middle frontal gyrus, precentral gyrus
high > low	12	3.08	-22	-16	48	L	precentral gyrus, superior frontal gyrus
high > low	11	2.84	62	-18	26	R	anterior supramarginal gyrus, postcentral gyrus
high > low	10	2.87	-16	-18	62	L	precentral gyrus, superior frontal gyrus

Table 6.3: Effect of Prestimulus EEG Alpha Magnitude on Task-related Auditory Processing. Per-voxel thresholded at $p < 0.005$ then cluster size thresholded at 10 voxels.

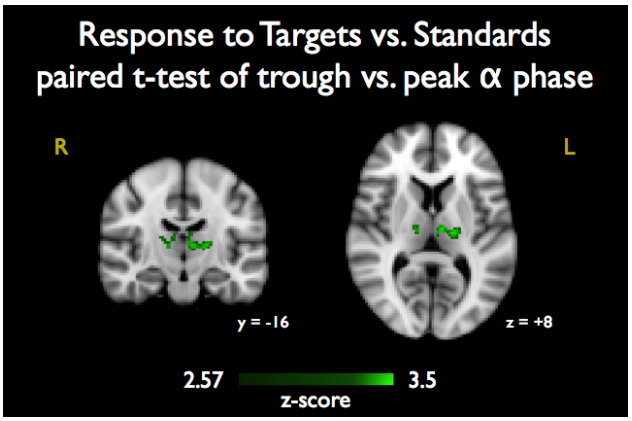

Figure 6.6: BOLD Correlates of Alpha Magnitude and Decision-Related Processing. Results of paired t-test comparing the target vs. standard contrast for trough vs. peak alpha alpha phase at stimulus onset. Images are shown in radiological coordinates on an MNI template.

brainstem, which was very slightly right lateralized. The increasing vs. decreasing t-test resulted in a positive correlate in right hippocampus and negative correlates in left middle frontal gyrus and paracingulate.

6.4 Discussion

We discuss our results mainly as they relate to the existing but limited EEG-fMRI literature investigating how prestimulus EEG alpha affects the BOLD response to visual stimuli. In this context, the novelty of our study is fourfold. Firstly we investigated stimulus processing in the auditory domain using an auditory oddball paradigm. Secondly we explored task-relevant stimulus processing (as opposed to stimuli that subjects ignored). Thirdly, we additionally investigated decision-related processing by contrasting the target vs. standard BOLD responses, and then performing paired t-tests. Fourthly we did not limit our investigation to ROIs, instead exploring the whole brain. Furthermore, only one previous published study (Scheeringa et al., 2011b) has investigated how the phase of the alpha oscillation at stimulus onset correlates with the BOLD response in addition to studying the prestimulus strength of alpha.

PHASE

paired t-test	Nvox	max z	MNIx	MNIy	MNIz	hem	region
waxing > waning	287	3.39	0	-74	36	L/R	precuneus cortex, cuneal cortex, superior lateral occipital cortex
negative > positive	121	3.30	-18	-18	8	L	thalamus
waxing > waning	97	3.24	4	60	4	L/R	frontal pole, paracingulate gyrus
waxing > waning	74	3.20	-10	-94	6	L	occipital pole, supracalcarine cortex,
negative > positive	61	2.97	14	-16	8	R	thalamus
decreasing > increasing	35	2.93	-40	-2	58	L	middle frontal gyrus, precentral gyrus, superior frontal gyrus
increasing > decreasing	28	3.29	20	-14	-18	R	hippocampus, amygdala, parahippocampal gyrus
decreasing > increasing	26	2.91	-12	44	8	L	paracingulate gyrus, anterior cingulate gyrus
waxing > waning	19	2.85	-20	-80	34	L	superior lateral occipital cortex
waxing > waning	17	2.80	62	-8	0	R	superior temporal gyrus
negative > positive	16	2.91	4	-24	-24	R	brainstem
positive > negative	15	2.90	-48	-26	32	L	postcentral gyrus, supramarginal gyrus
waxing > waning	14	3.07	-44	-6	34	L	precentral gyrus, postcentral gyrus, middle frontal gyrus
waxing > waning	13	2.96	-6	-72	48	L	precuneus cortex, superior lateral occipital cortex
positive > negative	12	3.20	-6	-86	50	L	superior lateral occipital cortex, precuneus cortex
increasing > decreasing	11	2.92	48	-42	34	R	supramarginal gyrus
decreasing > increasing	11	2.81	66	4	14	R	precentral gyrus, central opercular cortex
decreasing > increasing	10	2.84	22	2	28	R	caudate

Table 6.4: Effect of Prestimulus EEG Alpha Phase on Task-related Auditory Processing. Per-voxel thresholded at $p < 0.005$ then cluster size thresholded at 10 voxels.

6.4.1 Strength of EEG alpha activity correlates with BOLD activity following behaviorally-relevant auditory stimuli

We found an inverse correlation between prestimulus EEG alpha magnitude and the BOLD response throughout occipital areas and a positive correlate in the cerebellum (Table 6.1). These are consistent with what is seen in resting-state data (Goldman et al., 2002; Liu et al., 2012). Similar results have also been reported for visual task data (Becker et al., 2011; Mayhew et al., 2013), but Scheeringa et al. (2011b) found that after accounting for the underlying intrinsic correlation of the BOLD signal and ongoing alpha oscillations there was no significant effect of prestimulus alpha power on the BOLD response. Their study was able to remove this confound by subtracting the mean "pseudo trial" response (to no stimulus) from the mean "real trial" time courses within visual ROIs. This method was not reasonable in our study given our short (2–3 s) ITI between stimuli that were all relevant to the binary decision making task; our data contained no sufficiently long enough time series segments without task-relevant stimuli from which to create "pseudo trials." We instead addressed this potential confound in a different way, and that is discussed in Section 6.4.3.

6.4.2 Phase of alpha oscillation at stimulus onset affects distribution of BOLD response to auditory target stimuli

We also looked at the relationship of the alpha phase at stimulus onset to the BOLD response to target stimuli, by grouping the trials into 4 phase bins as was done by Scheeringa et al. (2011b) (see Figure 6.2). Our phase analysis shows that the phase of the alpha oscillation at stimulus onset affects the distribution of the BOLD response related to task-relevant stimulus processing. It is difficult to interpret the phase itself, but we see that when alpha oscillation is in one phase (peak/positive amplitude) the thalamus is recruited more strongly than when it is in the opposite phase (trough/negative amplitude). In the case of the trough phase of the alpha wave at stimulus onset, grey matter (right precuneus and left cerebellum) is recruited more strongly than in the peak phase condition. Scheeringa et al. (2011b), whose focus was task-irrelevant visual stimulus processing within visual cortex, found that the BOLD response in BA 17 and BA 18 was significantly greater when stimuli were presented during the trough vs. the peak of the alpha oscillation. We did not detect any supra-threshold (cluster-corrected $p < 0.05$) effect in that area for this auditory task.

6.4.3 Low task-engagement requires recruitment of additional brain regions for decision-related processing

Since the results discussed above (Section 6.4.1) were not directly interpretable based on a possible confound between low frequency BOLD signal fluctuations and the alpha rhythm, we performed an additional investigation. We analyzed the data in such a way that would remove this confound and also include more of the higher level processing such as decision-making, motor planning, and error monitoring. We first contrasted the BOLD response to target vs. standard stimuli, separately for each prestimulus alpha magnitude group (high, medium, low). Significant activations for this traditional type of analysis reveal the brain regions involved in the perceptual decision-making process, along with motor planning and behavioral performance monitoring. We then performed a paired t-test of these target vs. standard contrast for the high vs. low prestimulus alpha conditions, which reveals the effect of alpha on task-related processing.

We found that the main differences are in supplementary motor area (SMA) of the cingulate cortex and contralateral motor areas. These motor area activations are not an effect of RT variability, since RT was not correlated with prestimulus EEG alpha magnitude and we included RT as an additional noise regressor in our fMRI BOLD model. All of our activations resulting from the high vs. low t-test were positive in sign, interpreted as stronger decision-related response when the subject is less engaged in the task prior to the stimulus. This suggests that when task-engagement is low, target stimuli play greater role in refocusing attention to the task. Since the cingulate is commonly associated with self-monitoring of task performance, this large cluster (254 voxels at a $p < 0.005$ per voxel threshold) may represent increased awareness and error checking of the behavioral response following a less-attended target stimulus.

6.4.4 Support for thalamo-cortical loop provided by alpha phase analysis of perceptual decision processes

Although phase is not confounded by any intrinsic correlation of underlying alpha power fluctuations, we performed the same task-related processing investigation as we did for alpha magnitude (Section 6.4.1). We similarly grouped trials (this time into the 4 phase bins, and contrasted target vs. standard BOLD responses. We performed three paired t-tests of these contrasts: positive vs. negative (i.e. peak vs trough), increasing vs. decreasing (i.e. growing more positive or more

negative), and waxing vs. waning (i.e. alpha oscillation moving away from zero vs. toward zero).

We found that the decision-related BOLD response in bilateral thalamic regions was stronger when the stimulus was presented during the trough vs. the peak of the alpha wave. Though results shown (Figure 6.6, Table 6.4 are not thresholded based on cluster size, these activations were both large: 121 voxels in left thalamus and 61 in right thalamus, after a $p = 0.005$ per voxel threshold. This strongly supports the idea of a thalamo-cortical loop for modulation of the alpha rhythm, since here it is the phase of the cortical alpha that is modulating the BOLD response in the thalamus. The specific location appears to be the medial dorsal nuclei, which is consistent with a resting state study (Liu et al., 2012) that aimed to link cortical alpha to specific regions of the nuclei. However, given the resolution of our functional images we cannot identify specific nuclei with certainty.

6.5 Conclusion

The purpose of this study was to explore the influence of our internal attentional state on the neural processing required for a task. We used an easy auditory oddball task that left subjects' minds free to wander, and we simultaneously recorded EEG with fMRI. Our approach was to exploit the known link between attention and EEG alpha activity, treating EEG alpha magnitude prior to each stimulus as an index of task engagement on each trial. We used the fMRI BOLD response as a measure of neural activity related to the auditory task. The aim was then to investigate the relationship between the posterior alpha rhythm and the BOLD response to task-relevant auditory stimuli. Our results are largely consistent with previous findings for visual stimuli but extend to the auditory domain. We additionally investigated the BOLD response related to the perceptual decision making process and found stronger activity in SMA and contralateral motor areas when subjects were in a less attentive state. We conclude that for the high alpha (low attention condition), the subsequent auditory target stimuli pull subjects' attention back to the task, causing them to attend more to their responses and reflect on their performance. We additionally explored the relationship of alpha phase at stimulus onset to the BOLD response, and the activity revealed in bilateral thalamus provides support for a thalamo-cortical loop in attentional modulations.

Chapter 7

Pre-stimulus Pupil Diameter Correlates with Post-stimulus EEG Dynamics

Pupillary measures have been linked to arousal and attention as well as activity in the brainstem's locus coeruleus norepinephrine (LC-NE) system. There is also evidence that evoked EEG responses, such as the P3, might have LC-NE activity as their basis. Since it is not feasible to record electrophysiological data directly from the LC in humans due to its location in the brainstem, an open question has been whether pupillary measures and EEG variability can be linked in a meaningful way to shed light on the nature of the LC-NE role in attention and arousal. In this study we used a data-driven approach to learn task-relevant projections of the EEG for an auditory oddball task, temporally localizing the projections across the entire trial. We correlated the variability of the EEG along these projections with pre-stimulus (baseline pupil diameter) and post-stimulus (maximum evoked pupil dilation) pupillary measures. We found that baseline pupil diameter correlates with early (175–200 ms) and late (350–400 ms) EEG component variability, suggesting a relationship between baseline (tonic) LC-NE activity and evoked EEG. Surprisingly we found no correlation between EEG variability and evoked pupil dilation, which is often associated with evoked (phasic) LC activity. After regressing out reaction time (RT), we found that the correlation between EEG variability and baseline pupil diameter remains, suggesting that such correlation is not explainable

by RT variability. We also investigated the relationship between these pupil measures and pre-stimulus EEG alpha activity, which has been reported as a marker of attentional state, and found a negative correlation with evoked pupil dilation. In summary, our results demonstrate significant correlations between pre-stimulus and post-stimulus neural and pupillary measures, provide further evidence for tight coupling between attentional state and evoked neural activity, and also the role of cortical and subcortical networks underlying the process of target detection.

7.1 Introduction

The locus coeruleus (LC) is a small nucleus located in the dorsal pons. LC is known to have widespread ascending projections throughout the brain, and is the sole source for cortical norepinephrine (NE) (Aston-Jones & Cohen, 2005). Traditional studies have linked the LC- NE system with arousal and attention (Benarroch, 2009). Aston-Jones & Cohen (2005) proposed an adaptive gain theory of LC-NE function that suggests it plays an important role in modulating the trade-off between exploitation and exploration, which ultimately optimizes behavioral performance (Aston-Jones & Cohen, 2005). During the phasic LC mode, LC activity exhibits a strong phasic increase in response to task-relevant stimuli. Conversely, during tonic LC mode, LC experiences an increased level of baseline activity and absence of phasic responses (Abercrombie et al., 1988; Aston-Jones & Cohen, 2005).

In order to further investigate the links between the LC-NE system and brain function in humans, recent studies have suggested using pupil diameter as an index of LC activity (Nieuwenhuis et al., 2010). Although a direct anatomical connection between the LC and pupillary dilator muscle is yet to be determined, baseline pupil diameter has been found to closely track the dynamics of tonic LC activity in monkeys (Rajkowski et al., 1993). Pupil dilation has also been linked with phasic LC activity in previous studies (Gilzenrat et al., 2010).

While simultaneous pupil and fMRI recording enables inferences the relationship between LC activity and activity in spatially localized cortex (Critchley et al., 2005), the limited temporal resolution of fMRI makes it difficult to infer timing relationships in neural processing. While its spatial resolution is limited, scalp electroencephalography (EEG) provides millisecond-range temporal resolution to make such temporally precise inferences. However, with one notable exception (Murphy

et al., 2011), there have been no studies that examine the relationship between LC activity (indexed by pupillary measures) and scalp EEG. Thus potential correlations between LC activity and neural processing at specific post-stimulus times have remained largely unexplored.

While the study of Murphy et al. (2011) investigated links between pupil diameter and two event related potential (ERP) components (the N1 and P3), our present study utilized a data-driven approach to learn the most task-relevant EEG projections, spanning the entire trial, and correlates EEG fluctuations along these projections with pupil diameter. By exploiting this EEG single-trial variability, we were able to identify temporally specific task-relevant EEG components that are significantly correlated with pupil diameter, uncovering key timing information for inferring connections between specific post-stimulus neural processes and LC activity. We also investigated how pre-stimulus neural activity, specifically variability in the magnitude of alpha oscillations, correlates with post-stimulus pupil dilation. EEG alpha power has been shown to negatively correlate with attention and subjects' task engagement prior to each trial (Babiloni et al., 2006; Ray & Cole, 1985; van Dijk et al., 2008). In this way we provided further insight regarding the link between pre-stimulus and post-stimulus cortical and subcortical processes underlying target detection.

7.2 Methods

7.2.1 Subjects and Behavioral Paradigm

Fifteen subjects (7 female; mean age 26.8, range = 20–44 years) participated in the experiment. One participant was excluded because of excessive artifacts in the EEG data. All participants had normal or corrected-to-normal vision and no history of psychiatric illness or head injury. An auditory oddball paradigm with 80% standard and 20% oddball (target) stimuli was used (as described in Section 2.1). This simple target detection task allowed subjects' minds to wander while maintaining near-perfect behavioral response accuracy.

7.2.2 Simultaneous EEG and Pupil Data Acquisition

Experiments were performed in a dark electro-magnetically shielded room, and thus controlled for visual sensory input that might affect the pupil diameter. Throughout the entire experiment, subjects' pupil diameter was measured at a rate of 1 kHz with an EyeLink-1000 infrared eye-tracker

(SR Research, Mississaugu, ON, Canada). Subjects were instructed to fixate on a central white cross for the duration of each run. Subjects' EEG was simultaneously recorded using a 64 scalp electrode ActiveTwo system (Biosemi, The Netherlands) with electrodes in the standard 10/20 configuration. EEG was recorded with at a sampling rate of 2048 Hz.

7.2.3 EEG and Pupil Data Pre-processing

For continuous EEG data, a 0.5 Hz high-pass filter was used to remove DC drift, and 60 Hz and 120 Hz notch filters were used to remove electrical line noise. After standard EEG filtering (Section 2.3.1), the EEG data were re-referenced to the average, run through an anti-alias filter, and down-sampled to 1 kHz to match the sampling rate of the pupil data. For continuous pupil diameter data, periods of blinks were detected using Eyelink's on-line parsing system, and then linearly interpolated in Matlab (The Mathworks, Natick, MA, USA). In order to compare within and across subjects, the pupil trace for each trial was normalized to the mean pupil diameter of the corresponding subject, resulting in a percentage pupil diameter change.

EEG and pupil diameter data were epoched identically, from 1 s prior to 2 s following each stimulus, with baseline removal using the last 200 ms prior to stimulus onset. Trials with large amplitude deflection were excluded from future analyses. We also rejected trials on which subjects failed to respond to target stimuli or responded to standard stimuli.

7.2.4 Single-trial EEG Analysis

We used the same logistic regression sliding window method described in Section 2.4.

7.2.5 Pupil Diameter Analysis

We examined two pupil diameter measurements, namely the baseline pupil diameter and the evoked pupil dilation. The baseline pupil diameter was defined as pupil diameter at stimulus onset time. The evoked pupil dilation was defined as the maximum percentage deviation from baseline pupil diameter within each epoch.

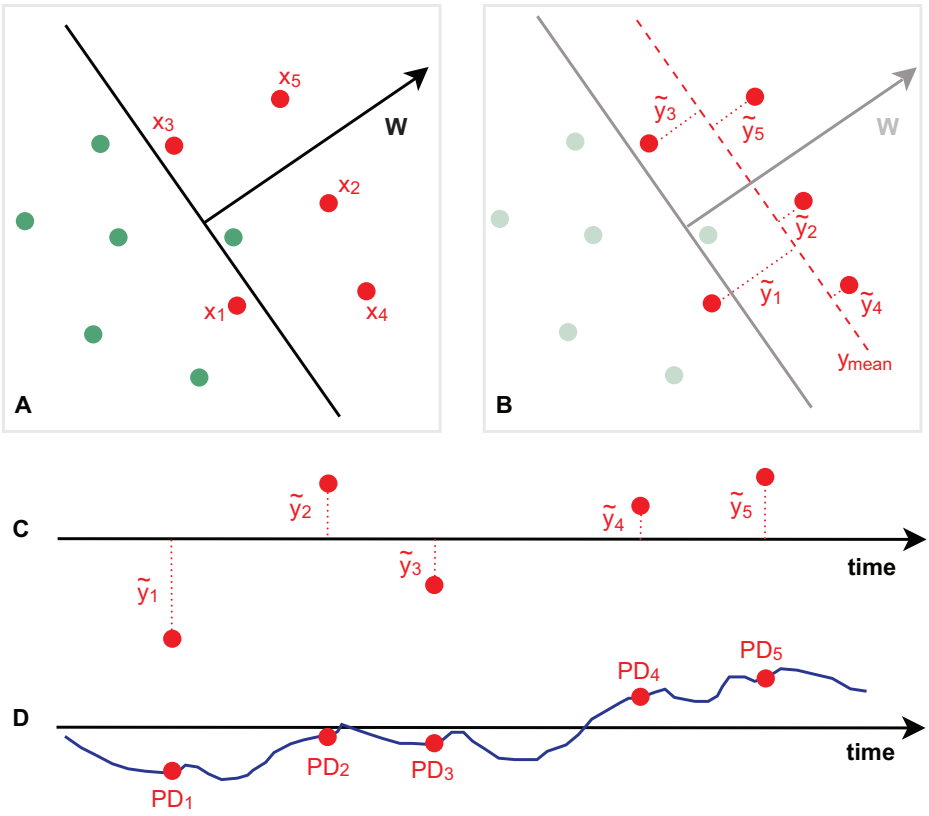

Figure 7.1: Method for correlating EEG single-trial variability with baseline pupil diameter. A. We first estimate $\mathbf{w}$, which is a linear weighting on the EEG sensors that maximally discriminates stimulus conditions: targets (red) vs. standards (green), shown in two dimensions for illustration purposes. This determines a task- relevant projection of the data, where the distance to the decision boundary reflects the decision certainty of the classifier. **B.** From $\mathbf{w}$ we compute $\tilde{y}_i$, which is the demeaned classifier output, $\tilde{y}_i = \mathbf{w}^\top \mathbf{x}_i - y_{\text{mean}}$, for each target trial, i. (In the text we refer to this variable as post-EEG$_{\text{comp}}$). **C.** Given the $\tilde{y}$'s (post-EEG$_{\text{comp}}$) and their corresponding stimulus-onset time points, we compute the correlation with **D.** baseline pupil diameter. This entire method was applied independently for multiple temporal windows, τ, spanning the trial.

7.2.6 Magnitude of Pre-stimulus Alpha Oscillations

Apart from baseline pupil diameter, we also investigated the magnitude of EEG alpha oscillations as another pre-stimulus measurement. Estimation of the alpha activity was performed similarly to Chapter 6 and is described below.

To estimate the magnitude of pre-stimulus alpha oscillations for each target trial, we first performed an independent component analysis (ICA) on the EEG data. We selected a single "alpha component" based on two criteria: (1) the component with the highest ratio of mean power in the 8–12 Hz alpha band relative to mean power in adjacent bands (5–8 Hz theta band and 12–20 Hz beta band) which (2) also had a posterior scalp topography. We estimated the alpha activity from this component using a band-pass filter (with a bandwidth of 4 Hz) centered on the subject-specific alpha frequency, which was determined based on the peak in the power spectral density of the unfiltered EEG. A Hilbert transform (Duoandikoetxea, 2001) was used to construct the envelope of alpha oscillations across time. Lastly, the magnitude of pre-stimulus alpha oscillations for each trial was obtained by averaging this envelope in the –500 to 0 ms time range prior to the stimulus.

7.2.7 Correlation Analysis and Statistics

For each time window, τ, between 0 ms and 1000 ms post-stimulus onset, we correlated the de-meaned output, $\tilde{y}_i = y_i - y_{\text{mean}}$, of the EEG discriminator for each trial, i (see Figure 7.1), with the following four measurements that we described in the preceding sections.

- reaction time (RT)
- magnitude of pre-stimulus alpha oscillations (pre-EEG$_\alpha$)
- baseline pupil diameter (pre-PD)
- evoked pupil dilation (post-PD)

We refer to the EEG discriminating component variability as post-EEG$_{\text{comp}}$. Specifically, Pearson correlation was used for testing the linear relationships between the $\tilde{y}$'s and the four measurements. For each correlation test, we obtained a vector of correlation coefficients for the different time windows, τ, resulting in a progression of correlations over time.

In order to estimate the significance level of these correlations and correct for multiple comparisons, we applied threshold-free cluster enhancement (TFCE) (Smith & Nichols, 2009). The use of TFCE on the time series of correlation values ensured detection of both diffuse, low-amplitude correlations (i.e. weak but long-lasting) and sharp, local correlations (i.e. strong but short-lived). For each of the four measures we tested, we constructed null distributions of TFCE scores by permuting the vector of single-trial measurements 1000 times, computing the correlation tests, and applying TFCE. We used family-wise error (FWE) correction to determine the corrected $p<0.05$ threshold.

In order to tease apart correlates that were observable in RT from latent variability in the post-EEG_{comp}, we repeated the correlation analyses after linearly regressing out RT from the discriminating component variability $\tilde{y}$.

Our primary analyses focused on correlations between the EEG discriminating component variability of target trials with RT, pre-EEG_{α}, pre-PD and post-PD. We also investigated pairwise correlations between these attention-related measures. In this way, we were able to study the relationships between behavioral, neural and pupillary measurements both before and after the stimulus.

7.3 Results

7.3.1 Behavioral Performance

All fourteen subjects performed the task at high accuracy with $99.3\% \pm 0.2\%$ of targets correctly detected. Average reaction time (RT) was 398.4 ± 23.9 ms.

7.3.2 Trial-averaged Evoked Analysis

We first analyzed trial-averaged event-related potentials (ERPs) and evoked pupil responses for both target and standard trials, quantifying the magnitude of the differences in the average evoked activity. Figure 7.2 shows the resulting ERPs. The N1-P2 complex can be seen at fronto-central electrode sites (Fz, Cz), followed by the N2 component, which was larger for targets than standards on posterior scalp sites (shown on Pz). In contrast, anterior N2 was larger for standards than targets, as seen from frontal and central electrodes (Fz, Cz). This is consistent with results from

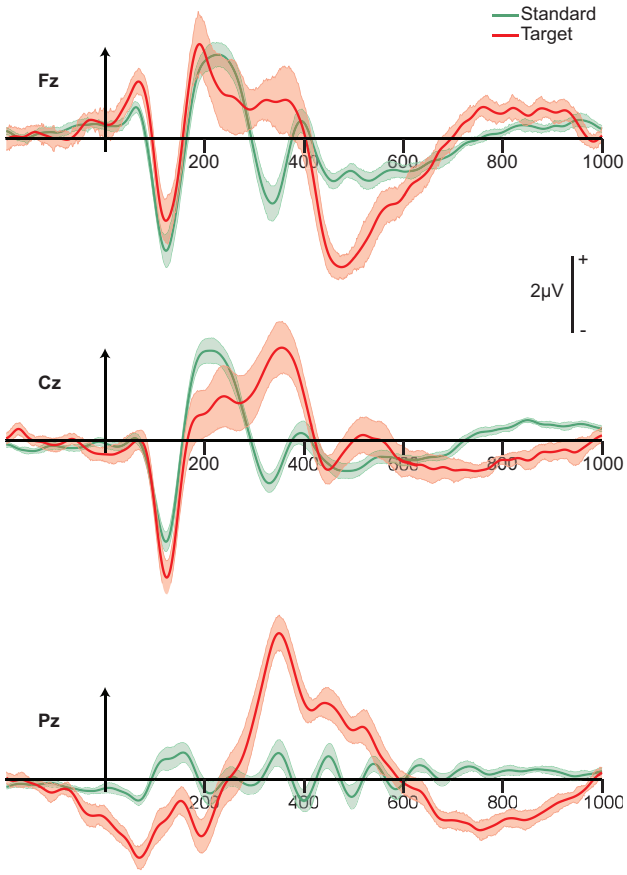

Figure 7.2: Grand mean ERPs at electrodes Fz, Cz and Pz. Shown are grand average (N=14) stimulus-locked curves from 200 ms pre-stimulus to 1000 ms post-stimulus for target (red) and standard (green) stimuli, with shaded bands indicating standard error.

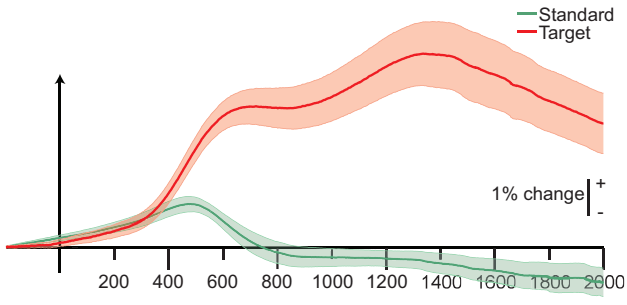

Figure 7.3: Evoked pupil dilation. Grand average (N=14) stimulus-locked curves from 200 ms pre-stimulus to 2000 ms post-stimulus for target (red) and standard (green) stimuli, with shaded bands indicating standard error. Traces have units of percentage change from the mean.

many oddball paradigms (Folstein & Van Petten, 2008). Lastly, the P3 component was evident and most prominent on the parietal (Pz) electrode, peaking at approximately 350 ms post-stimulus.

Both target and standard stimuli evoked pupil diameter increases (Figure 7.3). An early dilation peak was seen at 500–600 ms post-stimulus for both standard and target trials. This is consistent with the results of Steinhauer & Hakerem (1992), who described pupil dilations caused by inhibition of parasympathetic pathways. The primary dilation, i.e. the maximum pupil dilation evoked by target stimuli, was reached at approximately 1350 ms. Consistent with well-established pupillometry findings, the pupil dilation following target stimuli was larger than the dilation following standards (Steinhauer & Hakerem, 1992).

7.3.3 Single-trial Task-relevant EEG Components

We next analyzed the single-trial EEG in order to correlate fluctuations in pupil diameter with the temporally localized task-relevant EEG. Group mean single-trial EEG discriminator performance (shown in Figure 7.4A) was significant for all consecutive windows between 75 ms and 850 ms post-stimulus ($p < 0.01$ for AUC > 0.62, computed via permutation test). The subject-averaged performance reached its peak of AUC $= 0.91$ at 350 ms. Corresponding forward models for a subset of windows with significant discrimination are shown in the top row of Figure 7.4C. Discriminating activity around 200 ms was strongest at central sites and more negative for targets compared to standards. This spatial distribution and peak latency was characteristic of the N2 component. In addition, strong positive activity at parietal sites lasted from 350 ms to 500 ms and was consistent with the P3.

7.3.4 Correlation Analysis

We next conducted our correlation analysis between post-stimulus EEG discriminant component variability for target trials (which we refer to as post-EEG_{comp}, representing $\tilde{y}_i$'s for target trials for each window τ) and behavioral and pupil diameter measurements. First we considered correlations between post-EEG_{comp} and RT. Figure 7.4B indicates significant negative correlation between these two measurements for all but two consecutive windows from 150 ms to 575 ms. Previous work has shown that much of the LC activity and the late phases of the P3 response are locked to reaction time (Aston-Jones & Cohen, 2005; Gerson et al., 2005). In order to capture variability that is unique

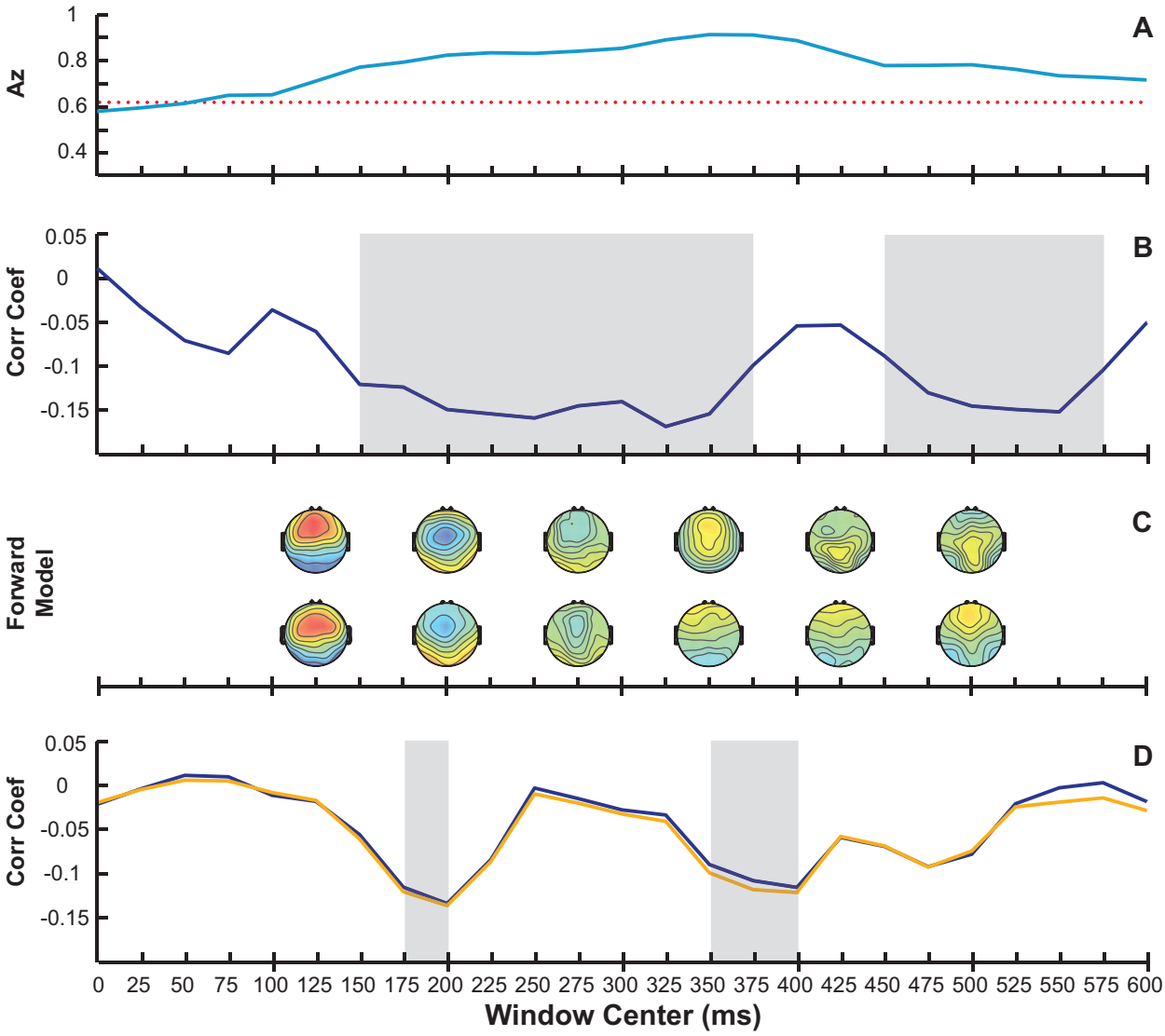

Figure 7.4: Correlation between RT, baseline pupil diameter (pre-PD) and EEG component variability (post-EEG$_{\text{comp}}$). Shown are group-level results for EEG windows spanning the trial, with shaded regions denoting p<0.05 (corrected) significance. **A.** EEG classifier performance as defined by area under the ROC curve (blue trace). p = 0.01 (AUC = 0.61) threshold is indicated with a red dotted line. **B.** Correlation coefficients between RT and post-EEG$_{\text{comp}}$ (classifier output y) as a function of window time. **C.** Subset of scalp topographies generated using y (top row) and residual y (after regressing out RT, bottom row). Color represents correlation between the discriminating component and the data (red = positive, blue = negative, green = 0). **D.** Correlation coefficients between pre-PD and post-EEG$_{\text{comp}}$ before (purple trace) and after (orange trace) regressing out RT.

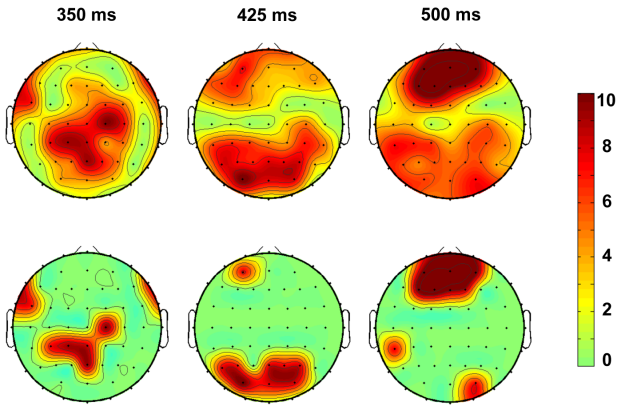

Figure 7.5: Statistical differences between forward models before and after regressing out RT. Pairwise t-tests were conducted on each electrode using forward models before and after regressing out RT, with h denoting the test decision (0 or 1) and p denoting the significance level. Shown are –log(p) and –log(p) × h values (top and bottom row, respectively) for selected windows.

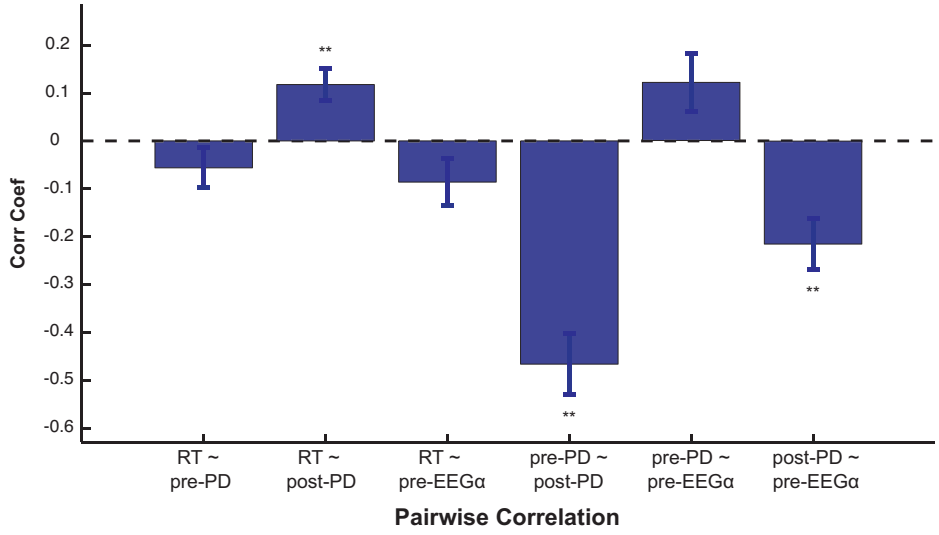

Figure 7.6: Pairwise correlations between RT, baseline pupil diameter, evoked pupil dilation and magnitude of pre-stimulus alpha. Shown are correlation coefficients between the four measurements: RT, pre-PD, post-PD and pre-EEG$_\alpha$. Standard error bars are across subjects (N=14). Significant correlations ($p < 0.01$) are denoted by double asterisks, with dashed line at zero correlation.

to the EEG latent states and not attributable to behavioral measures, such as RT, we regressed out RT from post-EEG_{comp}. The bottom row in Figure 7.4C shows the resulting forward models after the linear contribution of RT variability was removed. The major difference between these scalp topologies and the ones prior to decorrelating with respect to RT was seen during the P3 time window of 350 ms to 500 ms. Regressing out RT significantly reduced the posterior activations typically associated with the P3b, while making more apparent the frontal contributions associated with the frontal P3 (P3f) (see Figure 7.5). These results are consistent with the findings of Gerson et al. (2005); they showed a fronto-parietal transition of the P3 complex that begins with a stimulus locked P3f and ends with a classic response locked parietal P3b topography.

Figure 7.4D shows the results of correlating pre-PD with post-EEG_{comp} before and after regressing out RT from post-EEG_{comp}. Though regressing out RT did significantly change the forward models, it did not significantly change the correlations between pre-PD and post-EEG_{comp} (compare orange vs. purple curves in Figure 7.4D). The timing of significant correlations between pre-PD and post-EEG_{comp} aligned with the latencies of the N2 and P3 ERPs.

We investigated several additional correlations in our analysis. First we looked at whether pre-stimulus alpha (pre-EEG_{α}) covaried with post-EEG_{comp}. Previous work has suggested a link between pre-stimulus oscillatory measures and post-stimulus evoked responses (Rajagovindan & Ding, 2011). We found no significant correlations between pre-EEG_{α} and post-EEG_{comp} (highest correlation at $\tau = 450$ms, $p > 0.05$). However we did find significant correlations between pre-EEG_{α} and post-PD (see Figure 7.6). Figure 7.6 also shows pairwise correlations between the four measurements. Notably, post-PD is negatively correlated with pre-EEG_{α} .

7.4 Discussion

Our study investigated relationships between pre-stimulus and post-stimulus pupil and EEG measurements that have all been independently linked to attention, arousal, or anticipation. A summary of our findings is shown graphically in Figure 7.7. We based our analysis only on target trials (i.e. for identical stimuli), so the obtained EEG variability was driven purely by endogenous factors, primarily instantaneous attention to the task and anticipation for upcoming target stimuli. Therefore our results enable inferences of functional interactions between pre-stimulus and post-stimulus

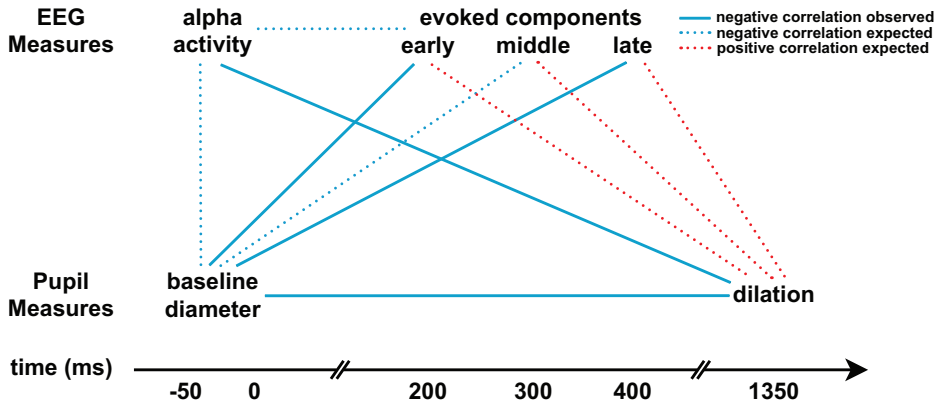

Figure 7.7: Summary of pairwise relationships between pupil and EEG measures. All measures are aligned according to their temporal order. Pre-stimulus measures of endogenous attentional state include baseline pupil diameter and magnitude of pre-stimulus EEG alpha oscillations. Post-stimulus measures (evoked responses) include EEG discriminating components at different window offsets (early ≈200 ms, middle ≈300 ms, late ≈400 ms) and evoked pupil dilation. Significant ($p<0.05$, corrected) findings are shown with solid lines, where red indicates positive correlation and blue negative. Dotted lines denote relationships that were hypothesized based on previous literature but not detected in our study.

neural processes that are known to modulate with various endogenous brain states.

Consistent with previous literature (Kammer et al., 1999), we found that much of the post-stimulus evoked EEG single-trial variability is reflected in the RT (Figure 7.4B). This demonstrated the need to regress out the RT variability, in that our goal was to study latent brain states. Within Section 7.4, unless otherwise noted, post-EEG_{comp} refers to the residual y's of targets after regressing RT out of the classifier output.

7.4.1 Baseline pupil diameter correlates with early and late neural responses

Prior work using highly invasive neurophysiological recordings in primates has demonstrated a close link between pre-stimulus pupil diameter and tonic LC activity (Aston-Jones & Cohen, 2005), which can be exploited to make inferences about LC activity in humans (Murphy et al., 2011). In contrast to the work of Murphy et al. (2011), which investigated single-trial pupil diameter correlates with only N1 and P3 ERP components, our study utilized the most task-relevant EEG projections spanning the entire trial and investigated their pupil diameter correlates. This approach enabled us to temporally localize specific task- related EEG components that are significantly correlated

with pupil measures, teasing them apart from EEG components that do not possess such pupil correlates.

We found negative linear relationships between post-EEG_{comp} and pre-PD within two post-stimulus time ranges. The late post-EEG_{comp}, at 350–400 ms, are closely related to the P3 ERP component, as evidenced by the ERP traces and forward models. Significant correlations between pre-PD and late post-EEG_{comp} suggest a relationship between underlying tonic LC activity (indexing arousal) and decision- related processing. We found no significant correlations between middle post-EEG_{comp} and pre-PD, suggesting that tonic LC activity does not influence task-related neural processing around 300 ms post-stimulus.

The early post-EEG_{comp} around 175–200 ms are representative of the N2 ERP component, which has not yet been studied in relation to pupil measurements. Our study found no correlations between pre-PD and neural responses at the typical N1 time, consistent with the findings of Murphy et al. (2011). Nevertheless, the correlation we found between pre-PD and EEG activity at 200 ms possibly indicates the influence of pre-stimulus tonic LC activity on early sensory processing of target stimuli.

7.4.2 Evoked pupil dilation correlates with pre-stimulus pupil diameter but not evoked EEG responses

As described by Aston-Jones & Cohen (2005), the fluctuations of tonic LC activity are known to affect the stimulus-driven phasic responses. In this study, we found that maximum pupil dilation is negatively correlated with baseline pupil diameter, which is consistent with the reports of Gilzenrat et al. (2010) and Murphy et al. (2011). Since our experiment was conducted in a dark room with the fixation cross supplying only very low ambient light, it was likely that the observed post-PD responses reached the physiological limit of the pupil. Therefore, the negative correlation between pre-PD and post-PD might have resulted simply because the pupil could not dilate any further on trials with high pre-PD (Lacey, 1956), an artifact caused by the limited dynamic range of the pupil. We also observed negative correlations between post-PD and pre-EEG_{α} ; further discussion regarding this relationship can be found below.

Since phasic LC activity has been linked to both evoked pupil dilations and the P3 ERP component, we initially expected to observe correlations between our post- PD measurement and post-

EEG_{comp}. However, although we found both post-PD and post-EEG_{comp} to be significantly correlated with pre-PD, our analysis did not detect any correlation between these two measures (refer to dotted red lines in Figure 7.7). Prior work also failed to detect such expected correlations between P3 ERP component variability and pupil dilations (Murphy et al., 2011). Multimodal studies with simultaneous pupillometry, EEG, and fMRI recording may be required for better understanding why this correlation is not seen with EEG and pupil measures alone. (Murphy et al., 2011) discussed possible sources of variance that obscured a more direct relationship between pupil dilation and P3 ERP component. One of the measurement issues mentioned is that pupil dilation and P3 have markedly contrasting latencies, and it is possible that they may reflect different combinations of distinct information processing stages.

As discussed in the previous section, decision-related cognitive processing may act as an early (prior to the P3) mediating factor in a chain of processes, while internally-driven performance monitoring after the behavioral response likely acts as a later mediator of neural activity. Furthermore, as Murphy et al. (2011) pointed out, the pupil dilation occurs on a much longer time scale than evoked neural responses, which allows additional endogenous processes to participate and influence the response. These mediating factors can potentially add enough variance to obscure a more direct connection between pupil dilation and neural responses.

7.4.3 RT is not closely linked with baseline pupil diameter

Previous animal studies have reported an inverted U-shaped relationship between tonic LC activity and task performance (Aston-Jones & Cohen, 2005), in which task performance is optimal during intermediate states of tonic LC activity. Murphy et al. (2011) reported this inverted U-shaped relationship between pre-stimulus pupil diameter and RT coefficient of variation, and thus suggested this quadratic relationship between pupil diameter and task performance supported the hypothesis that pre-stimulus pupil diameter is a valid proxy for tonic LC activity in humans. However, our study found no significant correlations between RT and pre-PD. One possible explanation is that while baseline pupil diameter fluctuates from trial to trial, RT does not exhibit much variability since all subjects responded quickly and achieved near-perfect accuracy throughout the experiment. We conclude that RT can hardly be treated as task performance in easy tasks such as oddball detection, and for that reason, this lack of correlation between pre-stimulus pupil diameter and RT

also suggests that tonic LC activity is not likely the source of RT variability.

Although we found no linear relationship between pre-PD and RT, we observed negative correlations between RT and post-EEG_{comp} for the majority of windows spanning the trial, which was expected based on previous findings on negative correlations between RT and ERP amplitudes (Gajewski et al., 2008). We also observed that large pupil dilations were linked with longer RTs.

7.4.4 Pre-stimulus alpha modulations correlate with evoked pupil dilation

It is well known that power in the EEG alpha band (8–12 Hz) is negatively correlated with attention to the task (Vazquez et al., 2001). High pre-stimulus alpha (i.e., low attention) has been linked with decreased behavioral response accuracy, but not with longer RTs. Consistent with previous literature, we found no correlation between pre-stimulus alpha and RT, but we did find a significant negative correlation between the magnitude of pre-stimulus alpha oscillations and the evoked pupil dilation. To the best of our knowledge, pupil measures have not been studied in relation to EEG alpha until now. Since pupil dilation has been proposed to index phasic LC activations (Murphy et al., 2011), our observed negative correlation between post-PD and pre-EEG_{α} could represent a connection between pre-stimulus attentional state and post-stimulus phasic LC activation.

Since we found evoked pupil dilations to have strong negative correlations with both pre-EEG_{α} and pre-PD, we might expect to find a relationship between these two measures of pre-stimulus attentional states. However, we did not find any significant correlation between pre-PD and pre-EEG_{α} . A possible explanation is that although both measures reflect endogenous attentional state to some extent, pre-PD is more closely tracking general arousal while pre-EEG_{α} is tracking task-related attention.

7.5 Conclusions

In this study, we used a data-driven analysis to investigate the complex dynamic relationships between pupillary measures and EEG variability. Specifically, we investigated correlations between pre-stimulus (baseline pupil diameter, magnitude of EEG alpha oscillations) and post-stimulus (evoked pupil dilation, temporally-specific EEG components) physiological variables that have all been independently linked to attention. Here by identifying correlates of temporally specific post-

EEG_{comp} with pre-PD, we provide key timing information regarding functional relationships between specific post-stimulus endogenous processes and pre-stimulus tonic LC activity. We believe our findings will promote future studies on utilizing noninvasive measurements to further investigate and index LC activity in a more direct way.

Chapter 8

Conclusions

8.1 Significance

No one is able to maintain fully focused attention to a task, and mind wandering is particularly inevitable during mundane tasks. In daily life for normal humans, the outcome of these attentional fluctuations is often limited to decreased productivity (e.g. slow or poor digestion of a journal article) but in rare cases the result can be deadly (e.g. inattentive driving leading to a fatal accident). The ability to track waning attention before it affects behavioral performance could thus lead to development of brain computer interfaces (BCIs) that optimize task performance and improve safety. This thesis work took steps toward a clearer understanding of the function and interaction of various attentional systems in healthy humans, which will lead to investigations of disordered attention networks. This work has even greater implications for the diagnosis and treatment of neurological disorders that affect task-engagement and general attention, including attention-deficit hyperactivity disorder (ADHD), Alzheimer's disease, Parkinson's disease dementia, traumatic brain injury, and stroke.

8.2 Summary

This thesis focused on the neural activity associated with naturally-fluctuating task-related attention, and investigated this activity non-invasively in healthy human subjects. Such endogenous modulations of attention are by definition not related to external events, so any attempt to control

them would negate the experiment. To overcome this challenge, we exploited well-known links between EEG and pupil measurements and endogenous attention. The EEG and pupil measurements provided a way to index internal attentional state during each trial of the experiments. We used multi-modal neuroimaging, namely simultaneous EEG-fMRI and EEG-pupillometry, and investigated correlates of these measurements in the simultaneously-acquired data.

In the EEG-fMRI studies of Chapters 3, 4, and 5, we used the amplitude of event-related EEG responses to represent attention to the tasks on each trial, and we used this to construct regressors for the fMRI general linear model (GLM). This approach required dimensionality reduction from the original 43-channel EEG space, which we achieved by applying machine learning methods to the EEG data to find the most task-relevant projections. The linear classifier output one scalar value for each trial, which served as an index of task-related attention. Results of the EEG-based fMRI analysis revealed brain regions with activity that modulates with attentional state. The fMRI data provided these correlates in both cortical and deep subcortical structures at high spatial resolution. Since multiple event-related EEG components with various latencies are known to have amplitude that modulates with attention, we repeated this analysis for narrow windows of EEG data spanning each trial, and this provided information about the temporal cascade of attention-related activity at high temporal resolution.

Since the behavioral response time (RT) is also highly correlated with endogenous attention, we first regressed out any variability correlated with RT, and this enabled us to study fluctuations of attention that are not observable in external events. We found that many brain regions previously shown to couple with EEG responses have variance that is completely reflected in the RT, while the variability in other areas is latent. We investigated these correlates specific to auditory (Chapter 3) and visual tasks (Chapter 4), as well as those that generalize across sensory input domains (Chapter 5). This enabled us to tease apart the temporal order and functional significance of the activations. Without aiming to study functional networks, which are commonly studied in resting-state fMRI data, we found correlates of EEG single trial variability in the default-mode network (DMN), ventral attention network (VAN), locus coeruleus norepinephrine (LC-NE) system, and areas previously implicated in the P300 target-related EEG response. Our DMN finding was specific to the visual domain and the others were shown to generalize.

In the novel supra-modal investigation that combined auditory and visual data at the subject

level (Chapter 5), we expanded upon our results by performing dynamic causal modeling (DCM) on the fMRI data. Using our EEG-based GLM clusters as regions of interest (ROIs), we designed and tested models to further investigate functional interactions between these attention systems. We found strong evidence for reciprocal connections between cortical networks and the brainstem. In addition to providing support for this theorized link using non-invasive methods in healthy humans, our results suggest that ACC activity early in the trial influences the phasic response of the LC, which then modulates activity in a number of attention-related cortical regions.

In the EEG-fMRI study described in Chapter 6, we used EEG activity to index endogenous attention in a different way. Power of the ongoing posterior EEG alpha oscillation is commonly associated with attention, so we used an estimate of its magnitude immediately prior to stimulus onset as a surrogate for attentional state on each trial. We contrasted the BOLD response related to the simple auditory perceptual decision for low vs. high attentional state to investigate the influence of subjects' internal attentional state on the neural processing required for a task. Our activations in primary and supplementary motor areas suggest that during periods of waning attention, target stimuli act to re-focus subjects' attention and lead them to monitor their behavioral performance. We additionally explored the relationship of EEG alpha phase at stimulus onset to the BOLD response, and the activity revealed in bilateral thalamus provides evidence for a thalamo-cortical loop in attentional modulations. Our findings are largely consistent with the limited alpha-EEG-fMRI literature, which all investigates task-irrelevant visual stimulus processing, but we extend our work to task-relevant decision-related processing in the auditory domain. Furthermore, we do not limit our fMRI analysis to ROIs, allowing us to make inferences regarding correlates of attentional fluctuations across the brain.

Finally, the EEG-pupillometry study of Chapter 7 exploited the close link between pupil size and activity in the LC-NE system, which modulates arousal and attention. Neural activity within the LC nucleus is particularly difficult to study in humans due primarily to its location within the brainstem. We used pupil diameter prior to stimulus as a surrogate for tonic LC activity since these have been shown to closely track each other in monkey studies. We again used our machine learning methods and our alpha EEG methods to generate EEG-based measures of attention. We then investigated pairwise correlations between attention-related EEG measurements and pupil diameter measurements, some of which were post-stimulus responses to target stimuli and some of

which were pre-stimulus measures of underlying attentional state. The sliding EEG window method enabled us to separately investigate correlates of attention at multiple temporal offsets spanning the trial, to determine which specific components of the evoked EEG response are influenced by LC activity. We again regressed out the affect of RT variability to focus our study on latent brain states. We found that both early and late (but not middle time range) EEG components correlate negatively with pupil diameter prior to stimulus onset, suggesting these components are modulated by tonic LC activity. We also found a negative correlation between the pre-stimulus EEG alpha magnitude and the evoked pupil response to auditory target stimuli, which can be related to the phasic LC response.

All of the studies described within this thesis investigated neural activity related to simple perceptual decision making tasks, and in particular how this activity is modulated by endogenous attentional state. We focus on fluctuations that are not detectable in behavioral response and not related to individual stimulus properties. Our data-driven multimodal methods were able to reveal information regarding temporally-specific functional interactions between known attention systems, some of which generalize across sensory input modality.

8.3 Pitfalls and Limitations

One of the first steps in this thesis work was to transition the auditory oddball EEG-fMRI study of Goldman et al. (2009), which used a 1.5T scanner, and expand upon it to include a visual task. We used a higher-field 3T scanner, providing a greater signal-to-noise ratio (SNR) of the fMRI signal and higher resolution functional images. However, this came at the potential cost of EEG discrimination performance, due to reduced SNR in the EEG caused by increased magnitude of magnetically-induced artifacts. This sacrifice in SNR, if large enough to decrease discrimination performance, would decrease the significance of the BOLD activations. We were able to overcome this limitation by increasing the saliency of our auditory and visual target stimuli.

Precise temporal localizations are difficult in traditional fMRI studies due to the slow, diffuse, and indirect nature of the BOLD measurement and to spatial variations in the HRF. Our method of combining single-trial EEG variability with fMRI was able to circumvent this limitation by finding BOLD correlates of the electrophysiological response at multiple temporal offsets. Despite the

temporal information it provides, our EEG-based GLM method is unable to infer causality. While effective connectivity fMRI analysis techniques such as DCM aim to infer causal relationships in a physiologically meaningful way, interpretation of the results are controversial. Hypothesis-based models compete against each other, and the winning model is used to make inferences about neural activity. The winning model is not necessarily a well-fit model—just the best fitting of the models that were tested. It is unrealistic if not impossible to test every permutation of intrinsic connectivity between the selected ROIs; even when including a small number of ROIs ($\ll 10$) the number of possible models is enormous.

Our EEG-based fMRI analysis methods reveal BOLD correlates of modulations in task engagement. We would intuitively expect positive activations to appear in areas that are more active when the subject is task-engaged and negative activations to appear when the subject is mind-wandering. However, it has been shown that low frequency electrophysiological variations, such as those measured by scalp EEG, are negatively correlated with the BOLD response (Mantini et al., 2007; Mukamel et al., 2005; Scheeringa et al., 2011a). The open question about the physiological meaning of directionality of electrophysiological BOLD correlates remains, and this leads to challenges in the interpretation of results.

Another challenge when using simultaneously-acquired EEG data to model the fMRI signal is dimensionality reduction. There are too many EEG channels to simply input their signals as individual GLM regressors. Additionally, the mismatched sampling rates of EEG and fMRI (milliseconds vs. seconds) as well as the very different timescales of the signals being measured (electrophysiology vs. hemodynamic activity) would render such a model essentially meaningless. Selection of a subset of electrodes or independent component analysis (ICA) projections can be arbitrary. Our machine learning methods were able to determine the most task-relevant projection of the EEG data and thus avoid an arbitrary electrode selection. Since this was performed for multiple windows of EEG data spanning the trial, it also avoided an arbitrary selection of ERP components at various latencies, which is common method reported in the literature. In the alpha analysis we selected our ICA projection based on specific criteria and were confident that we were investigating a meaningful attention-related projection of the EEG data. However, there exist multiple independent component projections possessing high ongoing alpha power, but which are out of phase with each other. For this reason, BOLD contrasts related to alpha phase at stimulus

onset must be interpreted with caution. Results can be viewed as a comparison between opposite phase conditions but inferences should not be made about the particular phase of the oscillation.

The EEG-pupil study described here investigated linear correlations between pre-stimulus and post-stimulus measures of attentional state; however, there is evidence to suggest existence of nonlinear relationships between LC activity and attention. Therefore, our negative findings cannot exclude the possibility of more complex relationships between these metrics.

8.4 Future Work

Follow-up studies beyond the scope of this thesis should use spectral analysis of EEG to explore the EEG frequency and BOLD directionality relationship. It would be particularly interesting to explore whether EEG spectral dynamics are responsible for the sign reversals we observed in the visual task results near RT and then shortly after the response. Frequency-dependencies of our numerous activations should also be investigated independently, since common resting-state networks have been associated with specific EEG frequency bands (Mantini et al., 2007) and some are anti-correlated with each other. The community should not neglect BOLD signals detected in white matter and draining veins, since they can provide a clearer understanding of the neural activity occurring upstream. Future studies should utilize diffusion tensor imaging (DTI) or arterial spin labeling (ASL) and co-registration with high resolution anatomical and functional MRI to investigate the EEG-based fMRI correlates we found in draining veins.

While this dissertation work made great strides toward understanding interactions between attention systems, causality remains an open question. Transcranial magnetic stimulation (TMS) is the optimal method to investigate causal relationships between neural activity in specific brain regions, since it is noninvasive and can thus be performed on healthy humans. Future studies should use TMS to test causal relationships and provide confident conclusions about dynamic causal interactions.

High SNR is valuable in all signal analyses, and particularly in fMRI where BOLD changes are tiny relative to the underlying signal. Future EEG-fMRI studies in our lab will use an upgraded and more user-friendly MR-compatible EEG system to provide greater quality EEG data. This new system can be used with a multiple channel MRI gradient coil, which will increase the SNR

of the fMRI data. Together this will enable studies of more complex tasks, including difficult decision-making tasks involving more natural stimuli.

The EEG-fMRI data of this thesis is proving its utility in the development and exploration of new data fusion methods, due to the simplicity of the auditory and visual oddball tasks and the special care taken during data acquisition. A fast bootstrapping and permutation testing technique for assessing reproducibility and interpretability of multivariate fMRI decoding models (called FaSTGLZ) has already been developed (Conroy et al., 2013a,b). Techniques of linking EEG and fMRI classifiers are also currently being explored.

An obvious next step in the EEG-pupil research project is to investigate quadratic relationships between pupil diameter and EEG measurements, and this work is already in progress. We believe our EEG-pupil work will promote future studies that use noninvasive measurements to further investigate and index LC activity. Simultaneous EEG, fMRI, and pupillometry experiments specifically designed to test hypotheses of LC-NE system behavior have the potential to provide much needed insight into the mechanistic role of this system.

Bibliography

Abercrombie, E. D., Keller, J., R. W., & Zigmond, M. J. (1988). Characterization of hippocampal norepinephrine release as measured by microdialysis perfusion: pharmacological and behavioral studies. *Neuroscience*, *27*(3), 897–904.

Arthurs, O. J., & Boniface, S. (2002). How well do we understand the neural origins of the fMRI BOLD signal? *Trends Neurosci*, *25*, 27–31.

Astafiev, S. V., Snyder, A. Z., Shulman, G. L., & Corbetta, M. (2010). Comment on "modafinil shifts human locus coeruleus to low-tonic, high-phasic activity during functional MRI" and "homeostatic sleep pressure and responses to sustained attention in the suprachiasmatic area". *Science*, *328*(5976), 309.

Aston-Jones, G., & Cohen, J. D. (2005). An integrative theory of locus coeruleus-norepinephrine function: adaptive gain and optimal performance. *Annu Rev Neurosci*, *28*, 403–50.

Aston-Jones, G., Rajkowski, J., Kubiak, P., & Alexinsky, T. (1994). Locus coeruleus neurons in monkey attended cues in a vigilance task activated by attended cues in a vigilance task. *J Neurosci*, *14*, 4467–4480.

Babiloni, C., Vecchio, F., Bultrini, A., Luca Romani, G., & Rossini, P. M. (2006). Pre- and poststimulus alpha rhythms are related to conscious visual perception: a high-resolution EEG study. *Cereb Cortex*, *16*(12), 1690–700.

Banerjee, S., Snyder, A. C., Molholm, S., & Foxe, J. J. (2011). Oscillatory alpha-band mechanisms and the deployment of spatial attention to anticipated auditory and visual target locations: supramodal or sensory-specific control mechanisms? *J Neurosci*, *31*(27), 9923–9932.

Barry, R. J., Kirkaikul, S., & Hodder, D. (2000). EEG alpha activity and the ERP to target stimuli in an auditory oddball paradigm. *Int J Psychophysiol*, *39*(1), 39–50.

Becker, R., Reinacher, M., Freyer, F., Villringer, A., & Ritter, P. (2011). How ongoing neuronal oscillations account for evoked fMRI variability. *J Neurosci*, *31*(30), 11016–27.

Benar, C.-G., Schn, D., Grimault, S., Nazarian, B., Burle, B., Roth, M., Badier, J.-M., Marquis, P., Liegeois-Chauvel, C., & Anton, J.-L. (2007). Single-trial analysis of oddball event-related potentials in simultaneous EEG-fMRI. *Hum Brain Mapp*, *28*, 602–13.

Benarroch, E. E. (2009). The locus ceruleus norepinephrine system: functional organization and potential clinical significance. *Neurology*, *73*(20), 1699–704.

Biancardi, M., Fukanaga, M., van Gelderen, P., de Zwart, J. A., & Duyn, J. H. (2011). Negative BOLD-fMRI signals in large cerebral veins. *J Cereb Blood Flow Metab*, *31*, 401–412.

Bledowski, C., Prvulovic, D., Goebel, R., Zanella, F. E., & Linden, D. E. J. (2004a). Attentional systems in target and distractor processing: a combined ERP and fMRI study. *NeuroImage*, *22*, 530–40.

Bledowski, C., Prvulovic, D., Hoechstetter, K., Scherg, M., Wibral, M., Goebel, R., & Linden, D. E. J. (2004b). Localizing P300 generators in visual target and distractor processing: a combined event-related potential and functional magnetic resonance imaging study. *J Neurosci*, *24*, 9353–60.

Boly, M., Balteau, E., Schnakers, C., Degueldre, C., Moonen, G., Luxen, A., Phillips, C., Peigneux, P., Maquet, P., & Laureys, S. (2007). Baseline brain activity fluctuations predict somatosensory perception in humans. *Proc Natl Acad Sci U S A*, *104*(29), 12187–92.

Bouret, S., & Sara, S. J. (2005). Network reset: a simplified overarching theory of locus coeruleus noradrenaline function. *Trends Neurosci*, *28*, 574–82.

Bressler, S. L., & Menon, V. (2010). Large-scale brain networks in cognition: emerging methods and principles. *Trends Cogn Sci*, *14*(6), 277–90.

Brookes, M. J., Woolrich, M., Luckhoo, H., Price, D., Hale, J. R., Stephenson, M. C., Barnes, G. R., Smith, S. M., & Morris, P. G. (2011). Investigating the electrophysiological basis of resting state networks using magnetoencephalography. *Proceedings of the National Academy of Sciences of the United States of America*, *108*(40), 16783–8.

Carter, R. M., Macinnes, J. J., Huettel, S. a., & Adcock, R. A. (2009). Activation in the vta and nucleus accumbens increases in anticipation of both gains and losses. *Front Behav Neurosci*, *3*, 1–15.

Cavanna, A. E., & Trimble, M. R. (2006). The precuneus: a review of its functional anatomy and behavioural correlates. *Brain*, *129*(Pt 3), 564–83.

Clayton, E. C., Rajkowski, J., Cohen, J. D., & Aston-Jones, G. (2004). Phasic activation of monkey locus ceruleus neurons by simple decisions in a forced-choice task. *J Neurosci*, *24*(44), 9914–20.

Conroy, B., Walz, J. M., Cheung, B., & Sajda, P. (2013a). Fast simultaneous training of generalized linear models (FaSTGLZ). *Journal of Machine Learning Research*, *(In revision)*.

Conroy, B., Walz, J. M., & Sajda, P. (2013b). Fast bootstrapping and permutation testing for assessing reproducibility and interpretability of multivariate fMRI decoding models. *PLoS One*, *(Accepted)*.

Corbetta, M., Patel, G., & Shulman, G. L. (2008). The reorienting system of the human brain: from environment to theory of mind. *Neuron*, *58*, 306–324.

Corbetta, M., & Shulman, G. L. (2002). Control of goal-directed and stimulus-driven attention in the brain. *Nat Rev Neurosci*, *3*, 201–215.

Critchley, H. D., Tang, J., Glaser, D., Butterworth, B., & Dolan, R. J. (2005). Anterior cingulate activity during error and autonomic response. *NeuroImage*, *27*(4), 885–95.

Crottaz-Herbette, S., & Menon, V. (2006). Where and when the anterior cingulate cortex modulates attentional response: combined fMRI and ERP evidence. *J Cogn Neurosci*, *18*, 766–780.

D'Ardenne, K., McClure, S. M., Nystrom, L. E., & Cohen, J. D. (2008). Bold responses reflecting dopaminergic signals in the human ventral tegmental area. *Science*, *319*, 1264–1267.

Dayan, P., & Yu, A. J. (2006). Phasic norepinephrine: a neural interrupt signal for unexpected events. *Network*, *17*, 335–50.

De Luca, M., Beckmann, C. F., De Stefano, N., Matthews, P. M., & Smith, S. M. (2006). fMRI resting state netwoeks define distinct modes of long-distance interaction in the human brain. *NeuroImage*, *29(4)*, 1359–1367.

de Pasquale, F., Della Penna, S., Snyder, A. Z., Lewis, C., Mantini, D., Marzetti, L., Belardinelli, P., Ciancetta, L., Pizzella, V., Romani, G. L., & Corbetta, M. (2010). Temporal dynamics of spontaneous meg activity in brain networks. *Proc Natl Acad Sci U S A*, *107*, 6040–5.

Diquattro, N. E., Sawaki, R., & Geng, J. J. (2013). Effective connectivity during feature-based attentional capture: Evidence against the attentional reorienting hypothesis of tpj. *Cereb Cortex*.

Donchin, E., & Coles, M. (1988). Is the P300 component a manifestation of context updating? *Behav Brain Sci*, *11*, 357–374.

Duda, R. O., Hart, P. E., & Stork, D. G. (2001). *Pattern Classification*. New York: John Wiley Sons.

Dugue, L., Marque, P., & VanRullen, R. (2011). The phase of ongoing oscillations mediates the causal relation between brain excitation and visual perception. *J Neurosci*, *31*(33), 11889–93.

Duoandikoetxea, J. (2001). *Fourier Analysis*, vol. Graduate Studies in Mathematics (29).

Eason, R., Harter, M., & White, T. (1969). Effects of attention and arousal on visually evoked cortical potentials and reaction time in man. *Physiol Behav*, *4(3)*, 283–289.

Eichele, T., Debener, S., Calhoun, V. D., Specht, K., Engel, A. K., Hugdahl, K., von Cramon, D. Y., & Ullsperger, M. (2008). Prediction of human errors by maladaptive changes in event-related brain networks. *Proc Natl Acad Sci U S A*, *105*, 6173–8.

Eichele, T., Specht, K., Moosmann, M., Jongsma, M. L. a., Quiroga, R. Q., Nordby, H., & Hugdahl, K. (2005). Assessing the spatiotemporal evolution of neuronal activation with single-trial event-related potentials and functional MRI. *Proc Natl Acad Sci U S A*, *102*, 17798–803.

Einhauser, W., Stout, J., Koch, C., & Carter, O. (2008). Pupil dilation reflects perceptual selection and predicts subsequent stability in perceptual rivalry. *Proc Natl Acad Sci U S A*, *105*(5), 1704–9.

Esposito, F., Bertolino, A., Scarabino, T., Latorre, V., Blasi, G., Popolizio, T., Tedeschi, G., Cirillo, S., Goebel, R., & Di Salle, F. (2006). Independent component model of the default-mode brain function: Assessing the impact of active thinking. *Brain Res Bull*, *70*, 263–9.

Esposito, F., Mulert, C., & Goebel, R. (2009). Combined distributed source and single-trial EEG-fMRI modeling: application to effortful decision making processes. *NeuroImage*, *47*, 112–21.

Feige, B., Scheffler, K., Esposito, F., Di Salle, F., Hennig, J., & Seifritz, E. (2005). Cortical and subcortical correlates of electroencephalographic alpha rhythm modulation. *J Neurophysiol*, *93*, 2864–72.

Fellinger, R., Klimesch, W., Gruber, W., Freunberger, R., & Doppelmayr, M. (2011). Pre-stimulus alpha phase-alignment predicts p1-amplitude. *Brain Res Bull*, *85*(6), 417–23.

Folstein, J. R., & Van Petten, C. (2008). Influence of cognitive control and mismatch on the N2 component of the ERP: a review. *Psychophysiology*, *45*(1), 152–70.

Fox, M. D., Corbetta, M., Snyder, A. Z., Vincent, J. L., & Raichle, M. E. (2006). Spontaneous neuronal activity distinguishes human dorsal and ventral attention systems. *Proceedings of the National Academy of Sciences of the United States of America*, *103*(26), 10046–10051.

Fox, M. D., & Raichle, M. E. (2007). Spontaneous fluctuations in brain activity observed with functional magnetic resonance imaging. *Nat Rev Neurosci*, *8*, 700–11.

Friston, K. J., Harrison, L., & Penny, W. (2003). Dynamic causal modelling. *NeuroImage*, *19*(4), 1273–1302.

Fuglo, D., Pedersen, H., Rostrup, E., Hansen, A. E., & Larsson, H. B. (2012). Correlation between single-trial visual evoked potentials and the blood oxygenation level dependent response in simultaneously recorded electroencephalography-functional magnetic resonance imaging. *Magn Reson Med*, *68*(1), 252–60.

Fuster, J. M. (2001). The prefrontal cortex–an update: time is of the essence. *Neuron*, *30*(2), 319–33.

Gajewski, P. D., Stoerig, P., & Falkenstein, M. (2008). ERP–correlates of response selection in a response conflict paradigm. *Brain Res*, *1189*, 127–34.

Gerson, A. D., Parra, L. C., & Sajda, P. (2005). Cortical origins of response time variability during rapid discrimination of visual objects. *NeuroImage*, *28*, 342–53.

Ghez, C., & Fahn, S. (1985). *The Cerebellum*. New York: Elsevier, 2 ed.

Gilzenrat, M. S., Nieuwenhuis, S., Jepma, M., & Cohen, J. D. (2010). Pupil diameter tracks changes in control state predicted by the adaptive gain theory of locus coeruleus function. *Cogn Affect Behav Neurosci*, *10*(2), 252–69.

Goense, J., Merkle, H., & Logothetis, N. K. (2012). High-resolution fMRI reveals laminar differences in neurovascular coupling between positive and negative BOLD responses. *Neuron*, *76*, 629–39.

Goldberg, I., Harel, M., & Malach, R. (2006). When the brain loses its self: prefrontal inactivation during sensorimotor processing. *Neuron*, *50*(2), 329–39.

Goldman, R. I., Stern, J. M., Engel, J., J., & Cohen, M. S. (2002). Simultaneous EEG and fMRI of the alpha rhythm. *Neuroreport*, *13*, 2487–92.

Goldman, R. I., Wei, C.-Y., Philiastides, M. G., Gerson, A. D., Friedman, D., Brown, T. R., & Sajda, P. (2009). Single-trial discrimination for integrating simultaneous EEG and fMRI: identifying cortical areas contributing to trial-to-trial variability in the auditory oddball task. *NeuroImage*, *47*, 136–47.

Green, D. M., & Swets, J. A. (1966). *Signal Detection and Psychophysics*. John Wiley Sons.

Hanslmayr, S., Aslan, A., Staudigl, T., Klimesch, W., Herrmann, C. S., & Bauml, K. H. (2007). Prestimulus oscillations predict visual perception performance between and within subjects. *NeuroImage*, *37*(4), 1465–73.

Hill, R. A., Chiappa, K. H., Huang-Hellinger, F., & Jenkins, B. G. (1995). EEG during MR imaging: differentiation of movement artifact from paroxysmal cortical activity. *Neurology*, *45*(10), 1942–3.

Hong, L., Walz, J. M., & Sajda, P. (2013). Your eyes give you away: Changes in pupil diameter correlate with task-related EEG dynamics. *PLoS One*, *(In revision)*.

Hopfinger, J. B., & West, V. M. (2006). Interactions between endogenous and exogenous attention on cortical visual processing. *NeuroImage*, *31*, 774–89.

Hyvarinen, A. (1999). Fast and robust fixed-point algorithms for independent component analysis. *IEEE Trans Neural Netw*, *10*(3), 626–34.

Ives, J. R., Warach, S., Schmitt, F., Edelman, R. R., & Schomer, D. L. (1993). Monitoring the patient's EEG during echo planar MRI. *Electroencephalogr Clin Neurophysiol*, *87*(6), 417–20.

Kammer, T., Lehr, L., & Kirschfeld, K. (1999). Cortical visual processing is temporally dispersed by luminance in human subjects. *Neurosci Lett*, *263*(2-3), 133–6.

Kelly, S. P., Gomez-Ramirez, M., & Foxe, J. J. (2009). The strength of anticipatory spatial biasing predicts target discrimination at attended locations: a high-density EEG study. *Eur J Neurosci*, *30*(11), 2224–34.

Keren, N. I., Lozar, C. T., Harris, K. C., Morgan, P. S., & Eckert, M. a. (2009). In vivo mapping of the human locus coeruleus. *NeuroImage*, *47*, 1261–7.

Key, A. P. F., Dove, G. O., & Maguire, M. J. (2005). Linking brainwaves to the brain: an ERP primer. *Dev Neuropsychol*, *27*, 183–215.

Kincade, J. M., Abrams, R. A., Astafiev, S. V., Shulman, G. L., & Corbetta, M. (2005). An event-related functional magnetic resonance imaging study of voluntary and stimulus-driven orienting of attention. *J Neurosci*, *25*, 4593–604.

Klimesch, W., Doppelmayr, M., Russegger, H., Pachinger, T., & Schwaiger, J. (1998). Induced alpha band power changes in the human EEG and attention. *Neurosci Lett*, *244*(2), 73–6.

Lacey, J. I. (1956). The evaluation of autonomic responses: toward a general solution. *Ann N Y Acad Sci*, *67*(5), 125–63.

Lange, J., Oostenveld, R., & Fries, P. (2013). Reduced occipital alpha power indexes enhanced excitability rather than improved visual perception. *J Neurosci*, *33*(7), 3212–20.

Laufs, H., Holt, J. L., Elfont, R., Krams, M., Paul, J. S., Krakow, K., & Kleinschmidt, A. (2006). Where the BOLD signal goes when alpha EEG leaves. *NeuroImage*, *31*(4), 1408–18.

Laurens, K. R., Kiehl, K. A., & Liddle, P. F. (2005). A supramodal limbic-paralimbic-neocortical network supports goal-directed stimulus processing. *Hum Brain Mapp*, *24(1)*, 35–49.

Linden, D. E. J. (2005). The P300: where in the brain is it produced and what does it tell us? *Neuroscientist*, *11*, 563–76.

Liu, Z., de Zwart, J. A., Yao, B., van Gelderen, P., Kuo, L. W., & Duyn, J. H. (2012). Finding thalamic BOLD correlates to posterior alpha EEG. *NeuroImage*, *63*(3), 1060–9.

Logothetis, N. K. (2008). What we can do and what we cannot do with fMRI. *Nature*, *453*(7197), 869–78.

Logothetis, N. K., Augath, M., Murayama, Y., Rauch, A., Sultan, F., Goense, J., Oeltermann, A., & Merkle, H. (2010). The effects of electrical microstimulation on cortical signal propagation. *Nat Neurosci*, *13*, 1283–91.

Loughlin, S., Foote, S., & Bloom, F. (1986). Efferent projections of nucleus locus coeruleus: topographic organization of cells of origin demonstrated by three-dimensional reconstruction. *Neuroscience*, *18*, 291–306.

Luck, S., Woodman, G., & Vogel, E. (2000). Event-related potential studies of attention. *Trends Cogn Sci*, *4*, 432–440.

MacDonald, r., A. W., Cohen, J. D., Stenger, V. A., & Carter, C. S. (2000). Dissociating the role of the dorsolateral prefrontal and anterior cingulate cortex in cognitive control. *Science*, *288*(5472), 1835–8.

Makeig, S., Delorme, A., Westerfield, M., Jung, T.-P., Townsend, J., Courchesne, E., & Sejnowski, T. J. (2004). Electroencephalographic brain dynamics following manually responded visual targets. *PLoS Biol*, *2*, 0747–0762.

Makeig, S., Westerfield, M., Jung, T. P., Covington, J., Townsend, J., Sejnowski, T. J., & Courchesne, E. (1999). Functionally independent components of the late positive event-related potential during visual spatial attention. *J Neurosci*, *19*, 2665–80.

Makeig, S., Westerfield, M., Jung, T. P., Enghoff, S., Townsend, J., Courchesne, E., & Sejnowski, T. J. (2002). Dynamic brain sources of visual evoked responses. *Science*, *295*(5555), 690–4.

Mantini, D., Perrucci, M. G., Del Gratta, C., Romani, G. L., & Corbetta, M. (2007). Electrophysiological signatures of resting state networks in the human brain. *Proc Natl Acad Sci U S A*, *104*, 13170–5.

Mathewson, K. E., Gratton, G., Fabiani, M., Beck, D. M., & Ro, T. (2009). To see or not to see: prestimulus alpha phase predicts visual awareness. *J Neurosci*, *29*(9), 2725–32.

Mattle, H., Edelman, R. R., Reis, M. A., & Atkinson, D. J. (1990). Flow quantification in the superior sagittal sinus using magnetic resonance. *Neurology*, *40*(5), 813–5.

Mayhew, S. D., Ostwald, D., Porcaro, C., & Bagshaw, A. P. (2013). Spontaneous EEG alpha oscillation interacts with positive and negative BOLD responses in the visual-auditory cortices and default-mode network. *NeuroImage*, *76*, 362–72.

Mazaheri, A., Nieuwenhuis, I. L., van Dijk, H., & Jensen, O. (2009). Prestimulus alpha and mu activity predicts failure to inhibit motor responses. *Hum Brain Mapp*, *30*(6), 1791–800.

Min, B. K., & Park, H. J. (2010). Task-related modulation of anterior theta and posterior alpha EEG reflects top-down preparation. *BMC Neurosci*, *11*, 79.

Mukamel, R., Gelbard, H., Arieli, A., Hasson, U., Fried, I., & Malach, R. (2005). Coupling between neuronal firing, field potentials, and fMRI in human auditory cortex. *Science*, *309*, 951–4.

Mulert, C., Seifert, C., Leicht, G., Kirsch, V., Ertl, M., Karch, S., Moosmann, M., Lutz, J., Mller, H.-J., Hegerl, U., Pogarell, O., & Jger, L. (2008). Single-trial coupling of EEG and fMRI reveals the involvement of early anterior cingulate cortex activation in effortful decision making. *NeuroImage*, *42*, 158–68.

Muri, R. M., Felblinger, J., Rosler, K. M., Jung, B., Hess, C. W., & Boesch, C. (1998). Recording of electrical brain activity in a magnetic resonance environment: distorting effects of the static magnetic field. *Magn Reson Med*, *39*(1), 18–22.

Murphy, P. R., Robertson, I. H., Balsters, J. H., & O'Connell R, G. (2011). Pupillometry and P3 index the locus coeruleus-noradrenergic arousal function in humans. *Psychophysiology*, *48*, 1532–43.

Murray, S. O., & Wojciulik, E. (2004). Attention increases neural selectivity in the human lateral occipital complex. *Nat Neurosci*, *7*(1), 70–4.

Nguyen, V. T., Breakspear, M., & Cunnington, R. (2013). Fusing concurrent EEG-fMRI with dynamic causal modeling: Application to effective connectivity during face perception. *NeuroImage*.

Nieuwenhuis, S., Aston-Jones, G., & Cohen, J. D. (2005). Decision making, the P3, and the locus coeruleus-norepinephrine system. *Psychol Bull*, *131*, 510–32.

Nieuwenhuis, S., De Geus, E. J., & Aston-Jones, G. (2010). The anatomical and functional relationship between the P3 and autonomic components of the orienting response. *Psychophysiology*.

Novitskiy, N., Ramautar, J. R., VandERPerren, K., De Vos, M., Mennes, M., Mijovic, B., Vanrumste, B., Stiers, P., Van den Bergh, B., Lagae, L., Sunaert, S., Van Huffel, S., & Wagemans, J. (2011). The BOLD correlates of the visual p1 and N1 in single-trial analysis of simultaneous EEG-fMRI recordings during a spatial detection task. *NeuroImage*, *54*(2), 824–35.

O'Connell, R. G., Dockree, P. M., & Kelly, S. P. (2012). A supramodal accumulation-to-bound signal that determines perceptual decisions in humans. *Nat Neurosci*, *15*(12), 1729–35.

Ossandn, T., Jerbi, K., Vidal, J. R., Bayle, D. J., Henaff, M.-A., Jung, J., Minotti, L., Bertrand, O., Kahane, P., & Lachaux, J.-P. (2011). Transient suppression of broadband gamma power in the default-mode network is correlated with task complexity and subject performance. *The J Neurosci : the official journal of the Society for Neuroscience*, *31*(41), 14521–30.

Palva, J. M., & Palva, S. (2012). Infra-slow fluctuations in electrophysiological recordings, blood-oxygenation-level-dependent signals, and psychophysical time series. *NeuroImage*, *62*(4), 2201–11.

Parra, L., Alvino, C., Tang, A., Pearlmutter, B., Yeung, N., Osman, A., & Sajda, P. (2002). Linear spatial integration for single-trial detection in encephalography. *NeuroImage*, *17*(1), 223–30.

Parra, L. C., Spence, C. D., Gerson, A. D., & Sajda, P. (2005). Recipes for the linear analysis of EEG. *NeuroImage*, *28*, 326–41.

Payzan-Lenestour, E., Dunne, S., Bossaerts, P., & O'Doherty, J. P. (2013). The neural representation of unexpected uncertainty during value-based decision making. *Neuron*, *79*(1), 191–201.

Penny, W. D., Stephan, K. E., Daunizeau, J., Rosa, M. J., Friston, K. J., Schofield, T. M., & Leff, A. P. (2010). Comparing families of dynamic causal models. *PLoS Comput Biol*, *6*(3), e1000709.

Philiastides, M. G., Ratcliff, R., & Sajda, P. (2006). Neural representation of task difficulty and decision making during perceptual categorization: a timing diagram. *J Neurosci*, *26*, 8965–75.

Philiastides, M. G., & Sajda, P. (2006). Temporal characterization of the neural correlates of perceptual decision making in the human brain. *Cereb Cortex*, *16*(4), 509–18.

Philiastides, M. G., & Sajda, P. (2007). EEG-informed fMRI reveals spatiotemporal characteristics of perceptual decision making. *J Neurosci*, *27*(48), 13082–91.

Picton, T. W. (1992). The P300 wave of the human event-related potential. *J Clin Neurophysiol*, *9*(4), 456–79.

Polich, J. (2007). Updating P300: an integrative theory of P3a and P3b. *Neurophysiol Clin*, *118*, 2128–48.

Polich, J., & Kok, A. (1995). Cognitive and biological determinants of P300: an integrative review. *Biol Psychol*, *41*(2), 103–46.

Raichle, M. E., MacLeod, A. M., Snyder, A. Z., Powers, W. J., Gusnard, D. A., & Shulman, G. L. (2001). A default mode of brain function. *Proc Natl Acad Sci U S A*, *98*(2), 676–82.

Rajagovindan, R., & Ding, M. (2011). From prestimulus alpha oscillation to visual-evoked response: an inverted-u function and its attentional modulation. *J Cogn Neurosci*, *23*(6), 1379–94.

Rajkowski, P., Kubiak, P., & Aston-Jones, G. (1993). Correlations between locus coeruleus (lc) neural activity, pupil diameter and behavior in monkey support a role of LCin attention. *Society for Neuroscience Abstracts*, *19*, 974.

Ray, W. J., & Cole, H. W. (1985). EEG alpha activity reflects attentional demands, and beta activity reflects emotional and cognitive processes. *Science*, *228*(4700), 750–2.

Romei, V., Brodbeck, V., Michel, C., Amedi, A., Pascual-Leone, A., & Thut, G. (2008). Spontaneous fluctuations in posterior alpha-band EEG activity reflect variability in excitability of human visual areas. *Cereb Cortex*, *18*(9), 2010–8.

Sajda, P., Goldman, R. I., Dyrholm, M., & Brown, T. R. (2010). *Chapter 9: Signal Processing and Machine Learning for Single-trial Analysis of Simultaneously Acquired EEG and fMRI*. Academic Press.

Sara, S. J., & Bouret, S. (2012). Orienting and reorienting: the locus coeruleus mediates cognition through arousal. *Neuron*, *76*, 130–41.

Scheeringa, R., Bastiaansen, M. C., Petersson, K. M., Oostenveld, R., Norris, D. G., & Hagoort, P. (2008). Frontal theta EEG activity correlates negatively with the default mode network in resting state. *Int J Psychophysiol*, *67*(3), 242–51.

Scheeringa, R., Fries, P., Petersson, K. M., Oostenveld, R., Grothe, I., Norris, D. G., Hagoort, P., & Bastiaansen, M. C. (2011a). Neuronal dynamics underlying high- and low-frequency EEG oscillations contribute independently to the human BOLD signal. *Neuron*, *69*(3), 572–83.

Scheeringa, R., Mazaheri, A., Bojak, I., Norris, D. G., & Kleinschmidt, A. (2011b). Modulation of visually evoked cortical fMRI responses by phase of ongoing occipital alpha oscillations. *J Neurosci*, *31*(10), 3813–20.

Scheibe, C., Ullsperger, M., Sommer, W., & Heekeren, H. R. (2010). Effects of parametrical and trial-to-trial variation in prior probability processing revealed by simultaneous electroencephalogram/functional magnetic resonance imaging. *J Neurosci*, *30*(49), 16709–17.

Schooler, J. W. (2011). Introspecting in the spirit of william james: comment on fox, ericsson, and best (2011). *Psychol Bull*, *137*(2), 345–50.

Singh, K. D., & Fawcett, I. P. (2008). Transient and linearly graded deactivation of the human default-mode network by a visual detection task. *NeuroImage*, *41*(1), 100–12.

Smit, D. J., Posthuma, D., Boomsma, D. I., & De Geus, E. J. (2009). Phenotypic and genetic correlations between evoked EEG/ERP measures during the response anticipation period of a delayed response task. *Psychophysiology*, *46*(2), 344–56.

Smith, S. M. (2012). The future of fMRI connectivity. *NeuroImage*, *62*(2), 1257–66.

Smith, S. M., Jenkinson, M., Woolrich, M. W., Beckmann, C. F., Behrens, T. E., Johansen-Berg, H., Bannister, P. R., De Luca, M., Drobnjak, I., Flitney, D. E., Niazy, R. K., Saunders, J., Vickers, J., Zhang, Y., De Stefano, N., Brady, J. M., & Matthews, P. M. (2004). Advances in functional and structural MR image analysis and implementation as FSL. *NeuroImage*, *23*, S208–19.

Smith, S. M., & Nichols, T. E. (2009). Threshold-free cluster enhancement: addressing problems of smoothing, threshold dependence and localisation in cluster inference. *NeuroImage*, *44*, 83–98.

Steinhauer, S. R., & Hakerem, G. (1992). The pupillary response in cognitive psychophysiology and schizophrenia. *Ann N Y Acad Sci*, *658*, 182–204.

Stelzer, J., Chen, Y., & Turner, R. (2013). Statistical inference and multiple testing correction in classification-based multi-voxel pattern analysis (MVPA): random permutations and cluster size control. *NeuroImage*, *65*, 69–82.

Stephan, K. E., Penny, W. D., Daunizeau, J., Moran, R. J., & Friston, K. J. (2009). Bayesian model selection for group studies. *NeuroImage*, *46*(4), 1004–17.

Stephan, K. E., Penny, W. D., Moran, R. J., den Ouden, H. E., Daunizeau, J., & Friston, K. J. (2010). Ten simple rules for dynamic causal modeling. *NeuroImage*, *49*(4), 3099–109.

Stevens, A. A., Skudlarski, P., Gatenby, J. C., & Gore, J. C. (2000). Event-related fMRI of auditory and visual oddball tasks. *Magn Reson Imaging*, *18*, 495–502.

Stoodley, C. J., & Schmahmann, J. D. (2009). Functional topography in the human cerebellum: a meta-analysis of neuroimaging studies. *NeuroImage*, *44*(2), 489–501.

Stoodley, C. J., Valera, E. M., & Schmahmann, J. D. (2012). Functional topography of the cerebellum for motor and cognitive tasks: an fMRI study. *NeuroImage*, *59*(2), 1560–70.

Strang, G. (2003). *Chapter 4: Orthogonality*. Wellesley, MA: Wellesley-Cambridge Press, 3 ed.

Taylor, K. S., Seminowicz, D. a., & Davis, K. D. (2009). Two systems of resting state connectivity between the insula and cingulate cortex. *Hum Brain Mapp*, *30*(9), 2731–45.

Thut, G., Nietzel, A., Brandt, S. A., & Pascual-Leone, A. (2006). Alpha-band electroencephalographic activity over occipital cortex indexes visuospatial attention bias and predicts visual target detection. *J Neurosci*, *26*(37), 9494–502.

van Dijk, H., Schoffelen, J. M., Oostenveld, R., & Jensen, O. (2008). Prestimulus oscillatory activity in the alpha band predicts visual discrimination ability. *J Neurosci*, *28*(8), 1816–23.

Vanhaudenhuyse, A., Demertzi, A., Schabus, M., Noirhomme, Q., Bredart, S., Boly, M., Phillips, C., Soddu, A., Luxen, A., Moonen, G., & Laureys, S. (2011). Two distinct neuronal networks mediate the awareness of environment and of self. *J Cogn Neurosci*, *23*(3), 570–8.

Vazquez, M. M., Vaquero, E., Cardoso, M. J., & Gomez, C. M. (2001). Temporal evolution of alpha and beta bands during visual spatial attention. *Brain Res Cogn Brain Res*, *12*(2), 315–320.

Vossel, S., Weidner, R., Driver, J., Friston, K. J., & Fink, G. R. (2012). Deconstructing the architecture of dorsal and ventral attention systems with dynamic causal modeling. *J Neurosci*, *32*(31), 10637–48.

Walz, J. M., Goldman, R. I., Carapezza, M., Muraskin, J., Brown, T. R., & Sajda, P. (2013a). Simultaneous EEG-fMRI reveals a temporal cascade of task-related and default-mode activations during a simple target detection task. *NeuroImage*, *(In press)*.

Walz, J. M., Goldman, R. I., Muraskin, J., Carapezza, M., Brown, T. R., & Sajda, P. (2013b). Simultaneous EEG-fMRI reveals temporal evolution of coupling between supramodal attention systems and the brainstem. *J Neurosci*, *(In press)*.

Warbrick, T., Mobascher, a., Brinkmeyer, J., Musso, F., Richter, N., Stoecker, T., Fink, G. R., Shah, N. J., & Winterer, G. (2009). Single-trial P3 amplitude and latency informed event-related fMRI models yield different BOLD response patterns to a target detection task. *NeuroImage*, *47*, 1532–44.

Waszak, F., & Herwig, A. (2007). Effect anticipation modulates deviance processing in the brain. *Brain Res*, *1183*, 74–82.

Weissman, D., Roberts, K., Visscher, K. M., & Woldorff, M. G. (2006). The neural bases of momentary lapses in attention. *Nature Neurosci*, *9*, 971–978.

Worsley, K. J. (2001). *Chapter 14: Statistical Analysis of Activation Images*. Oxford University Press.

Yarkoni, T., Barch, D. M., Gray, J. R., Conturo, T. E., & Braver, T. S. (2009). Bold correlates of trial-by-trial reaction time variability in gray and white matter: a multi-study fMRI analysis. *PLoS One*, *4*(1), e4257.

Yarkoni, T., Poldrack, R. A., Nichols, T. E., Van Essen, D. C., & Wager, T. D. (2011). Large-scale automated synthesis of human functional neuroimaging data. *Nat Methods*, *8*(8), 665–70.

Appendices

Appendix A

Publications Resulting from this Work

JOURNAL PAPERS

J.M. Walz, R.I. Goldman, M. Carapezza, J. Muraskin, T.R. Brown, and P. Sajda (2013) "Simultaneous EEG-fMRI Reveals a Temporal Cascade of Task-Related and Default-Mode Activations During a Simple Target Detection Task," *NeuroImage* (In press)

J.M. Walz, R.I. Goldman, J. Muraskin, M. Carapezza, T.R. Brown, and P. Sajda (2013) "Simultaneous EEG-fMRI Reveals Temporal Evolution of Coupling Between Supramodal Attention Systems and the Brainstem," *Journal of Neuroscience* (In press)

B. Conroy, J.M. Walz, and P. Sajda (2013) "Fast Bootstrapping and Permutation Testing for Assessing Reproducibility and Interpretability of Multivariate fMRI Decoding Models," *PLoS ONE* (Accepted)

L. Hong, J.M. Walz*, and P. Sajda (2013) "Your Eyes Give You Away: Changes in Pupil Diameter Correlate with Task-related EEG Dynamics," *PLoS ONE* (In revision) *co-first-author

B. Conroy, J.M. Walz, B. Cheung, and P. Sajda (2013) "Fast Simultaneous Training of Generalized Linear Models (FaSTGLZ)," *Journal of Machine Learning Research* (In revision)

J.M. Walz, R.I. Goldman, M. Carapezza, T.R. Brown, and P. Sajda (2013) "Prestimulus EEG Alpha Oscillations Modulate Distribution of fMRI BOLD Response to Auditory Stimuli" (In preparation)

CONFERENCE PAPERS

B. Lou, J.M. Walz, J.V. Shi, and P. Sajda (2011) "Learning EEG Components for Discriminating Multi-Class Perceptual Decisions," 5th Annual International IEEE EMBS Conference on Neural Engineering, April 27-May 1, Cancun, Mexico. pp. 675-678 in conference proceedings.

B. Conroy, J.M. Walz, and P. Sajda (2012) "Fast Simultaneous Training of Generalized Linear Models (FaSTGLZ) for Multi-voxel Pattern Analysis in fMRI," 2nd NIPS workshop on Machine Learning and Interpretation in Neuroimaging (MLINI), December 7-8, Lake Tahoe, NV.

ABSTRACTS

J.M. Walz and P. Sajda (2010) "Time Domain vs. Frequency Domain Single-Trial EEG Analysis of a Perceptual Decision-Making Task," 16th Annual Meeting of the Organization for Human Brain Mapping, June 6-10, Barcelona, Spain.

J. Sherwin, J.M. Walz, and P. Sajda (2010) "Using Hierarchical Temporal Memories to Track the Constituent Brain States Underlying Perceptual Decision Making," DARPA NEST Meeting, Nov. 18-22, San Diego, CA.

B. Lou, J.M. Walz, J.V. Shi and P. Sajda (2011) "Single-trial EEG Discriminators Predict Pre-stimulus Alpha Power During Perceptual Decision-making," Computational and Systems Neuroscience (COSYNE) Meeting, Feb. 24-27, Salt Lake City, UT.

J.M. Walz, J. Muraskin, R.I. Goldman, T.R. Brown, and P. Sajda (2012) "Single-trial EEG Discriminant Components Acquired During 3T fMRI," ISMRM 20th Annual Meeting, May 5-11, Melbourne, Australia.

B. Lou, Y. Li, J.M. Walz, and P. Sajda (2012) "Post-stimulus Trial-by-trial EEG Variability Indexes Mean and Variance of Pre-stimulus Alpha Power," 18th Annual Meeting of the Organization for Human Brain Mapping, June 10-14, Beijing, China.

J.M. Walz, L. Hong, and P. Sajda (2012) "Correlates of Pupil Diameter and Single-Trial EEG Variability in an Auditory Oddball Task," 18th Annual Meeting of the Organization for Human Brain Mapping, June 10-14, Beijing, China.

J.M. Walz, J. Muraskin, R.I. Goldman, T.R. Brown, and P. Sajda (2012) "The Superposition of Task-dependent and Default Mode Networks During a Mundane Target Detection Task," 18th Annual Meeting of the Organization for Human Brain Mapping, June 10-14, Beijing, China.

L. Hong, J.M. Walz, and P. Sajda (2012) "Temporally Specific EEG Components Correlate with Perceived Anticipation and Task Engagement," Society for Neuroscience Annual Meeting, October 13-17, New Orleans, LA.

J.M. Walz, M. Carapezza, J. Muraskin, R.I. Goldman, T.R. Brown, and P. Sajda (2012) "BOLD fMRI Correlates of Spontaneous Eye Blinks Detected Using Simultaneously-acquired EEG," Society for Neuroscience Annual Meeting, October 13-17, New Orleans, LA.

J.M. Walz, M. Carapezza, B. Lou, R.I. Goldman, T.R. Brown, and P. Sajda (2013) "Variability in Distribution of fMRI BOLD Response Linked to Prestimulus Alpha Power in Simultaneously-acquired EEG," ISMRM 21st Annual Meeting, April 20-26, Salt Lake City, UT. Oral presentation.

B. Conroy, J.M. Walz, and P. Sajda (2013) "Fast Validation Testing of Sparse Classification and Regression Models for Multi-Voxel fMRI Analysis," 19th Annual Meeting of the Organization for Human Brain Mapping, June 16-20, Seattle, WA.

J.M. Walz, R.I. Goldman, J. Muraskin, B. Conroy, T.R. Brown, and P. Sajda (2013) "Brainstem Modulation of the P300: Evidence from Simultaneous EEG-fMRI," 19th Annual Meeting of the Organization for Human Brain Mapping, June 16-20, Seattle, WA.

Appendix B

List of Abbreviations

General

BOLD	blood-oxygen level dependent
EEG	electro-encephalography
fMRI	functional magnetic resonance imaging
ICA	independent components analysis
ITI	inter-trial interval
PCA	principal components analysis
PD	pupil diameter
RT	reaction time

EEG Analyses

AUC	area under the ROC curve
EOG	electro-oculogram
ERP	event-related potential
LR	logistic regression
RL	response-locked
SL	stimulus-locked
STV	single-trial variability

fMRI Analyses

BCG	ballisto-cardiogram
BMS	Bayesian model selection
BPA	Bayesian parameter averaging
DCM	dynamic causal model
EPI	echo-planar imaging (functional data)
FWE	family wise error
GLM	general linear model
HRF	hemodynamic response function
MNI	Montreal Neurological Institute (brain template)
RF	radio frequency
ROI	region of interest
SPGR	spoiled gradient recalled (structural data)
TE	echo time
TFCE	threshold-free cluster enhancement
TR	repetition time

Brain Regions

ACC	anterior cingulate cortex
BS	brainstem
DLPFC	dorso-lateral prefrontal cortex
DMN	default-mode network
IFG	inferior frontal gyrus
LC	locus coeruleus
LOC	lateral occipital cortex
MFG	middle frontal gyrus
NE	norepinephrine
OFC	orbito-frontal cortex
PCC	posterior cingulate cortex
SFG	superior frontal gyrus
SMA	supplementary motor area
VAN	ventral attention network